Analysis of assembly and function of bacterial type III secretion systems

Dissertation

der Mathematisch-Naturwissenschaftlichen Fakultät

der Eberhard Karls Universität Tübingen

zur Erlangung des Grades eines

Doktors der Naturwissenschaften

(Dr. rer. nat.)

vorgelegt von

Nidhi Singh

aus Lucknow, Uttar Pradesh, Indien

Tübingen

2021

Gedruckt mit Genehmigung der Mathematisch-Naturwissenschaftlichen Fakultät der Eberhard Karls Universität Tübingen.

Tag der mündlichen Qualifikation:	*27.07.2021*
Dekan:	*Prof. Dr. Thilo Stehle*
1. Berichterstatter:	*Prof. Dr. Samuel Wagner*
2. Berichterstatterin:	*apl. Prof. Dr. Evi Stegmann*

Erklärung

Ich erkläre hiermit, dass ich die zur Promotion eingereichte Arbeit selbständig verfasst, nur die angegebenen Quellen und Hilfsmittel benutzt und Stellen, die wörtlich oder inhaltlich nach den Werken anderer Autoren entnommen sind, als solche gekennzeichnet habe. Eine detaillierte Abgrenzung meiner eigenen Leistungen von den Beiträgen meiner Kooperationspartner habe ich in „Declaration of author contribution“ vorgenommen.

.....

Unterschrift

For my family

Table of Contents

List of tables and figures

Summary[1]

Gram-negative bacterial pathogens utilize virulence-associated type III secretion systems (T3SS) to inject effector proteins into eukaryotic host cells. These effector proteins modulate the host cell biology to promote colonization and infection. Hence, T3SS are essential bacterial pathogenicity factors. The transmembrane export apparatus at the core of T3SS contains a unique helical complex of the hydrophobic proteins SctR, SctS, SctT, and SctU. These components comprise several highly conserved charged residues within their hydrophobic domains. Based on the closed state structure of the core complex $SctR_5S_4T_1$, we know several of these residues form both inter- and intramolecular salt bridges, which should break to facilitate pore opening. Mutagenesis of individual residues compromises the assembly or secretion of both the virulence-associated and the related flagellar T3SS. However, the exact role of these conserved charged residues in the assembly and function of T3SS remains elusive. Hence, to understand the role of these residues in the T3SS of *Salmonella* Typhimurium, we performed an in-depth investigation. Our investigation included mutagenesis, blue native PAGE, *in vivo* photocrosslinking and luciferase-based secretion assays. Our data show that these conserved salt bridges are not critical for the assembly of the respective protein but rather aid in incorporating the following subunit into the assembling complex. Our data also indicate that these conserved charged residues are critical for type III-dependent secretion and reveal a functional link between $SctS_{E44}$ and $SctT_{R204}$ and the cytoplasmic domain of SctU in gating the T3SS injectisome.

T3SS includes various proteins, and the exact interactions amongst constituent proteins and the complex assembly are not fully understood. The interaction amidst the inner ring protein and the sorting platform components is critical for the principal activity of type III secretion systems. SctK is one of the least studied cytoplasmic component and hence lack of information poses a major impediment in advancing our understanding of its interactions. Additionally, many aspects related to the organization, configuration and function of the sorting platform in the needle complex are still unclear. We performed an in-depth analysis of the different positions of SctD with *in vivo* photocrosslinking, luciferase-based secretion assays and different functional assays. Our results provide the plausible orientation model of SctD protein highlighting the interacting interface of SctD-SctK where the cytoplasmic component

[1] Parts of this summary were adapted from the submitted manuscript “Conserved salt bridges facilitate assembly of the helical core export apparatus of a *Salmonella enterica* type III secretion system”.

SctK establishes itself as the interacting partner of SctD in the inner membrane. Our newly established functional assays could successfully elucidate that low external pH and blockage of PMF can lead to a temporary dissociation and change in dynamics of the cytosolic components from T3SS respectively. Our investigation also characterizes the effect of single-gene deletions on the SctD-SctK interactions confirming that different secretion states have no substantial effect on the interaction of the ring protein with the cytosolic protein.

Zusammenfassung

Gram-negative bakterielle Pathogene nutzen Virulenz-assoziierte Typ-III-Sekretionssysteme (T3SS), um Effektorproteine in eukaryotische Wirtszellen zu injizieren. Diese Effektorproteine modulieren die Biologie der Wirtszelle, um die Kolonisierung und Infektion zu fördern. Daher sind T3SS wesentliche bakterielle Pathogenitätsfaktoren. Der Transmembran-Exportapparat im Kern des T3SSs enthält einen einzigartigen helikalen Komplex aus den hydrophoben Proteinen SctR, SctS, SctT und SctU. Diese Proteine umfassen mehrere hoch konservierte geladene Seitenketten innerhalb ihrer hydrophoben Domänen. Basierend auf einer Struktur des Kernkomplexes $SctR_5S_4T_1$ im geschlossenen Zustand ist es, dass mehrere dieser Seitenketten sowohl inter- als auch intramolekulare Salzbrücken bilden. Diese Salzbrücken sollten aufbrechen, um die Porenöffnung zu erleichtern. Mutationen an den Seitenketten der ausgebildeten Salzbrücken beeinträchtigen die Assemblierung oder auch die Sekretion sowohl beim Virulenz-assoziierten als auch beim verwandten flagellaren T3SS. Die genaue Rolle dieser konservierten geladenen Seitenketten bei der Assemblierung und deren Funktion am T3SS bleibt unklar. Um die Bedeutung dieser Seitenketten im T3SS von Salmonella Typhimurium zu verstehen, haben wir eine eingehende Untersuchung durchgeführt. Unsere Untersuchung umfasste Mutagenese, blue native PAGE, *in vivo* Photocrosslinking und Luciferase-basierte Sekretionsassays. Es stellte sich heraus, dass diese konservierten Salzbrücken unkritisch für die Assemblierung sind, aber den Einbau der nachfolgenden Untereinheit in den Kernkomplex begünstigen. Desweiteren haben wir herausgefunden, dass diese Salzbrücken kritisch für die Typ-III-abhängige Sekretion sind und zeigen eine funktionelle Verbindung zwischen $SctS_{E44}$ und $SctT_{R204}$ und der zytoplasmatischen Domäne von SctU beim Gating des T3SS auf.

Das T3SS besteht aus vielen verschiedenen Proteinen die korrekt aufgebaut sein, und miteinander interagieren müssen, um einen funktionellen Komplex zu bilden. Die genauen Interaktionen zwischen den konstituierten Proteinen und dem Aufbau des Komplexes ist nicht vollständig geklärt. Die Interaktion zwischen dem inneren Ringprotein und den Proteinen der Sortierplattform ist entscheidend für die Hauptaktivität des Typ-III-Sekretionssystems. SctK ist eine der am wenigsten untersuchten zytoplasmatischen Komponenten und daher stellt der Mangel an Informationen ein großes Hindernis dar, um unser Verständnis seiner Interaktionen voranzutreiben. Zusätzlich sind viele Aspekte, die mit der Organisation, Konfiguration und Funktion der Sortierplattform im Nadelkomplex zusammenhängen, noch unbekannt. Wir haben eine eingehende Analyse der verschiedenen Positionen von SctD mit *in vivo*

Photocrosslinking, Luciferase-basierten Sekretionsassays und verschiedenen funktionellen Assays durchgeführt. Unsere Ergebnisse liefern ein plausibles Orientierungsmodell des SctD-Proteins, das die interagierende Schnittstelle von SctD-SctK hervorhebt, an der sich die zytoplasmatische Komponente SctK als Interaktionspartner von SctD in der inneren Membran etabliert. Wir konnten mit unseren neu etablierten funktionellen Assays erfolgreich aufklären, dass ein niedriger äußerer pH-Wert und die Blockierung von PMF zu einer temporären Dissoziation bzw. Veränderung der Dynamik der zytosolischen Komponenten von T3SS führen kann. Unsere Untersuchung charakterisiert auch den Effekt von Einzelgen-Deletionen auf die SctD-SctK-Interaktionen und bestätigt, dass unterschiedliche Sekretionszustände keinen wesentlichen Einfluss auf die Interaktion des Ringproteins mit dem zytosolischen Proteinen haben.

List of Publications

- **Publication 1 (Research Article)**

  Conserved salt bridges facilitate assembly of the helical core export apparatus of a *Salmonella enterica* type III secretion system
  Singh N, Kronenberger T, Eipper A, Weichel F, Franz M, Macek B, Wagner S (revision submitted)

- **Publication 2 (Review Article)**

  Investigating the assembly of the bacterial type III secretion system injectisome by *in vivo* photocrosslinking.
  Singh N, Wagner S.
  Int J Med Microbiol. 2019 Sep;309(6):151331. doi: 10.1016/j.ijmm.2019.151331. Epub 2019 Jul 15.

- **Publication 3 (Research Article)**

  Yeast can express and assemble bacterial secretins in the mitochondrial outer membrane.
  Natarajan J, Moitra A, Zabel S, **Singh N**, Wagner S, Rapaport D.
  Microb Cell. 2019 Nov 19;7(1):15-27. doi: 10.15698/mic2020.01.703.

- **Publication 4 (Review Article)**

  Assembly and targeting of secretins in the bacterial outer membrane.
  Natarajan J, **Singh N**, Rapaport D.
  Int J Med Microbiol. 2019 Nov;309(7):151322. doi: 10.1016/j.ijmm.2019.06.002. Epub 2019 Jun 19.

- **Publication 5 (Review Article)**

  Bacterial type III secretion systems: a complex device for the delivery of bacterial effector proteins into eukaryotic host cells.
  Wagner S, Grin I, Malmsheimer S, **Singh N**, Torres-Vargas CE, Westerhausen S.
  FEMS Microbiol Lett. 2018 Oct 1;365(19):fny201. doi: 10.1093/femsle/fny201.

- **Publication 6 (Research Article in preparation)**

  Interaction of SctD with SctK in *Salmonella enterica* type III secretion system.
  Singh N, Kronenberger T, Ulrich S, Grin I, Wagner S.

Declaration of personal contribution to the publications

Publication 1: Conserved salt bridges facilitate assembly of the helical core export apparatus of a *Salmonella enterica* type III secretion system.

I contributed to the design and execution of the experiments. I performed and analysed all experiments with the exception of the MD simulation, mass spectrometric analysis and size exclusion chromatography. I wrote the paper together with Prof. Samuel Wagner.

Publication 2: Investigating the assembly of the bacterial type III secretion system injectisome by in vivo photocrosslinking.

I participated in writing this review article with Prof. Samuel Wagner.

Publication 3: Yeast can express and assemble bacterial secretins in the mitochondrial outer membrane.
I created the InvG (SctC) strains used in this study, performed crude membrane preparation for analysis and contributed to the methodology section of this research article.

Publication 4: Assembly and targeting of secretins in the bacterial outer membrane.
I did VMD modelling of InvG (SctC) protein from type II and type III secretion systems and contributed with Figure 1 in this review article.

Publication 5: Bacterial type III secretion systems: a complex device for the delivery of bacterial effector proteins into eukaryotic host cells.

I participated in writing this review article with all the other authors.

Publication 6: Interaction of SctD with SctK in *Salmonella enterica* type III secretion system (in preparation).

I contributed to the design and execution of the experiments and established the methodology used for the experiments. I performed all the experiments with the exception of structure modelling and few additional crosslinking experiments. I wrote the first draft of this paper. This version of paper is liable to changes as per requirement during the publication procedure.

Parts of this introduction section have already been published in:

- Investigating the assembly of the bacterial type III secretion system injectisome by *in vivo* photocrosslinking

  Nidhi Singh, Samuel Wagner.

- Conserved salt bridges facilitate assembly of the helical core export apparatus of a *Salmonella enterica* type III secretion system

  Nidhi Singh, Thales Kronenberger, Andrea Eipper, Felix Weichel, Mirita Franz, Boris Macek, Samuel Wagner (revision submitted).

1. Introduction

Bacteria are microscopic single-celled organisms that can thrive in almost every environment on Earth [1]. They are found in enormous numbers in a variety of extreme environmental conditions such as hot sulfur springs, high pressure, or freezing temperatures. The diversity of their habitats or niches ranges from deep-sea vents to the human skin and gastrointestinal systems. Such environments set forth many challenges to the survival of bacteria. Hence, bacteria have evolved unique features, including a cell envelope, to withstand environmental stresses [2,3]. The bacterial cell envelope protects from unfavorable circumstances. It is involved in maintaining membrane integrity, communication with the environment, nutrient uptake, and the use of ion gradients as an energy source, which are all critical for bacterial survival [4]. The ability to adapt to extreme conditions makes bacteria remarkably successful pathogens. Poor sanitation and contamination of food and water sources give rise to multiple debilitating diseases such as salmonellosis caused by *Salmonella* species [5–7]. *Salmonellae* are rod-shaped, Gram-negative, facultative, non-spore-forming intracellular bacteria that belong to *the Enterobacteriaceae* family [7,8]. The family comprises two *Salmonella* species, namely *Salmonella bongori* and *Salmonella enterica [9,10]*. The model organism of this thesis is *Salmonella enterica* subsp. *enterica* serotype Typhimurium, which will be referred to throughout as *Salmonella*.

Every year, on average, approximately 1.3 billion cases of gastroenteritis and 16 million cases of typhoid fever are reported worldwide, which ultimately cost about 3 million lives every year [11]. The looming issue of antibiotic resistance in bacteria and their impending threat to the human population need redressal through an extensive investigation of bacterial infection mechanisms, followed by developing alternative anti-infective strategies.

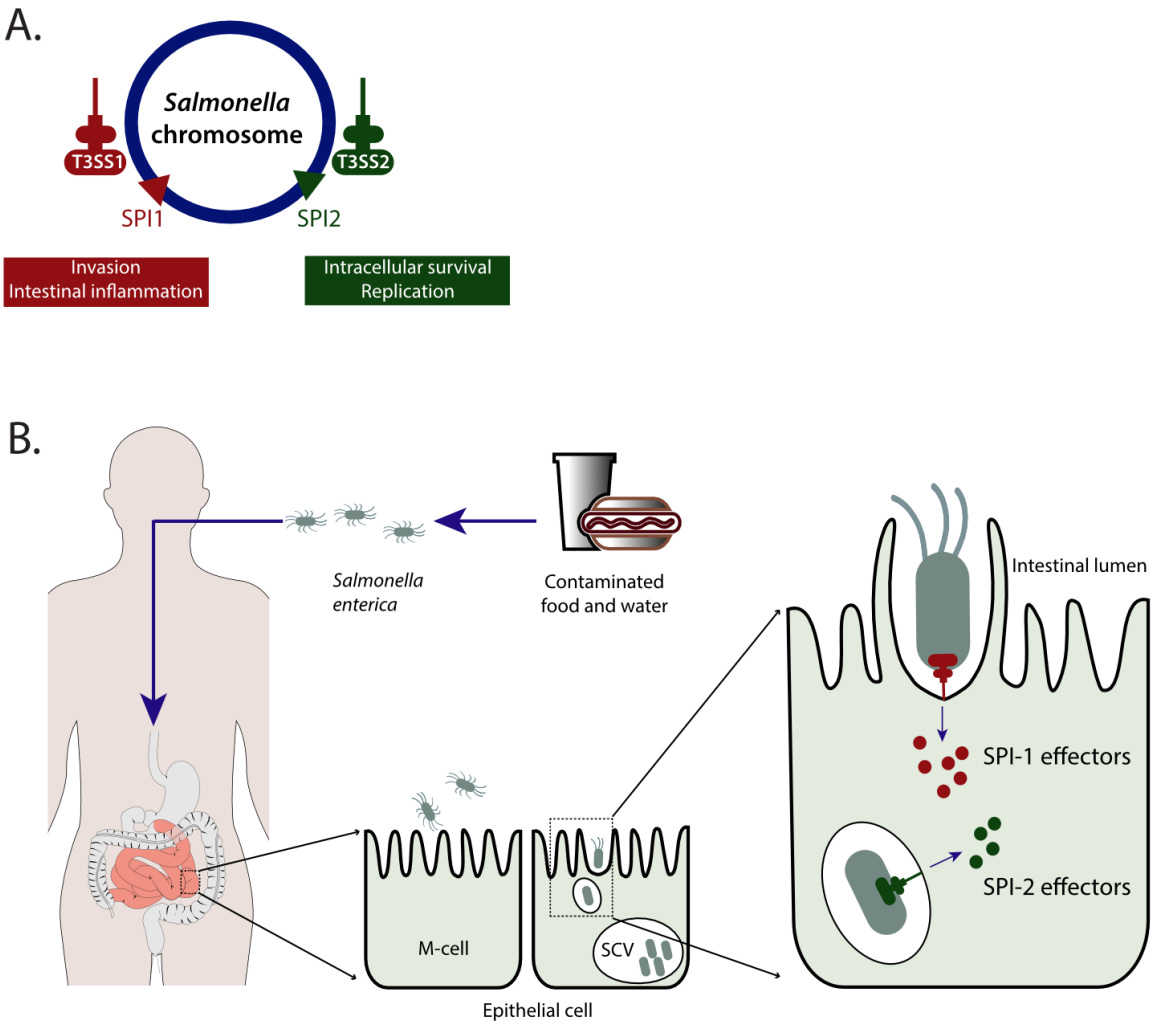

Figure 1: Pathogenicity and invasion model of *Salmonella* Typhimurium

A. T3SS is the molecular secretion machinery responsible for the infection process and is encoded on two separate pathogenicity islands, SPI-1 and SPI-2. Once host cell contact is established, invasion of *Salmonella* gets triggered by SPI-1 effector proteins. Thereafter, for manifestation of a systemic infection, SPI-2 effector proteins get secreted across the vacuolar membrane. SPI-2 effector proteins facilitate intracellular replication and survival of the bacteria. **B.** Exposure to contaminated food or water leads to ingestion of *Salmonella*. After reaching the small intestine *Salmonella* promotes its intrusion into the non-phagocytic enterocytes (preferentially specialized M-cells) with the help of T3SS1 effectors. Bacterial adherence to the host epithelial M-cells is mediated by fimbrial adhesins, and subsequently results in endocytosis. A phagosomal compartment called SCV is formed. Bacteria can survive and propagate intracellularly in this compartment with the help of another set of T3SS2 effectors. **Modified from** [6]. **Abbreviations:** T3SS, Type III secretion system; SPI, *Salmonella* pathogenicity island; SCV, *Salmonella* containing vacuole; M cells, microfold cells.

1.1 Pathogenicity and Invasion of *Salmonella*

Once *Salmonella* enters the digestive tract, a relatively small number of bacteria successfully survive the acidic pH of the stomach and reach the distal small intestine because of the expression of virulence genes which enable the bacterium to withstand the low pH environment [12,13]. *Salmonella* then colonizes the gastrointestinal tract by preferentially adhering to the specialized epithelial cells that superimpose the gut-associated lymphoid tissues via fimbrial adhesions [14] and thereafter penetrates and destroys the specialized epithelial microfold cells (M cells) of Peyer's patches via phagocytosis [15]. An alternative pathway for its' entry is by an invasion of non-phagocytic enterocytes [16]. The pathogenicity of *Salmonella* depends on virulence-associated molecular secretion machinery known as the type III secretion system (T3SS). T3SS is crucial for pathogenesis in several enteropathogens, namely *Salmonella* Typhimurium [17].

The specific stage of infection determines the expression of either of the two distinct virulence-associated T3SSs (T3SS1 and T3SS2), which are genetically expressed at two distinct loci encoding *Salmonella* pathogenicity island 1 (SPI-1) and 2 (SPI-2) [18,19] (Fig.1). Both pathogenicity islands were acquired by horizontal gene transfer and contribute to the pathogenic abilities. *Salmonella* employs both of these systems for invasion, replication, and survival within the host cells [6]. On the one hand, the host cell contact followed by invasion is activated by the SPI-1, while on the other hand, SPI-2 elicits intracellular survival and propagation (Fig. 1). SPI-1 encoded virulence effector proteins get secreted into the host cell cytoplasm through T3SS1. The microaerophilic environment of the distal small intestine, the neutral pH, high osmolarity together lead to the induction of SPI-1 expression [15,19,20]. The effector proteins prompt actin rearrangements, membrane ruffling, and invagination of the host cell's cytoskeleton, thereby commencing the engulfment of *Salmonella [18]*. *Salmonella* inhabits and replicates in a phagosomal compartment called *Salmonella* containing vacuole (SCV) [21]. The altered environmental conditions inside the SCV, such as low Mg2+ or Ca2+ concentrations and phosphate starvation compared to that of the intestinal lumen, trigger radical changes in the gene expression profile of SPI-2 in *Salmonella*. The switch from T3SS1- to T3SS2-dependent secretion of effectors is vital for ensuring intracellular survival and replication of bacteria as well as evasion of the immune system inside the macrophages, contributing to an escalation of systemic infection [18,22–25]. Interaction and synergy amongst distinct regulatory elements of both secretion systems enable a well-regulated and secured transition from T3SS1 mediated invasive state to T3SS2 mediated intracellular survival state

[26]. The T3SS2 effector proteins are also responsible for stimulating bacterial migration into the neighboring epithelial cells [27].

1.2 Secretion systems

Bacteria evolved several secretion systems to influence their surroundings, invade host cells, compete with the other microbes for their survival, and deliver specific molecules to their desired location [28].

Export of diverse proteins such as adhesion factors, toxins, effector proteins, proteases, or transcription factors, is the key to facilitate the interaction of bacteria with their surroundings. Protein export mainly occurs with the help of Sec and Tat translocons which translocate unfolded and folded substrate proteins, respectively, across the cytoplasmic membrane [28,29].

Given that Gram-positive bacteria possess only one membrane, protein export across the cell envelope is relatively simple. Conversely, the Gram-negative bacteria require extended and sophisticated mechanisms for protein export across the two membranes of their cell envelope. Simpler mechanisms utilized by bacterial exotoxins could not cater to the much-complicated feat of delivering bacterially encoded effector proteins into the host cells. Hence, evolutionary forces compelled and eventually led to the emergence of distinct complex machinery to deliver an array of diverse bacterial proteins into the target cells. Nine different protein secretion systems (type I to type IX) have been identified to date. Their classification is based on the characteristic buildup of their secretion machinery, secretion signal, source of energy for secretion (ATP vs. PMF, or both), substrate status (unfolded vs. folded), and the number of steps involved in the secretion process (one step vs. two steps) across the two membranes of their cell envelope into the extracellular space or the target cells [30].

Three secretion systems (type III, type IV, and type VI) amongst the given nine systems are capable of delivering bacterially encoded effector proteins directly into the cytosol of the target cells (Fig. 2A) [31]. Secretion systems are coming forth as prime targets for advancing prevention strategies and novel therapies targeting different pathogens because of their central role in bacterial pathogenesis [32,33].

Furthermore, these machines also reveal themselves as highly beneficial tools for discerning the fundamental questions related to protein transport across membranes, signal transduction, and organelle assembly [31]. Large protein complexes of typically 100 subunits or beyond constitute the protein injection machines, and therefore, the size of these whole entities ends

up in several megadaltons. Usually, secretion systems broadly consist of cytosolic, inner membrane, periplasmic, outer membrane, and extracellular components that span across the cell envelope's membranes. The biogenesis and assembly of these machines is a multi-step regulated sophisticated task that demands meticulous orchestration.

1.3 Virulence associated type III secretion system: structure and function

Virulence-associated T3SSs are highly conserved, complex membrane-localized molecular nanomachines. Many pathogenic or symbiotic Gram-negative bacteria utilize this machinery to inject effector proteins into the eukaryotic host cells to promote their survival and colonization [34]. T3SS is the focal point of this thesis. T3SS traverses multiple membranes of Gram-negative bacteria to deliver semi-folded proteins into the target host cells in a one-step secretion process (Fig. 2B) [35]. Since the core function of such nanomachines is the efficient delivery of effector proteins, T3SS is also termed as injectisomes. Injectisomes or virulence-associated T3SSs are evolutionary derivatives of bacterial flagellar systems that contain a flagella-associated T3SS (fT3SS) as their core component [36]. fT3SS exports structural components of the flagellar filament for self-assembly of bacterial flagella, thereby facilitating bacterial movement [37]. Nonetheless, injectisomes are substantially advanced and capable of secreting a wide range of substrate proteins [38]. Furthermore, their perception of host-cell contact, their ability to interact with the host cells and inject substrate proteins via the translocation pore into the host cell also gives insight into their evolutionary progression [39,40].

Injectisomes consist of approximately 20 different proteins with an extensive spectrum of copy numbers ranging from 1 to more than 100 (Fig. 2B) [41]. Electron microscopy of *S.* Typhimurium gave first visualizations in 1998 [42]. Further advancements in cryo-electron microscopy (cryo-EM) particularly assisted in resolving the structural components of T3SSs at a much higher resolution [43].

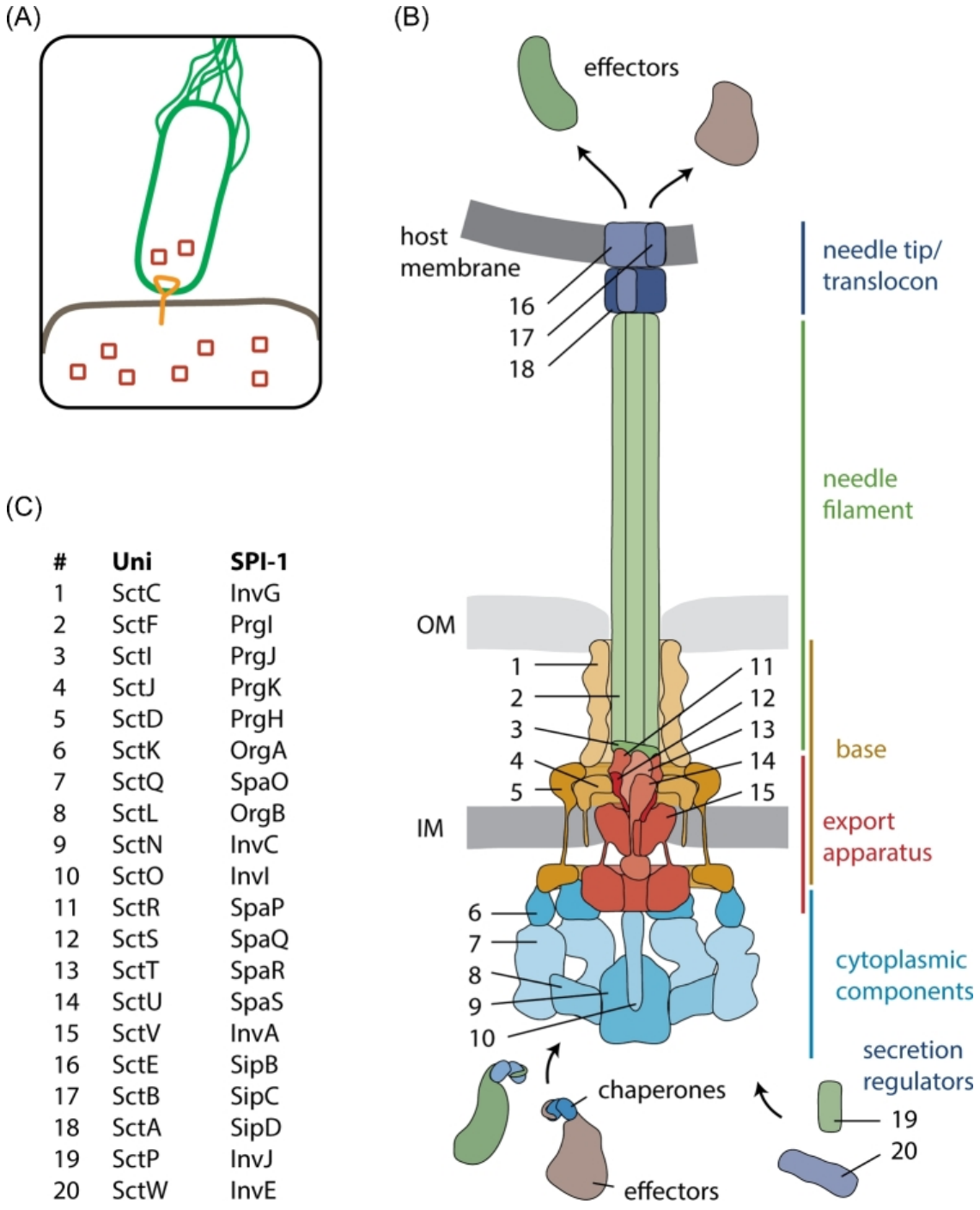

(C)

#	Uni	SPI-1
1	SctC	InvG
2	SctF	PrgI
3	SctI	PrgJ
4	SctJ	PrgK
5	SctD	PrgH
6	SctK	OrgA
7	SctQ	SpaO
8	SctL	OrgB
9	SctN	InvC
10	SctO	InvI
11	SctR	SpaP
12	SctS	SpaQ
13	SctT	SpaR
14	SctU	SpaS
15	SctV	InvA
16	SctE	SipB
17	SctB	SipC
18	SctA	SipD
19	SctP	InvJ
20	SctW	InvE

Figure 2: Molecular structure and function of T3SS injectisome.

A. T3SS serves as a tool for the injection of bacterial effector proteins into the eukaryotic host cells. **B.** Structure of the T3SS. Different subunits, namely cytoplasmic components, base, export apparatus, needle filament, and translocon, constitute the T3SS. All of the structural units are color-coded, and each component is labeled and designated with its protein name in **C.** according to the unified nomenclature of T3SS components (Uni, left column) [44], as well as to the nomenclature of T3SS encoded by *Salmonella* pathogenicity island 1 (SPI-1, right column). **Adapted from** [45]**. Abbreviations:** Sct, secretion and cellular translocation; IM, inner membrane; OM, outer membrane.

Both plant Gram-negative bacteria such as *Pseudomonas syringae* or *Xanthomonas* etc., and human pathogens such as enteropathogenic *Escherichia coli* (EPEC), *Salmonella*, Chlamydia, *Shigella,* and *Yersinia* etc., employ T3SS in order to modulate their host cell by influencing a variety of cellular functions. [34]. Determination and recognition of each effector protein's biochemical activities and enhanced understanding of their prospective contribution to pathogenesis have exposed common themes in these significant bacterial proteins' evolutionary scheme and function [46]. The repository of the injected effector proteins is remarkably structurally diversified to cater to various cellular functions: avoidance of phagocytosis (e.g., *Yersinia*), elimination of macrophages (e.g., *Salmonella*), impinging immune responses (e.g., *Salmonella*, *Yersinia*, and *Xanthomonas*) or procurement of nutrients (e.g., *Chlamydia* and *Salmonella*) [46].

Henceforth, in this thesis, I will be using the unified nomenclature of T3SS components, as already mentioned in Fig. 2C [44,47].

1.3.1 Base

The injectisome is firmly embedded in the bacterial cell envelope by virtue of a basal body composed of three distinct proteins SctC, SctD, and SctJ. The injectisome base incorporates 15.5 SctC subunits, which together construct the outer membrane secretin complex (OR) [48,49] along with 24 subunits each of SctD and SctJ that form the inner membrane concentric rings (IR) [50,51]. These secretins are similar to the ones present in type II secretion systems [51–53].

Primarily, the secretin structure encompasses N-domains, a C-domain, and S-domains [54]. The N-terminus of secretins contain three N-domains (N0, N1, and N3) which protrude deeply into the periplasm, forming a neck that connects the secretins with the inner membrane concentric rings [55]. The outer membrane portal is formed by a unique double-layered β-barrelled C-domain [51]. A concave membrane association domain is established by its outer β-barrel that extends itself towards the outer membrane. Simultaneously, the inner β-barrel reaches out into the lumen leading to the formation of a gate that separates the periplasmic space from the outside [51]. A cognate pilotin binds to the S-domain (site of interaction for cognate chaperones) of the secretin and conducts its targeting and assembly. Pilotins are outer-membrane targeted small lipoproteins involved in assembly, localization, and outer-membrane insertion of secretins [56].

Once the assembly of the needle filament commences, the continued polymerization of needle filament pushes the closed gate conformation formed by the SctC subunits in the outer membrane to open up [51,54]. The elementary sites of these conformational changes belong to the conserved core secretin region, mainly the N3 ring domain, inner β-barrel, and the membrane associating lip of the core secretin domain. Reorientation and conformational changes in all these sites pave the path for lodging the needle filament. The most pronounced conformational change occurs in the inner β-barrel upon needle assembly [51,54].

The N0 domain of SctC connects SctD [55]. N0 and N1 domains form the structural motifs found in SctD as well as SctJ. SctD consists of a single transmembrane segment (TMS), a small N-terminal forkhead associated (FHA) domain in the cytoplasm, and a periplasmic domain comprising of two ring-building motifs which interact with SctJ and also with the N-terminus of SctC [57]. The term 'ring-building motifs' for the base components SctD and SctJ is associated with their potential role in the execution of concentric ring formation [57]. Two ring-building motifs collectively structure the periplasmic domain of SctJ, which has an N-terminal lipid anchor and usually a C-terminal TMS [58]. Twenty-four SctD subunits and 24 SctJ subunits form the two concentric rings so that SctD is on the outer periphery enclosing the SctJ ring. Considering its orientation, SctD was also named as the outer inner ring protein and SctJ as the inner ring protein [50].

1.3.2 Cytoplasmic components

Five proteins SctK, SctQ, SctL, SctN, and SctO are the cytoplasmic components of the T3SS (Fig. 2B) [59]. They exist both in an injectisome-bound form as well as free soluble cytoplasmic complexes [60,61]. SctK, SctQ, and SctL together construct the sorting platform. As the name suggests, the sorting platform recruits chaperone-bound substrate complexes and arranges them per the hierarchical state of secretion [59].

Injectisome-bound SctK and SctQ organize themselves into six pod configurations which directly bind via single SctK to the cytoplasmic domains of four SctD subunits each [62,63]. These pods are linked to a homodimer of SctL, which couples them to the hexameric ATPase SctN. SctN is believed to be responsible for the recognition and stripping of the chaperones and unfolding the T3SS substrates [63–65]. A single copy of SctO is situated at the center of the hexameric ATPase SctN and extends towards the major export apparatus protein SctV [63,66]. *SctQ,* due to the presence of an internal start codon*,* gets translated into two polypeptides of varying lengths ($SctQ_{FL}$ and $SctQ_C$), and both polypeptides are vital for the assembly of the injectisome and T3SS function [67–73]. Nonetheless, $SctQ_C$ might not be a

structural component of the pods [69]. The stoichiometric estimations provided by fluorescence microscopy [60,61] along with the structural investigations of the SctQ complexes indicate that 24 $SctQ_{FL}$ (4 $SctQ_{FL}$ per pod), including 48 $SctQ_C$ (8 $SctQ_C$ per pod), are associated with each injectisome [67,70,74,75].

1.3.3 Export apparatus

The export apparatus is one of the most important building blocks of the T3SS consisting of five hydrophobic proteins SctR, SctS, SctT, SctU, and SctV (Fig. 2B) [76]. These proteins, which are highly conserved in both injectisomes and flagellar T3SS (fT3SS) [77], are essential for secretion [78]. Also, the assembly of the injectisome begins with the formation of the export apparatus [77,79]. A distinctive helical assembly is established on the periplasmic side of the inner membrane with the help of one SctU, one SctT, four SctS, and five SctR subunits enclosed within the SctJ rings of the needle base [41,80–83]. The predicted transmembrane hairpins of SctR, SctS, and SctT constitute one helix-forming module of $SctR_5S_4T_1U_1$ complex, of which SctR contributes two of these modules, SctS one, and SctT three to the helical complex. SctT results from the structural integration of SctR and SctS. This fusion compensates for the helical rise between the first and the fifth SctR and maintains the assembled structure [43,80]. SctU shuts the helical complex by contributing two extra helix-forming modules in an alternative topology by allocating its soluble C-terminal domain in the cytoplasm [83].

The export apparatus constituents are classified into two distinct groups: major and minor export apparatus. The denotation' major export apparatus' is derived from the fact that the two components: SctU and SctV, are prominently oversized compared to all other components. In addition to their transmembrane segments, both of these components consist of large cytoplasmic domains and exert distinctive functions in the system [78,84]. The structures of these cytoplasmic domains exist for both SctU and MixA (SctV homolog) in *Shigella [85,86]*.

SctU portrays a significant role in substrate specificity switching [87]. Implying that SctU is engaged in transferring T3SS secreted sets of early substrates to intermediate substrates, hence it is titled as 'switch protein' [88–91]. Both SctU and SctV possess a sizable cytoplasmic domain consisting of four and two predicted TMS, respectively [79]. The cytoplasmic domain of SctU and other homologous T3SS switch proteins harbor an NPTH motif, after which the protein is capable of autocatalytically cleaving itself [85,89]. Therefore, besides contributing its predicted TMS to the helical assembly, the cytoplasmic C-terminal domain encounters autocleavage at a conserved NPTH motif [85,92–95]. Although exhaustive crosslinking

analysis could identify protein-protein interactions amidst the predicted TMDs of SctU and SctR while positioning SctU in the center [80], still specific placement of SctU within the complex has recently been possible where the cryo-electron microscopic structure of the export gate from a *Vibrio* flagellar system revealed that the switch protein SctU is wrapped around the SctRST complex by its four predicted transmembrane helices [83].

Mutants become incompetent in switching the early substrates to intermediate substrates secretion when they are unable to autocleave. Nevertheless, this auto-cleavage is plausibly not the switch signal as such but is instead responsible for securing SctU into such a conformation that allows it to exercise its switch function [91]. The crystal structure of SctV homolog MxiA disclosed that its cytoplasmic domain configures a nonameric ring [86]. A prospective role in substrate recognition of the SctV homologs *Xanthomonas* HrcV and FlhA in the fT3SS was suggested based on their interaction with the effector proteins and their chaperones [96–98]. SctV is seated centrally inside the inner membrane part of the needle base (Fig. 2B) [86]. The N-terminal half of SctV forms a transmembrane domain (TMD) with eight predicted TMS. A TMD, along with a sizable conserved loop in between, most likely forms the entrance of the translocation channel inside the inner membrane [99,100]. The C-terminal half lies exposed to the cytoplasm, and its four subdomains assemble into a nonameric ring with a central pore of 50 Å in width [86]. $SctV_C$ establishes the hierarchy of substrate secretion by binding secretion adaptor proteins of early and intermediate substrates [101–105] in addition to the substrate-chaperone complexes [106]. The inner membrane proton gradient gets exploited by N-terminal TMDs of SctV for secretion [100].

The minor export apparatus proteins SctR, SctS, and SctT contain four, two, and six predicted transmembrane segments (TMS), respectively [79]. Notably, recent updates provided by cryo-electron microscopic analysis of the structure of SctRST complex from flagellar homologs disclosed that these proteins are supramembraneously positioned and barely make any membrane contact in the final assembled injectisome. Instead, they are gripped within the SctJ ring above the membrane in a periplasmic position [43].

Dietsche et al. suggested that the assembled SctRST complex form a translocation pore (Fig. 2B) with an inner diameter of 15 Å seated within the inner membrane [80]. The complex displays three gates in the pre-secretion state: highly conserved Gln and Met line mouth of the pore, the pore entrance closes from inside via a loop from SctT, and the pore's exit portal gets constricted by the N-termini of both SctR and SctT [43]. The very distal end of the assembled SctRST complex gets in close proximity with the inner rod after the assembly of the helical filament leading to the stabilization of the pore in an open conformation [80].

The entire export apparatus is indispensable for a functionally competent T3SS [107]. Nevertheless, many specific details related to the precise structure and function, especially of the minor export apparatus components SctR, SctS, and SctT, are still unknown. A comprehensive study, characterization, and investigation of this substructure will undoubtedly help us understand the secretion mechanisms of this highly complex machinery. Hence, this became one of the primary objectives of my thesis.

1.3.4 Filament, needle tip, and translocon

After the successive assembly of the export apparatus, the base, and the cytoplasmic components, the system becomes secretion competent. Various T3SS secreted proteins, except the cytoplasmic and membrane-associated components, associate as structural elements of the assembled injectisome. The extracellular needle filament protein SctF provides the highest number of subunits to the system [108]. SctF organizes into a helical hairpin configuration, with a poorly conserved and disorganized N-terminus facing outwards, a conserved loop, and a C-terminus facing inwards [109–111].

The helical needle filament in *Salmonella* is roughly composed of about 120 copies of SctF [112], which polymerize and assemble into a right-handed helical conduit having an approximate needle length of 35 nm [91,108,109,113].

The needle filament is firmly connected to the distal end of the SctRSTU complex within the base via six copies of the inner rod protein SctI, which serves as an adaptor protein (Fig.2B) [41,43,80,113,114]. This firm association of the export apparatus and the base is ensured because of the identical helical rise of the SctRST complex and the needle filament (4.0 and 4.3 Å per subunit, respectively) and subunit counts involved per turn (5.7 and 5.6, respectively) [43]. On the one hand, the SctRST complex's termini faces outwards, and on the other hand, the needle filament protein (SctF) termini faces inwards. This orientation gives a plausible explanation why the adaptor protein SctI is critical for a compact association of the export apparatus and needle filament.

The inner cavity of the needle with a radial diameter of 15 Å is coated with highly conserved polar and hydrophobic residues with alternative positive and negatively charged sections. This grants passage of only unfolded substrates across this channel [54,109].

The hydrophilic translocator protein SctA forms the pentameric needle tip complex at the end of the needle of the majority of the injectisomes. SctA serves as a scaffold for the hydrophobic translocon complex [112,115,116].

Previous studies revealed that a hetero-complex of defined stoichiometry is formed by multiple copies of two different translocator proteins, namely SctE and SctB, in the host membrane, and this very complex is the prerequisite for translocon formation [40,117–121]. The complex seems to be big enough to house multiple copies of the SctE-SctB complex and penetrate the host cell membrane by setting up a protein channel [40]. These proteins putatively have 1–2 TMS, which get inserted into the host cell membrane with the assistance of the tip complex during bacterial infections. Hence, the establishment of the translocon is coordinated by the tip complex of the injectisome [122]. Although the constituents of the translocon get effectively secreted in the absence of the tip protein SctA, they eventually are incompetent in constructing the translocon [123,124].

1.3.5 Hierarchy of the secreted components

An explicit aspect of the T3SS is ordered hierarchical export of proteins wherein proteins destined for establishing the needle complex filament and the associated structures are secreted in the first place. Subsequently, the secretion of effector proteins that promote their translocation across the channel to the target host cell occurs. The order of secretion of different substrates in injectisomes determines a three-level hierarchical system. The term ‘early substrates’ in most T3SSs is assigned to four different substrates: the needle filament proteins SctF, the inner rod protein SctI, the non-structural needle length control protein SctP, and OrgC in *Salmonella* functioning in conjunction with SctF in order to achieve efficient needle assembly [125–127]. This designation is self-explanatory because these substrates are secreted at first once the assembly of the secretion competent system concludes. Commencement of secretion elicits a conformational change in the outer membrane secretin protein SctC, and its closed gate conformation opens up upon assembly of the needle filament by radially projecting the hairpin structure formed by two β-sheets of each SctC subunit constituting the periplasmic gate [43,51,54]. This substrate-induced gate opening of the secretin pore does not occur if the polymerizing needle filament proteins are absent [51]. Accumulation of the secreted proteins in the periplasm in the absence of needle filament proteins strengthens the above proposition [101].

The needle length control protein SctP estimates the length of polymerizing needle filament in a ruler-like fashion and, along with the switch protein SctU, induces the switch of early substrates to intermediate substrate secretion [128]. Assembly of the hydrophilic tip protein SctA with two other hydrophobic translocator proteins SctE and SctB, occurs at the top of the needle [129]. SctE, SctB, and SctA are the intermediated secretion substrates and still serve

as the structural components of perfectly assembled and functionally competent T3SS. As mentioned before, SctA, together with the other two proteins, constitutes the translocation pore complex in the host cell membrane [118,130]. Consequently, a continuous channel is created that bridges the *Salmonella* cytoplasm to the host cell cytoplasm.

Furthermore, a second switch step of substrate specificity switching comes into action where the switch from intermediate effectors to late effector protein secretion occurs. This involves the cytoplasmic gatekeeper protein SctW. The late effector proteins act in different ways in the target host cell [131–133].

1.3.6 Substrate specificity switching

SctU is named the 'switch protein' because of its distinct role in switching of early substrate secretion to intermediate substrate secretion, which depends on the autocleavage of its cytoplasmic domain resulting in two polypeptides [89,90,134].

Inhibition of the autocleavage of SctU helps implement needle-length control and substrate specificity switching as two independent processes instead of one [91,135,136]. With hindered autocleavage of SctU, mutants can regulate the needle length but have no command over the switching of early substrate secretion to intermediate substrate secretion owing to the differences in their signal sequence. Insertion of a late effector signal sequence into the needle tip protein revives the secretion and assembly function at the needle tip [91]. Therefore, cleavage of the switch protein cannot be the regulatory signal administering substrate switching. Control of the needle length in relation to its further elongation or stoppage was neither accomplished by the assembly of the needle tip nor by switching to intermediate substrate secretion, eventually leading to diminished early substrate secretion [91,135]. For this reason, needle length control seems to involve either undesignated mechanisms responsible for active termination of further early substrates secretion or conformational rearrangements of the needle filament proteins impeding its further assembly.

Autocleavage of the switch protein SctU is an unrestrained process that takes place after its folding and before its internalization into the needle complex. Also, its cleavage is obligatory for acquiring an adaptable conformation in accordance with its secretion activity [91].

Overall, substrate specificity switching not only triggers the secretion of needle tip proteins along with their consequential assembly at the needle filament's distal proximity but also allocates hydrophobic translocators to the sorting platform of the needle complex and aids in their premature secretion as well [59]. At this juncture, the injectisome is completely

assembled and is completely prepared for target host-cell interaction, i.e., host-cell contact, formation of translocon pore, and injection of the effector proteins.

1.3.7 Host cell interaction: sensing and injection

Host cell sensing by the tip of the needle complex instigates secretion across the injectisome *in vivo*. The signals responsible for switching to late effector protein secretion in this sensing mechanism are relayed to the cytoplasmic end of the injections. The gatekeeper protein SctW is the most crucial T3SS component that is indispensable for the activation of secretion of late substrate effector proteins. Removal of the gatekeeper protein results in discontinuation of the secretion of translocators and hypersecretion of the late effectors [131,137,138]. Chemical signals (such as congo red, calcium chelation, etc.) can also imitate host cell sensing situations in T3SS of some bacteria [139–141].

The SctV-SctW communication contributes to the administration and control of the secretion process by delivering a committed binding site for translocator-chaperone complexes and blocking the binding site for late effectors [102]. SctW gets released from SctV once a host cell connection is established in order to enable late substrate secretion. Unbound and free SctW is eliminated from the injectisome either by secretion or by degradation [102,138,142,143]. Hydrophobic translocators insert inside the host cell membrane after sensing the host cell and form multimeric pores accountable for the disposition of the substrates into the host cell cytoplasm [121]. The genesis of the translocation pore concludes the pathway spanning from the bacterial cytoplasm until the host cell cytoplasm for effector protein injection [144].

1.4 Type III secretion-independent assembly of the injectisome

Appropriate and precise assembly of individual components in an extremely synchronized manner is the prerequisite for needle complex assembly because of a multitude of substructures involved in the process. This highly coordinated orchestration ensures a complete functionally competent nanomachine.

The injectisome assembly occurs in two phases:

(1) Assembly of the principle secretion competent machine depending on Sec-mediated translocation along with membrane insertion of the involved components.

(2) Assembly of needle filament, needle tip and translocon by type III secretion-dependent process.

Detention of both the inner as well as outer membrane-inserted parts in a two-dimensional space and perforation of the peptidoglycan layer are the two basic factors that restrict the assembly of the principle secretion competent machinery. The earliest components initially are inserted into the membrane by a Sec-dependent pathway followed by Sec-independent pathway of assembly once the machinery develops secretion competence. Hence, Diepold et al. recommended a bipolar assembly model for the assembly of the injectisome [78], asserting the dependence of base assembly on:

(1) Nucleation of the assembly by the export apparatus components that provide secretion competence to the machinery (Fig. 3A).

(2) Secretin formation that assures outer membrane translocation (Fig. 3B).

The three minor export apparatus components SctR, SctS and SctT nucleate the assembly in the inner membrane, as shown for SPI-1 encoded T3SS [77]. All of the inner membrane associated T3SS components get inserted into the membrane via a Sec-dependent pathway [107]. SctR assembles into multimers independently and employment of SctT stabilizes its association [80]. Detection of SctS-SctT interactions exclusively in the presence of SctR advocates the notion that the assembly of the export apparatus nucleates with SctR and proceeds further by assignment of SctT and SctS [80]. Additionally, structural informations from the the helical complex of the flagellar SctRST homolog FliPQR as well as other structures of an equivalent complex from Shigella virulence systems indicated that five SctR multimers initiate the assembly followed by subsequent employment of one SctT and four SctS subunits [43,81]. Nonetheless, at this point, it cannot be excluded that SctRS heterodimers with the subsequent addition of SctT result in the assembly of the SctRST complex.

Intramolecular salt bridge formations in the predicted TMS mediate the assembly of SctR and stabilize the staggered conformation of the protein [43]. Similarly, assembly of SctS upon the SctRT subcomplex is promoted by the formation of intermolecular salt bridges. The incremental stepwise winding of the SctRST complex whilst assembling raises the complex above the inner membrane towards the periplasm. This helical assembly is supported by strong hydrophobic interactions amongst the predicted TMS of the core export apparatus proteins SctR, SctS, and SctT [43]. Nevertheless, many attributes and further details still remain elusive. Before the recruitment of SctV, the switch protein SctU congregates the

SctRST complex [80]. In some T3SS, SctV is essential for the needle base assembly [145], while for others, it seems completely dispensable [77]. SctV ring formation surrounding the assembled SctRSTU complex possibly drives the upliftment of the helical SctRST complex from the inner membrane and thereby assists the interaction with SctJ and its multimerization into a 24-mer SctJ ring (Fig. 3A).

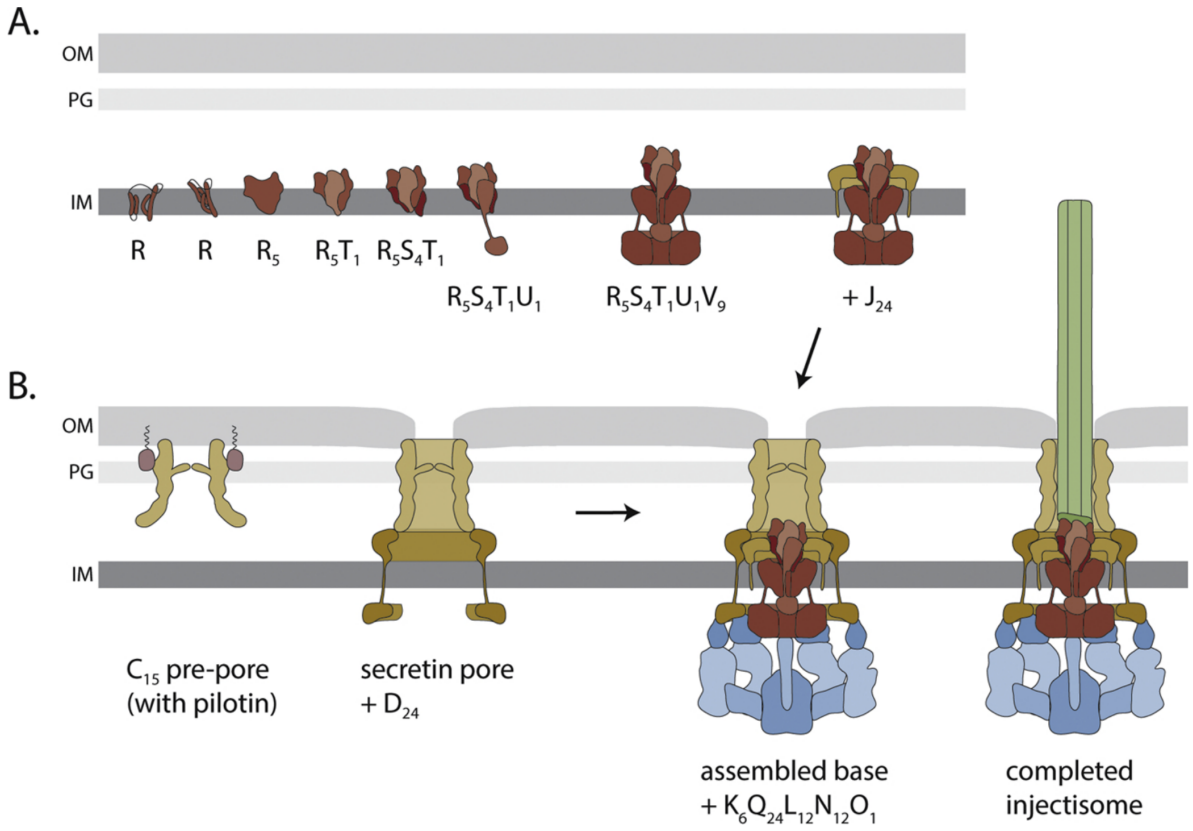

Figure 3: Assembly of the T3SS injectisome

Protein names are represented by their last letter, excluding "Sct". The assembly pathways are in sequence from left to right. **A.** Assembly of the injectisome begins with the formation of export apparatus at the inner membrane with membrane-integrated SctR. SctR (also SctS and SctT, not shown) folds into such conformation which permits helical assembly. Thereafter, five SctR, joined by one SctT and four SctS subunits assemble together into a helical complex winding up supra-membraneously. Integration of one SctU further with addition of nine SctV subunits culminates in assembled export apparatus, which is then encompassed by 24 subunits of the IR protein SctJ. **B.** 15 secretin monomers assemble together with the help of pilotins forming a pre-pore. Secretins form a pore in the OM and recruit the outer IR protein SctD. Closure of the outer IR is not enabled until the SctJ-export apparatus assembly gets incorporated. Employment of the cytoplasmic components and further assembly of the needle filament finishes the assembly of the injectisome. **Adapted from** [45]**. Abbreviations:** IM, inner membrane; OM, outer membrane; PG, peptidoglycan; IR, inner ring; Sct, secretion and cellular translocation

Secretins from type II secretion systems have been widely studied concerning their assembly and outer membrane targeting and have helped derive basic inferences and better understanding other secretion systems. In most cases, targeting and assembling secretins does not require any additional T3SS factors except the pilotins [107,145,146]. SctC is translocated across the inner membrane via a Sec-dependent pathway. Secretin subunits assemble independently at the outer membrane and form a pre-pore with the assistance of the pilotin protein, as reported in *Yersinia* [145]. Pilotins are small lipoproteins targeted to the outer membrane by the Lol pathway [147] and are essential for proper assembly of the secretin complex, localization of SctC subunits, and their insertion as well as anchoring in the outer membrane [148,149]. Pilotin binds to the S-domain of cognate secretins [150].

Interactions amongst adjoining N3 domains in addition to the interactions of S-domain with the C-domain of the neighboring subunit direct the formation of the pre-pore by facilitating the multimerization of the SctC subunits [51]. Peptidoglycan lytic enzymes expedite the pre-pore formation [151]. It is known that Bam machinery directs targeting of non-lipidated proteins to the outer membrane [152]. The insertion of the pre-pore into the outer membrane is a Bam independent process [152] and is supposed to develop by membrane affiliation of an amphipathic helical loop succeeded by insertion of the distal hydrophobic β-barrel lip region [51]. Upon the independent assembly of the secretin in the outer membrane, recruitment of the outer inner ring protein SctD occurs, leading to the further incorporation of the SctJ bound export apparatus complex [145] (Fig. 3B).

The cytoplasmic domain of SctD interacts with SctK, and this interaction aids in lodging the cytoplasmic components onto the assembling complex [63]. In *Yersinia*, the employment of the cytoplasmic components is reported to be dependent on SctK, SctQ, SctL, and SctN, whereas, in *Salmonella*, SctN is not crucial for the same. The cytoplasmic components integrate into a subcomplex even before lodging onto the injectisome [59–61]. Nevertheless, no such distinct injectisome-free subcomplexes of the cytoplasmic components could be designated. Instead, an adaptive and dynamic network of cytosolic interactions was found to be responsible for incorporating new components at any point in time [60]. Confirmations based on cryo-EM and fluorescence microscopy results revealed that interactions between SctO and the cytoplasmic domain of SctV were not accountable for docking cytoplasmic components onto the injectisome [61,63,101,145]. Assembly of the cytoplasmic components appears to bank nearly equally on all of its components except the stalk protein SctO. SctO seems less critical for injectisome assembly in *Yersinia*. In *Salmonella*, the assembly of SctK, SctQ, and SctL lead towards the subsequent integration of SctN and SctO [61]. After

successfully integrating the assembled base and the cytoplasmic components, the system acquires secretion competence.

1.4.1 A comprehensive overview of the two assembly models

Due to different starting points and numerous discrete steps of the assembly involved in the constitution of the needle complex, many conceptual disputes exist that remain uncovered. Moreover, the assembly might differ in various bacterial species. The complete assembly process pertaining to the integration of the inner and outer membrane subcomplex assemblies can be sorted into two different model systems: -

(1) Inside-out assembly model: Independent assembly of the secretin ring in the outer membrane followed by recruitment of the outer inner ring protein SctD leading to the final association of the SctJ bound export apparatus subcomplex [145] (Fig. 4).

(2) Outside-in assembly model: Assembly of secretins accelerated by clearance of the peptidoglycan overhead of the inner membrane assembly [153] (Fig. 5).

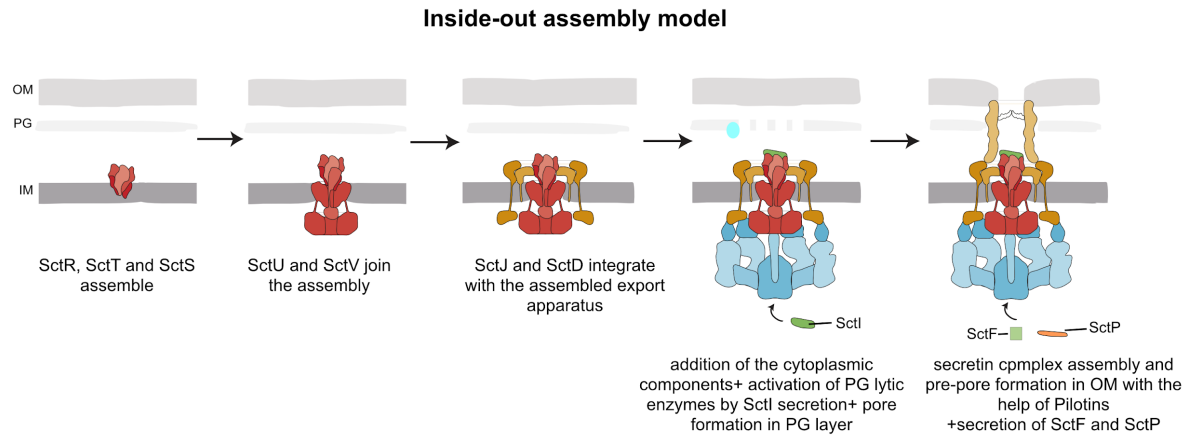

Figure 4: Inside-out assembly model

Assembly of T3SS commences by integrating export apparatus components SctR, SctT, and SctS at the inner membrane with subsequent integration of SctU and SctV. Further oligomerization of IR proteins SctD and SctJ encompasses the export apparatus. Thereafter, cytoplasmic components join the assembly process authorizing the secretion of SctI. The PG lytic enzyme gets activated by the secretion of SctI. Secretins then assemble into the secretin complex, and secretion of SctF and SctP begins. Polymerization of the needle leads to the opening of the periplasmic gate. (Modified from Westerhausen 2021). **Abbreviations:** T3SS, Type III secretion system; OM, outer membrane; PG, Peptidoglycan; IM, inner membrane; IR, inner ring; Sct, secretion and cellular translocation.

The inside-out assembly model suggests that the inner membrane is the primal nucleating site for the assembly of the export apparatus [77]. The assembled SctRSTU complex together with

SctV appoints the two inner membrane ring proteins SctD and SctJ. Subsequently, the cytoplasmic apparatus assembles with the needle base, thereby authorizing early substrate secretion [49,79]. Secretion of the early substrate SctI triggers the peptidoglycan lytic enzymes above the assembled inner membrane complex. Secretin subunits assemble into a pre-pore at the outer membrane [153], and eventually, it gets associated with the inner membrane components [51]. Polymerization of the needle filament culminates the assembly process of the injectisome. This assembly model is supported by various supportive observations [79], such as the augmented enzymatic activity of the lytic enzymes in the peptidoglycan, especially in the presence of SctI [153]. Also, an extensive interaction of SctD with SctJ compared to the nominal interaction of SctD with SctC evokes the affirmation for this model [51,153].

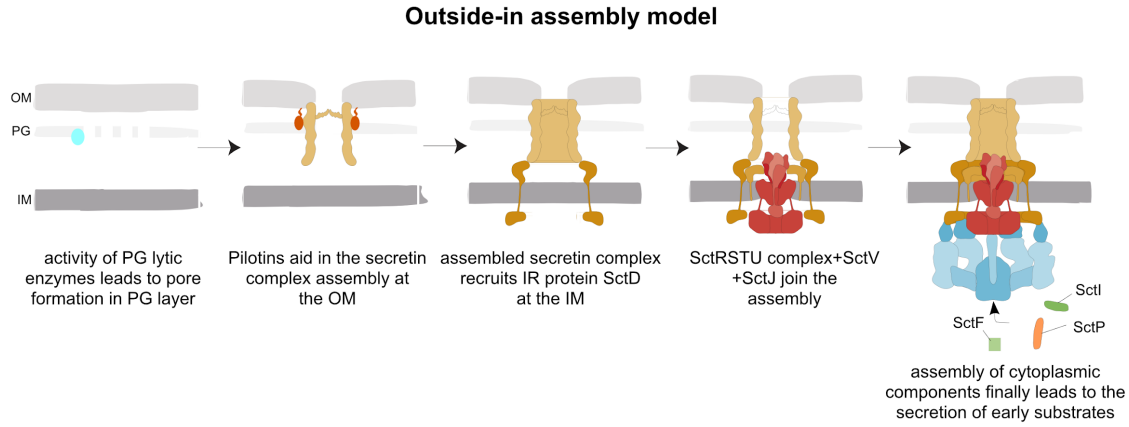

Figure 5: Outside-in assembly model

Secretin assembly initiates the assembly process. The activity of PG lytic enzymes leads to pore formation in the PG layer, and with the assistance of pilotins, secretin complex assembly takes place at the OM. SctD integrates with SctC, following up with further addition of the assembled export apparatus. After that, the cytoplasmic components assemble with the ATPase, eventually permitting early substrate secretion. (Modified from Westerhausen 2021). **Abbreviations:** T3SS, Type III secretion system; OM, outer membrane; PG, Peptidoglycan; IM, inner membrane; IR, inner ring; Sct, secretion and cellular translocation.

The outside-in assembly model is basically in accordance with the establishments made in *Yersinia,* which indicated that SctC subunits assemble independently at the outer membrane prompting the pre-pore formation with the help of peptidoglycan lytic enzymes [145,151]. Next, the outer inner ring protein SctD gets associated with the secretin ring. After that, the core export apparatus (SctRST) assembles before adding SctU and SctV in a sec-dependent manner [80,107]. Next, SctJ gets employed in the ongoing assembly, followed by SctC. Subsequently, SctC gets connected to the export apparatus via the inner membrane rings [145].

1.5 Characterization of the interaction between SctD and SctK in *Salmonella enterica* type III secretion system

The injectisome is firmly embedded in the bacterial cell envelope by a basal body composed predominantly of three principal structural proteins spread across the bacterial inner and outer membranes, namely SctC, SctD, and SctJ (see section 1.3.1). The IR has a 24 fold symmetry and is formed by SctD and SctJ. These multimeric membrane-spanning IRs anchor the proximal end of the needle filament. In contrast, the OR has a 15.5 fold symmetry and is formed by SctC [49–51,154]. SctK, SctQ, SctL, and SctN are the four soluble T3SS components that interact linearly [155]. Each of these four components is indispensable for assembly as well as effector secretion [60,145]. A single-pass transmembrane helix bridges the periplasmic and cytoplasmic domains of SctD. SctK, SctQ, and SctL together construct a high molecular weight complex known as the sorting platform, which lies underneath the basal body and binds chaperones and effector proteins [59] (see section 1.3.2).

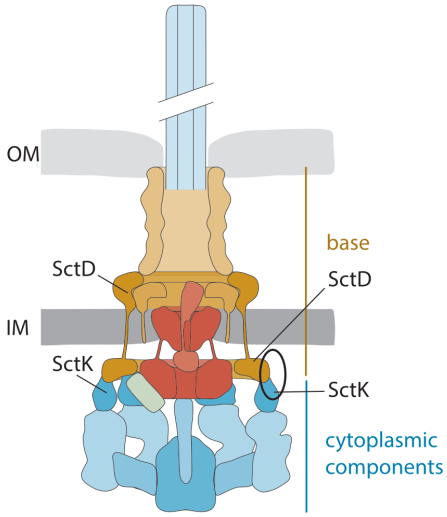

Figure 6: Cartoon representation for depiction of interaction between SctD and SctK. Cartoon representation of the interaction between the cytoplasmic domain of SctD and sorting platform protein SctK. Site-directed mutagenesis of various key residues within the potential interacting surface confirmed the interaction of these two proteins. **Abbreviations:** T3SS, Type III secretion system; OM, outer membrane; PG, Peptidoglycan; IM, inner membrane; IR, inner ring; Sct, secretion and cellular translocation.

The comprehensive organization of SPI-1 encoded T3SS in *Salmonella* structure closely resembles the structural organization in *Shigella* [63], which agrees with the extraordinary level of conservation of its constituents across different T3SSs. Nevertheless, the sorting platform of T3SS remarkably differs from the flagellar complex [62]. The sorting platform in *Shigella*

manifests a six-pod structure capped by a central hub at one end [62] and is discreetly different from the evolutionarily related cytoplasmic C-ring structure in flagella [156].

Owing to difficulties in the co-purification of the cytosolic components together with the remaining needle complex, insight into the structural arrangement of these cytosolic components could not be achieved until recently when the *in situ* cryo-electron tomographic study could show the organization of the six pod structures [63]. Rearrangement of the cytosolic domains of SctD ($SctD_C$) in the presence of SctK leads to the formation of six individual pods of four $SctD_C$ each that interact with a single adaptor protein SctK, which further connects SctQ, SctL, and SctN [62,63,157,158]. The cytosolic components exist in a bound state as injectisome-bound pod structures or in a readily diffusing cytosolic state by a constant exchange of proteins between the two different states [68]. The interplay of these cytosolic proteins together with their exchange rates remarkably coordinates with the activity of the needle complex [60,68,159]. The interaction of SctD with SctK protein is supposedly crucial, and the symmetry transition that transpires between them might be indicative of dynamic interactions taking place at this interface. Concerning the dynamics at this interactive surface, it is fascinating to observe *in situ* that $SctD_C$ from *Salmonella* forms clusters while interacting with SctK [63]. In disagreement with this observation, $SctD_C$ domains from *Shigella* ($MxiG_C$) continue to exist in an evenly spaced 24-fold symmetry without any distinguished clustering [157]. One could argue that protein movements or rearrangements take place at this interface. Therefore, comprehension of this interface, including the conceivable protein dynamics that might occur here, would be required for a better grasp of the radical mechanisms regulating the secretion. Until now, there is no data available on any facet of the various molecular interactions taking place between the sorting platform and the basal body.

A dynamic adaptive network consisting of diversified complexes consisting of varied stoichiometries is formed in the cytosol by SctK, SctQ, SctL, and SctN components of T3SS. Although altered external conditions have been shown to trigger changes in the composition of these dynamic complexes [60,160], it is still obscure how premature effector secretion is restricted during infection. A recent study conducted in *Yersinia* reported temporary release of the cytosolic components of the injectisome at low external pH conditions, thereby forbidding protein secretion in acidic environments [161]. Exposure of the periplasm to low external pH is suggested to cause partial uncoupling of the inner membrane protein SctD, which in turn leads to the dissociation of the cytosolic T3SS components [161]. These findings by Wimmi et al. inspired us to investigate the effect of acidic pH conditions in *Salmonella* on our already established SctD-SctK interactions. Since the restoration of neutral pH values was also shown

to reactivate the T3SS [161]. It seemed logical to investigate these findings for analyzing the role of the cytosolic components in the institution of an adaptive regulatory interface. This adaptive regulatory interface possibly is responsible for synchronizing the T3SS activity.

In summary, the interactions between the sorting platform components and the IR protein SctD are evidently significant for establishing the activity of T3SSs. Nonetheless, the explicit role of the cytosolic T3SS components in the process of secretion remains elusive to date. Recently, structure of PscK (member of T3SS SctK protein family) from *Pseudomonas aeruginosa* was solved thereby permitting computational modeling of the potential interacting interface between the cytosolic protein PscK and the cytoplasmic domain of the SctD homolog protein $PscD_C$ [158]. Since the discrete structure of the PscK-$PscD_C$ complex could not be determined, we also analyzed our data in light of these recent advancements. Based on our crosslinking data, we are in a position to make reasonable assumptions regarding the identification of the interaction surfaces of the two involved SctD and SctK proteins.

Therefore, this thesis aims to exhaustively study these interactions and the environmental factors that possibly lead to a change in the protein dynamics (see section 4: Part 2).

1.6 Conserved salt bridges in the export apparatus of T3SS

The export apparatus of T3SS spans the inner membrane and is a homolog of the flagella-associated T3SS [36]. SctR, SctS, SctT, SctU, and SctV together constitute the injectisomes, while FliP, FliQ, FliR, FlhB, and FlhA constitute the flagellar system (Fig. 7A).

Five subunits of SctR, one SctT, four SctS, and one SctU together integrate into a unique helical complex which is superposed on the inner membrane at the core of the injectisome base [43,81,83] (Fig. 7A). In addition to serving as a base ground for the assembly of the needle adapter and the needle filament, this helical complex apparently gates the secretion pore of the injectisome too [114,163]. Sequential successive addition of SctR subunits is followed by SctT, SctS, and SctU in a defined and fixed order to integrate into the $SctR_5S_4T_1U_1$ helical complex [80], which nucleates the course of injectisome assembly [77]. The predicted transmembrane hairpins of SctR, SctS, and SctT form one helix-forming module of $SctR_5S_4T_1U_1$ complex (see section 1.3.3). SctU seals the helical complex by contributing two extra helix-forming modules in an alternative topology by allocating its soluble C-terminal domain in the cytoplasm [83]. An outstretched loop between the two and three predicted transmembrane segment (TMS) of SctU passes through the gateway of the $SctR_5S_4T_1$ pore, thereby establishing contact with the loop of each SctS subunit, consequently playing a

potential role in the gating mechanism of opening and closing of the $SctR_5S_4T_1$ pore [83]. Therefore, in this thesis, we also took up the task of investigating the gating mechanism during the active secretion state of the injectisome (see section 4: Part 1).

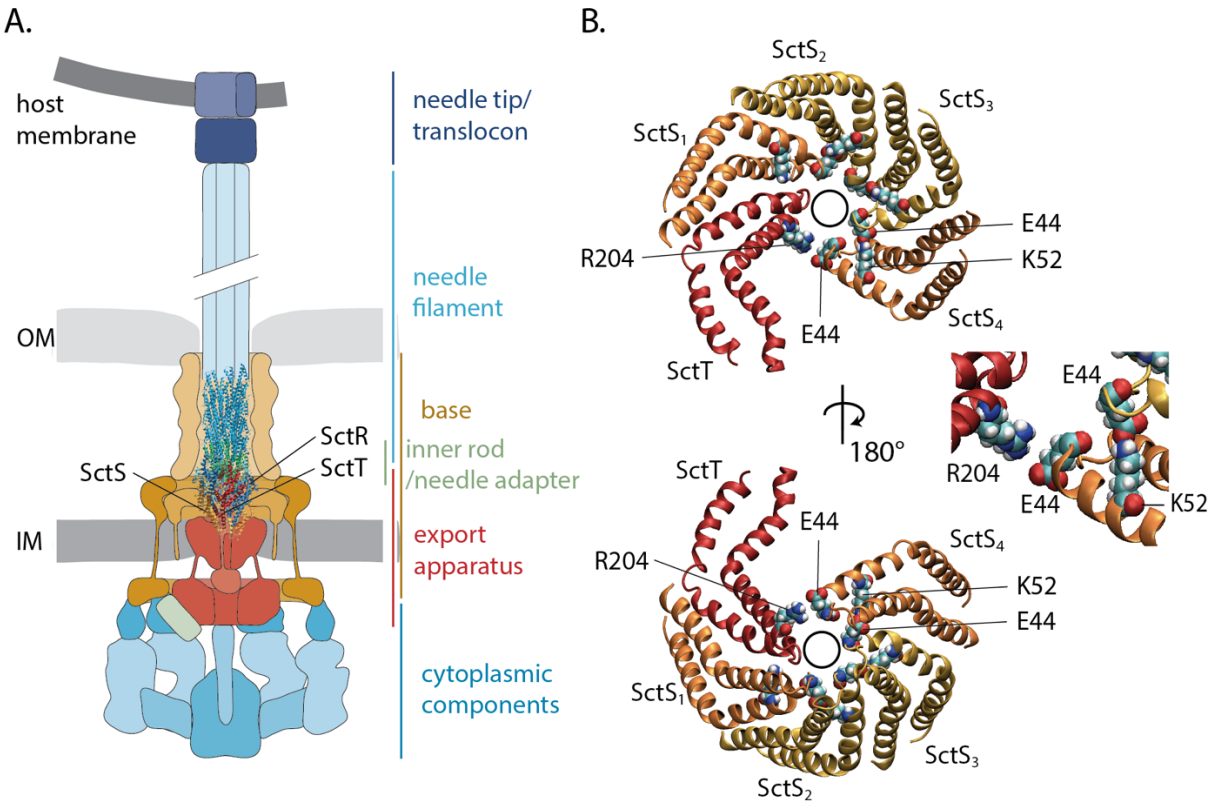

Figure 7: Cartoon of the T3SS injectisome and localization of the salt bridge-forming residues $SctS_{E44}$, $SctS_{K52}$, and $SctT_{R204}$. A. The cartoon of the T3SS injectisome is adapted and modified from [79]. Proteins of interest pertaining to this part are named according to the unified nomenclature [162], and their structure is shown. **B.** Homology model of the *Salmonella* $SctR_5S_4T_1$ core complex based on the *Shigella flexneri* Sct $R_5S_4T_1$ structure [114]. Four different copies of SctS are represented in different shades of orange and SctT in red. SctT and SctS positions reportedly forming salt bridges are represented in spheres. Top and bottom views of the complex are shown along with a close-up view of the salt bridge-forming residues and their interactions. **Abbreviations:** T3SS, Type III secretion system; OM, outer membrane; IM, inner membrane; Sct, secretion and cellular translocation.

The export apparatus constituents are predicted to embody multiple TMS and configure a hydrophobic helical complex (see section 1.3.3), yet several extremely conserved charged residues are present within their hydrophobic domains. Genetic characterization of a multitude of these conserved charged residues in the major export apparatus protein FlhA of flagellar type III secretion system was implicated in utilizing inner membrane proton-motive force to permit the opening of the export apparatus [100,164]. The conserved charged residues of the flagellar SctR homolog FliP have been reported as important but not essential for secretion

function [100]. Nonetheless, a D171A mutation located in the core of SctR of the T3SS of enteropathogenic *Escherichia coli* (EPEC) resulted in the loss of assembly and secretion competence of the injectisome. This residue appeared to be involved in mediating TMD-TMD interactions and consequently eliciting the activity of the full-length protein and the function of the T3SS [165]. Similarly, the substitution of the conserved E46 and K54 positions within the flagellar SctS homolog FliQ of *Salmonella* Typhimurium terminated flagellar motility, presumably by disturbing FliQ stability and complex assembly [100]. Furthermore, the replacement of $SctS_{K54}$ in the EPEC T3SS strongly impaired injectisome assembly and secretion [16]. Additionally, the substitution of $SctS_{K54}$ in EPEC T3SS impeded the injectisome assembly and secretion to a large extent [166].

Strikingly, intermolecular salt bridges are formed by the conserved charged residues of FliQ and SctS, reportedly based on the structures of the flagellar $FliP_5Q_4R_1$ and virulence $SctR_5S_4T_1$ complexes. These salt bridges link one FliQ/SctS subunit to the next adjacent one and the last FliQ/SctS subunit to FliR/SctT by another salt bridge via a corresponding conserved basic residue of FliR/SctT (Fig. 7B) [43,81]. The structure of flagellar $FliP_5Q_4R_1$ and virulence $SctR_5S_4T_1$ complexes also revealed that salt bridges occurred in the closed complex states, which meant opening the secretion pore demanded breakage of these salt bridges [167]. Also, the stability of the secretion pore apparently is upheld by a network of salt bridges in FliQ [168]. Analysis of flagellar $FliP_{E46D}$ mutants suggested a possible role of this residue in the gating mechanism of the flagellar FliPQR core complex [168]. An intriguing aspect of these conserved charged residues is their potential role in assembling the helical core export apparatus complex. Hence, assessing the roles of E44 and K52 in SctS and R204 in SctT in the assembly and function of the injectisome became another target of this thesis.

2. Research objectives

Many recent studies concentrated on characterizing the structure and assembly of the export apparatus components. The closed state structure of the helical core complex SctR5S4T1 revealed that the constituent hydrophobic proteins SctR, SctS, and SctT consist of numerous highly conserved charged residues within their hydrophobic domains. Amongst these, several residues participate in both inter- and intramolecular salt bridges. Thus, we assumed that these conserved charged residues might have potential roles in type III-dependent secretion and pore opening. Therefore, one of the goals for this thesis was to decipher the exact role of these conserved charged residues in the assembly and function of T3SS (Section 4: Part 1).

Despite recent advancements in high-resolution structural studies, we barely understand the organization, configuration and function of the injectisome in any detail. One of the blind spots is the sorting platform, which is the cytosolic component of the needle complex. The other goal of this thesis was to capture molecular interactions between the ring protein SctD and cytosolic protein SctK with a focus on obtaining the plausible orientation of the SctD protein. Along with various photocrosslinking studies, we used functional assays to investigate the interplay of the T3SS structural components. Consequently, we aimed to acquire detailed insights into the explicit role of different secretion states on the SctD-SctK interaction. In order to link changes in external pH and PMF to their distinct roles, we aimed to design specific functional assays that could help us better understand the acquired changes in the protein dynamics due to change in environmental factors of the needle complex (Section 4: Part 2).

Parts of this materials and methods section have been published in:

- Investigating the assembly of the bacterial type III secretion system injectisome by *in vivo* photocrosslinking

  Nidhi Singh, Samuel Wagner

- Conserved salt bridges facilitate assembly of the helical core export apparatus of a *Salmonella enterica* type III secretion system

  Nidhi Singh, Thales Kronenberger, Andrea Eipper, Felix Weichel, Mirita Franz, Boris Macek, Samuel Wagner (revision submitted)

3. Materials and Methods

3.1 Chemicals, Enzymes, Media and Buffers

All of the chemicals as well as enzymes used in this study were purchased from Sigma-Aldrich (München), Eppendorf, Thermo Fisher Scientific (Rockford, USA), Novagen (Darmstadt), New England Biolabs (Frankfurt am Main), Merck (Darmstadt), Carl Roth (Karlsruhe), Becton Dickinson (Le Pont De Claix, France), Biozym (Oldendorf) or AppliChem (Darmstadt) unless specified otherwise. Media and buffers used in this study are enlisted in table 1.

3.2 Antibodies

Antibodies used in this study (table 2) were all diluted in TBS-T before usage. The primary antibody α-FLAG was purchased from Sigma-Aldrich (München). The secondary antibody used in this study was conjugated to the fluorophore DyLight 800 4 x PEG and was purchased from Thermo Fisher Scientific (Rockford, USA). This conjugation enabled the detection of the secondary antibodies by a LI-COR Odyssey system (ODY-3191).

3.3 Bacterial strains and culture growth conditions

The bacterial strains used in this study are enlisted in table 3. All of the *Salmonella* strains were derived from *Salmonella enterica* serovar Typhimurium strain SL1344 [169] and created by allelic exchange [170]. *Escherichia coli* strains NEB5α and λpir116 which were used for molecular cloning were grown in either liquid Lennox broth (LB) medium at 37 °C, 180 rpm or on LB agar medium at 37 °C. *Salmonella enterica* serovar Typhimurium (*S.* Typhimurium)

strains were also grown in either liquid LB medium at 37 °C, 180 rpm or on LB agar medium at 37 ℃ with low aeration. As per requirements all media were supplemented with the respective antibiotics, which were used in the following concentrations: streptomycin (Strep): 50 µg/ml, tetracycline (Tet): 12.5 µg/ml, kanamycin (Kan): 25 µg/ml, ampicillin (Amp): 100µg/ml, and chloramphenicol (Cm): 25 µg/ml. *E. coli* β2163 cells which were used for allelic exchange required additional supplementation of 100 µg/ml diaminopimelic acid (DAP) in the medium for their growth. Gene expression of the SPI-1 encoded T3SS was induced by growing *S.* Typhimurium strains in liquid LB medium supplemented with 0.3 M NaCl with low aeration. As per usage, bacterial cells were stored either on LB agar medium at 4 °C for up to 4 weeks or frozen in 1.5 ml stock medium at -80 °C for long term storage.

3.4 Site-directed mutagenesis

In order to reconstruct pTACO10 (pT10) plasmids, we used a kit namely Q5 site-directed mutagenesis kit (NEB, E0552S). For this we designed non-overlapping site-directed mutagenesis primers (table 5) as per the manufacturer's instructions and thereafter amplified the plasmid DNA by polymerase chain reaction (PCR) using Q5 Hot Start High-Fidelity DNA Polymerase. The PCR products obtained were incubated with a provided KLD enzyme mix containing kinase, ligase and Dpn1. All these enzymes together enabled rapid circularization of the PCR products and removal of the template DNA. For amplification of the new plasmid DNA, transformation of chemically competent NEB5α cells was done by following a standard heat shock transformation procedure (30 min on ice, 30 secs at 42°C, 2 min on ice). At last the plasmids were extracted with the help of QIAprep Spin Miniprep Kit (Qiagen) and the positive mutants were identified by sequence analysis (Eurofins Genomics).

3.5 QuikChange site-directed mutagenesis

For *in-vivo* photo-crosslinking, amber stop codons are prerequisites. These amber stop codons hence needed to be introduced in the target genes. QuikChange site-directed mutagenesis (QC) [171] was used in order to introduce them in the genes of choice or target genes. KOD Hot Start DNA Polymerase and designed QC primers (table 5) were used according to manufacturer's protocol and a PCR was performed. The PCR product obtained was then digested with Dpn1 for 2 h at 37 °C in order to remove the template DNA. Thereafter 5 µl of this reaction product was used for a standard heat shock transformation into chemically competent NEB5α or pir116. Extraction of the plasmids was done by using the QIAprep Spin

Miniprep Kit (Qiagen) and sequence analysis (Eurofins Genomics) at last enabled identification of the positive mutants.

3.6 Gibson cloning and plasmid construction

Vector and insert DNA fragments were assembled by using Gibson cloning method [172] in order to reconstruct plasmids. The fragment amplification was done by PCR with the help of respectively designed Gibson primers along with Q5 Hot Start High-Fidelity DNA Polymerase. Thereafter, the PCR product was digested with Dpn1 for approximately 2 h at 37 °C and analyzed on 1% agarose gel in the TAE buffer for verification. Once successful, the amplified vector and insert fragments were assembled together in a 12.5 µl Gibson master mix consisting of DNA ligase, DNA polymerase, and T5 exonuclease for 1 h at 50°C. We proceeded with the transformation procedure thereafter. For this, 5 µl of the reaction product bearing the assembled plasmids was transformed either into heat shock competent *E. coli* or into electrocompetent *Salmonella* strains. Finally, the plasmids were extracted using QIAprep Spin Miniprep Kit (Qiagen) and the positive mutants were identified by sequence analysis (Eurofins Genomics). While dealing with the pT10 plasmids, it was ensured that their expression was induced additionally by supplementing the culture medium with 100 µM rhamnose.

Other required DNA modifications in this study were introduced either by QuikChange using KOD polymerase or by Q5 polymerase (NEB). Taq polymerase (NEB) was used for colony PCRs. Eurofins and Integrated DNA Technologies synthesized the required oligonucleotides used for plasmid constructions. As mentioned before, the Qiagen kits were used for plasmid purifications by following the manufacturer's instructions.

3.7 Transformation of electro-competent cells

Plasmids enlisted in table 4 were used for my project and as per requirements and suitability they were either introduced into *Salmonella* strains or into *E. coli* β2163 by electroporation. The cells were washed three times with ice cold 10 % glycerol [173] in order to make them electrocompetent. An electroporator (Eppendorf) was used at 1.8 kV, 200 Ω and 25 µF for electroporation.

3.8 Allelic exchange

Any kind of genetic modification such as gene insertion or deletion in *Salmonella* chromosome was performed by allelic exchange [174]. In order to do so, a tetracycline resistant suicide plasmid pSB890 was used. This suicide plasmid encoded the mutated gene of interest along with flanking regions of approximately plus 1000 bp upstream as well as 1000 bp downstream. The flanking regions are homologous to the chromosomal destination locus. Cloning and propagation of the suicide plasmid (pSB890) was performed in *E. coli* pir116 strain. This strain expresses Π protein which is responsible for initiating the replication of plasmids containing the R6K origin of replication. Thereafter, the suicide plasmid was transformed by electroporation into the *E. coli* β2163 donor strain. This donor strain is able to mate with *Salmonella* strains and hence successfully assist in the integration of the suicide plasmid into the Salmonella chromosome. β2163 donor strain was cultured in LB/Tet/DAP medium overnight (o/n) while the recipient *Salmonella* strain in LB/Strep medium. Following day 900 µl each from both cultures were mixed and spun down at 6000 rpm (Eppendorf MiniSpin, rotor F-45-12-11), 2 min at room temperature (RT) and thereafter washed with 1 ml LB/DAP in order to get rid of the antibiotics. The supernatant was then removed and the pellet was resuspended in 30 µl LB/DAP. This mixture was spotted on LB/DAP agar culture dish which was incubated at 37 °C for at least 8 h. As a result, the suicide plasmid got transferred to *Salmonella* strains by mating. pSB890 was finally integrated in the chromosome via homologous recombination thereby creating merodiploids *Salmonella*. These merodiploids were carefully selected by following their growth on LB/Strep and LB/Tet plates. Merodiploids that grew on LB/Strep plates and didn't on LB/Tet plates were selected. The chosen merodiploid colony was then grown for 24 h in 5 ml LB/Strep medium. Following day, 100 µl of the culture was plated on a sucrose agar plate and incubated o/n at 30 °C. Given the fact that the suicide plasmid carries a counter selection marker *sacB* encoding the enzyme levansucrase, which is responsible for conversion of sucrose to a cytotoxic metabolite called levan, we counterselected *Salmonella* colonies on sucrose plates which had lost the suicide plasmid. The resulting colonies were screened for either insertion or deletion by colony PCR and verified by sequence analysis (Eurofins Genomics).

3.9 *In vivo* photo-crosslinking

In vivo photocrosslinking was performed as described previously [80,175]. *S.* Typhimurium *flhD::tet* strains were transformed with pBAD-HilA, pSup-*p*Bpa and a pT10 plasmid encoding proteins of interest. HilA is the main transcriptional regulator of SPI-1 and this regulator is

arabinose-inducible. Therefore, addition of 0.05 % (w/v) arabinose ensured the activation of the expression of the invasion genes which yielded high levels of T3SSs within each cell. Gene expression of the pT10 plasmids was induced by addition of 500 µM rhamnose to the media. *S.* Typhimurium strains were grown o/n in 3 ml LB Lennox supplemented with 0.3 M NaCl along with their respective antibiotics (Strep, Tet, Cm, Amp, and Kan) and were back diluted next morning to an OD600 of approximately 0.05. Generally, the amount of inoculant culture (o/n culture) was approximately 300 µl that was added to 10 ml LB media supplemented with 0.3 M NaCl and the required antibiotics (Amp). In this case, all other antibiotics were not necessary because low copy number plasmids such as pT10 and pSup-*p*Bpa are stable enough for a short period of a few hours. Additionally, *p*Bpa (Bachem, Bubendorf, CH) was dissolved in 1 M NaOH and then was added in the culture media to a final concentration of 1 mM whilst shaking. These cultures were grown for 5 h at 37 °C ,180 rpm. Two times 4 ODU (2 sets for UV- and UV+) were harvested by centrifugation (6000 x *g*, 2 min, 4 °C). When a secretion assay was performed in parallel for the same samples then another 1.8 ml of the culture was collected separately and filtered (0.2 µm) for performing TCA precipitation of the culture supernatant (SN) (see 3.11). Moving on with the crosslinking samples, the harvested cells were washed with 5 ml ice cold PBS, centrifuged (6000 x *g*, 2 min, 4 °C) and resuspended in 2 ml ice cold PBS. One set of samples which was untreated called as UV- (UV negative control) was stored at -20 °C while the other set of samples which were UV+ (UV irradiated samples) were resuspended in 1 ml PBS and UV_{365nm} irradiated for 30 min on a CELLSTAR® 6 well cell-culture plate (Greiner Bio-One). After the UV exposure, the samples were centrifuged again and the pellets were washed with cold PBS. Thereafter, the pellets were either frozen o/n at -20 °C before analyzing on a SDS-PAGE followed by western blot, or shock frozen in liquid nitrogen and stored at -80 °C for blue native polyacrylamide gel electrophoresis (BN PAGE) analysis.

3.10 Crude membrane preparation

Crude membranes were prepared by following the published protocol [80]. The cell pellets (≥ 4 ODU) were resuspended in ice-cold 750 µl buffer K which was supplemented with 10 µg/ml lysozyme, 10 µg/ml DNase, 1 mM $MgCl_2$, 1 mM EDTA and 1:100 protease inhibitor cocktail (Sigma Aldrich, #P8849). This suspension was then incubated for 30 min at 4 °C. After 30 min, the samples were added to pre-cooled screw cap tubes containing 500 µl glass beads (150-212 µm in size, acid-washed, Sigma-Aldrich) and were bead milled for 2 min in a SpeedMill PLUS (Analytik Jena) at continuous mode. The lysed samples were then

centrifuged at 1000 x *g*, 1 min, 4 °C and the supernatant obtained was transferred to a fresh 1.5ml tube. The glass beads in the screw cap tubes were washed once again with 1 ml buffer K (without supplements). Again the beads were pelleted by centrifugation (1000 x *g*, 1 min, 4 °C) and the supernatant was collected in the same tube as before. In order to get rid of aggregates, cell debris, remaining glass beads and unlysed whole cells, the samples were finally centrifuged at 10000 x *g*, 10 min, 4 °C. Thereafter, 1.3 ml of the supernatant was collected and transferred into ultracentrifugation tubes. Crude membranes in the supernatant were isolated by ultracentrifugation at 52000 rpm, 50 min, 4 °C in a TLA55 rotor (Beckman Coulter). At last, the membrane pellets obtained after centrifugation were either frozen at -20 °C or directly subjected to further treatment for their analysis. For SDS-PAGE analysis, the crude membrane pellets corresponding to 4 ODU each were resuspended in a 40 µl SB buffer (see section 3.13) and heated at 75°C for 10 min. From this suspension 20 µl of sample (corresponding to 2 ODU) was loaded in each well of the SDS gel.

3.11 Classical Secretion assay

Type III dependent secretion of proteins into the culture medium was analyzed as described previously [91]. *S*. Typhimurium strains were cultured with 0.3 M NaCl at 37 °C for 5 h under low aerated conditions in LB broth. Bacterial suspensions were then centrifuged at 10,000 × *g* for 2 min at 4 °C to separate whole cells and supernatants. Whole cell pellets were directly resuspended in SDS PAGE loading buffer (1x) whereas supernatants were filtered through 0.2 µm pore size filters and supplemented with 0.1% (w/v) of Na- deoxycholic acid. Proteins present in the supernatant were precipitated by addition of 10% (v/v) of trichloroacetic acid (TCA) for 30 min at 4 °C. Precipitated proteins were pelleted by centrifugation at 20,000 × *g* for 20 min at 4 °C. These pellets were then washed with acetone and resuspended in SDS PAGE loading buffer. Whole cell pellets and secreted protein samples were analyzed by SDS PAGE, Western blotting and immunodetection.

3.12 NanoLuc luciferase (NL) secretion assay

T3SS effector proteins tagged with NL at the C-terminus facilitate a fast quantitative secretion analysis. Therefore, in order to measure T3SS effector protein secretion, SipA was C-terminally tagged to the Nano-Luciferase (NL). The overnight cultures of *S*. Typhimurium strains were back diluted to an OD600 of approximately 0.05 in LB media supplemented with 0.3 M NaCl. Simultaneously, the gene expression was also induced with the addition of 0.05 % (w/v) arabinose 100 µM rhamnose. The cultures were then grown for 5 h. Thereafter, the

samples were centrifuged (10000 x *g*, 2 min, 4 °C). Duplicates of 25 µl of supernatant per well were then transferred to a Nunc® MaxiSorpTM 384 well plate (Thermo Fisher Scientific) and 25 µl NanoGlo luciferase buffer (Promega) along with 1:50 NanoGlo luciferase substrate (Promega) mixture was added to the supernatant in each well. The plate was gently shaken for effective mixing of the substrate and the buffer with the samples and then incubated for 5 min at RT. NanoLuc exploits the substrate (furimazine) in order to produce luminescence of high intensity. Hence, the emitted high intensity luminescence signal could be measured and analysed by Infinite M200 Pro (Tecan) with acquisition settings as recommended by the manufacturer.

3.13 Sodium dodecyl sulfate polyacrylamide gel electrophoresis (SDS PAGE)

SDS PAGE was performed to separate the denatured protein samples according to their molecular weight. For comparison of the molecular weight of proteins a reference, Precision Plus Protein All Blue standards (Bio-Rad) was used. Separation of the denatured proteins according to their molecular weight was done on ServaGel TG Prime 8-16 % precast gels (Serva) by performing electrophoresis in the SDS running buffer at 110 V for 15 min followed by a run at 210 V for 85 min.

3.14 One- dimensional BN PAGE

Eight ODU of crude membranes were resuspended in 90 µl PBS. Homogenized solubilization was achieved by pipetting approximately 80-120 times up and down. Afterwards, a final concentration of 10 % (w/v) LMNG (Lauryl Maltose Neopentyl Glycol)**)** was added to the membranes. Thereafter, the membrane proteins were solubilized at 4°C for 1 hr (Thermomix, 500 rpm) by shaking and then unsolubilized material was removed with a clarifying spin of 20000 x g, 30 min at 4 °C. Next, the solubilized membrane aliquot was collected and split for SDS PAGE and blue native (BN) PAGE. The blue native samples were then resuspended in the blue native loading buffer. Native protein complexes were separated according to their molecular weight by using Native PAGE TM 3 - 12 % Bis-Tris protein gels (Invitrogen). Electrophoresis of the native protein complexes was performed as previously described [176].

3.15 Western blot analysis and immunodetection of proteins

After separation of the denatured protein samples according to their molecular weight via SDS by using SERVAGel^{TM} TG Prime^{TM} 8-16 % precast gels or by BN PAGE, proteins were blotted on a polyvinylidene difluoride (PVDF) membrane (Bio-Rad) using wet conditions. For comparison of the molecular weight of proteins a reference, Precision Plus Protein All Blue standards (Bio-Rad) was used. The gels were then transferred to a PVDF membrane (Bio-Rad) in the Trans-BlotTM Cell (Bio-Rad) chamber by standard protocols. Membranes were then probed with primary antibodies α- SctP (InvJ), α- SctE (SipB) [91] and M2 anti- FLAG (1:5,000) (Sigma- Aldrich). Secondary antibodies were goat anti- mouse IgG DyLight 800 conjugate (Thermo Fischer). Detection and analysis were performed by using Odyssey imaging system (LiCor) and Image Studio 5.1 (LiCor). In case BN gels were blotted then the membrane was first washed properly with methanol in order to remove Coomassie and then the standard protocol for blotting was followed.

3.16 Spheroplasting

For spheroplasting the overnight bacterial cultures were firstly back diluted and then cultured at 37 °C until an OD_{600} of 1 was achieved. Spheroplasting was performed at room temperature after pelleting the bacterial cultures. The harvested pellets were resuspended in 0.8 M sucrose solution for keeping the fragile spheroplasts in a hypertonic solution. Thereafter, 60 mM Tris solution (pH 8.0) was added followed by sequential addition of 20 µg/ml lysozyme, 1.3 mM EDTA, 50 µg/mL DNase and protease inhibitor from Sigma-Aldrich (1:100 from stock). The outer membrane of the bacterial pellets was then disrupted by multiple mixing steps. The suspension was then incubated for 20 min at RT and 4 mM $MgCl_2$ was later added to stop the spheroplasting reaction. The periplasmic fraction was separated from the spheroplasts by centrifugation at 6000 x *g*, 4 °C for 10 min. Thereafter, the periplasmic fraction was further supplemented with sodium deoxycholate to a final concentration of 0.1 % (w/v). Addition of 10 % (w/v) trichloroacetic acid for 30 mins at 4 °C precipitated the proteins. After this incubation, the precipitated proteins were centrifuged and pelleted for 20 mins at 20,000 x *g*, 4 °C. The supernatant was discarded and the cells were very carefully dissolved in fresh sucrose solution. Spheroplasts were then further treated as per requirements of the experimental goals.

Table 1: Media, buffers and solutions used in this study

Name	**Contents**
LB medium	5 g NaCl, 10 g tryptone and 5 g yeast extract were dissolved in 1 L H2O and autoclaved.
LB-0.3M NaCl medium	12.5 g NaCl, 10 g tryptone and 5 g yeast extract were dissolved in 1 L H2O and autoclaved.
LB agar medium	6 g LB Lennox and 4.5 g agar were dissolved in 300 ml H2O and autoclaved. Afterwards, respective antibiotics were added. For Tet/DAP agar medium, 480 µl Tet and 20 ml DAP were added to 1 L LB agar.
SOB medium	40 g bacto-tryptone, 10 g yeast extract, 1 g NaCl and 0.373 g KCl were dis- solved in 2 L H2O and autoclaved. Then, sterile filtered (0.22 µm) 1 M MgCl2 and 1 M MgSO4 solutions were added to achieve a final concentration of 10 mM.
SOC medium	20 ml sterile filtered (0.22 µm) 1 M glucose were added to 1 L SOB medium.
Sucrose agar medium	5 g tryptone, 2.5 g yeast extract and 7.5 g agar were dissolved in 400 ml H2O and autoclaved. Afterwards, 100 ml sterile filtered (0.22 µm) 50 % (w/v) sucrose was added.
Stock medium	63 g glycerol and 10 g peptone were dissolved in 500 ml H2O and thereafter autoclaved.
10X PBS	80 g NaCl, 2 g KCl, 14.4 g Na2HPO4 · 2 H2O and 2.4 g KH2PO4 were dissolved in 1 L H2O and the pH was adjusted to 7.4 with NaOH. Before usage, the buffer was diluted 1:10 with H2O.

50X TAE buffer	242 g Tris base, 57.1 ml glacial acetic acid and 37.2 g EDTA were dissolved in 1 L H2 O. Before usage, the buffer was diluted 1:50 with H2O.
4X SB buffer	10 ml 0.5M Tris-HCl pH6.8, 5 ml 80% (v/v) glycerol, 1.6 g SDS and 10 mg bromophenol blue were filled up to 16 ml with H2O. Before usage, the buffer was appropriately diluted with H2O and supplemented with a final concentration of 5 % (v/v) β-mercaptoethanol.
10X TBS	84 g NaCl and 30 g Tris base were dissolved in 1 L H2O. The pH was then adjusted to 8.0 with HCl. Before usage, the buffer was diluted 1:10 with H2O.
TBS-T	Already prepared TBS was supplemented with 0.05 % (v/v) Tween20.
10X Transfer buffer	30g Tris base, 144 g glycine and 2.5 g SDS were dissolved in 1 L H2O. Before usage, the buffer was diluted 1:10 with H2O and supplemented with a final concentration of 10 % (v/v) methanol.
SDS running buffer	30 g Tris base, 144 g glycine and 10 g SDS were dissolved in 1 L H2O. Before usage, the buffer was diluted 1:10 with H2O.
Buffer K	50 mM TEA, 250 mM sucrose and 1 mM EDTA pH 8 were dissolved in 500 ml H2 O. Then, the pH was adjusted to 7.5 with acetic acid.
6X DNA loading buffer	1.9 ml 80%(v/v) glycerol, 20 µl Tris-HCl pH 8.8 and a small piece of bromophenol blue was added to 3 ml H2 O.
5X ISO mix	300 µl 1 M Tris-HCl pH 7.5, 30 µl 1 M MgCl2, 60 µl 10 mM dNTP Mix, 30 µl 1 M DTT, 150 mg PEG 8000, 30 µl 100 mM NAD together

	with 600 µl H2O were mixed.
Gibson master mix	100 µl 5x ISO mix, 0.2 µl T5 exonuclease, 6.25 µl Phusion DNA polymerase and 50 µl *Taq* DNA Ligase were mixed in 218.6 µl H2 O.

Table 2: Antibodies used in this study

Antibody	**Origin**	**Dilution**	**Order**
α-FLAG (M2-monoclonal)	mouse	1:5000	primary
α-SctP (monoclonal)	mouse	1:1000	primary
α-SctE (monoclonal)	mouse	1:1000	primary
α-Mouse800 (polyclonal)	Goat	1:5000	secondary

Table 3: *Escherichia coli* and *Salmonella enterica* serovar Typhimurium strains used in this study

Strain name	**Species**	**Genotype**
NEB5α	*Escherichia coli*	*fhuA2Δ(argF-lacZ)U169 phoA glnV44 Φ80Δ(lacZ)M15 gyrA96 recA1 relA1 endA1 thi-1 hsdR17*
pir116	*Escherichia coli*	*endA1 hsdR17 glnV44 (= supE44) thi-1 recA1 gyrA96 relA1 Φ80dlacΔ(lacZ)M15 Δ(lacZYA-argF)U169 zdg-232 uidA::pir116*
β2163	*Escherichia coli*	*(F-) RP4-2-Tc::Mu DdapA::(erm-pir) [KmR ErmR]*
SB300	*Salmonella enterica*	*Salmonella enterica* subspecies *enterica* serovar Typhimurium strain SL1344 (WT)

SB762	*Salmonella enterica*	wild type (SL1344, flhD::tet)
MIB4592	*Salmonella enterica*	SB300, ΔspaPQRS, SipA-NL, flhD::tet
MIB5180	*Salmonella enterica*	$SpaR^{FLAG}$,SipA-NL, flhD::tet
MIB5182	*Salmonella enterica*	$SpaS^{FLAG}$,SipA-NL, flhD::tet
MIB5184	*Salmonella enterica*	$SpaS_{N258A}{}^{FLAG}$,SipA-NL, flhD::tet
MIB5236	*Salmonella enterica*	$SpaR_{R204A}$, $SpaS^{FLAG}$, SipA-NL, flhD::tet
MIB5238	*Salmonella enterica*	$SpaR_{R204Q}$, $SpaS^{FLAG}$, SipA-NL, flhD::tet
MIB5240	*Salmonella enterica*	$SpaQ_{E44D}$, $SpaS^{FLAG}$, SipA-NL, flhD::tet
MIB5272	*Salmonella enterica*	$SpaQ_{E44Q}$, $SpaS^{FLAG}$,SipA-NL, flhD::tet
MIB5274	*Salmonella enterica*	$SpaR_{R204A}$, $SpaS_{N258A}{}^{FLAG}$, SipA-NL, flhD::tet
MIB5276	*Salmonella enterica*	$SpaR_{R204Q}$, $SpaS_{N258A}{}^{FLAG}$, SipA-NL, flhD::tet
MIB5278	*Salmonella enterica*	$SpaQ_{E44D}$, $SpaS_{N258A}{}^{FLAG}$, SipA-NL, flhD::tet
MIB5280	*Salmonella enterica*	$SpaQ_{E44Q}$, $SpaS_{N258A}{}^{FLAG}$,SipA-NL, flhD::tet
MIB5282	*Salmonella enterica*	$SpaQ_{E44D}$, $SpaR^{FLAG}$,SipA-NL, flhD::tet
MIB5284	*Salmonella enterica*	$SpaQ_{E44Q}$, $SpaR^{FLAG}$,SipA-NL, flhD::tet
MIB5286	*Salmonella enterica*	$SpaR_{R204A}{}^{FLAG}$, SipA-NL, flhD::tet
MIB5288	*Salmonella enterica*	$SpaR_{R204Q}{}^{FLAG}$, SipA-NL, flhD::tet
MIB5432	*Salmonella enterica*	$SpaQ_{K52A}$, $SpaS_{N258A}{}^{FLAG}$, SipA-NL, flhD::tet

MIB5434	*Salmonella enterica*	$SpaQ_{K52Q}$, $SpaS_{N258A}^{FLAG}$, SipA-NL, flhD::tet
MIB5436	*Salmonella enterica*	$SpaQ_{K52A}$, $SpaR^{FLAG}$,SipA-NL, flhD::tet
MIB5438	*Salmonella enterica*	$SpaQ_{K52Q}$, $SpaR^{FLAG}$,SipA-NL, flhD::tet
MIB4438	*Salmonella enterica*	$InvG^{FLAG,A104X}$, flhD::tet
MIB4854	*Salmonella enterica*	$OrgA^{FLAG}$, SipA-NL, flhD::tet
MIB4856	*Salmonella enterica*	$PrgH^{FLAG}{}_{T47X}$, flhD::tet
MIB4858	*Salmonella enterica*	$PrgH^{FLAG}{}_{G50X}$, flhD::tet
MIB4860	*Salmonella enterica*	$PrgH^{FLAG}{}_{F60X}$, flhD::tet
MIB5122	*Salmonella enterica*	$PrgH^{FLAG}{}_{F61X}$, flhD::tet
MIB5124	*Salmonella enterica*	$PrgH^{FLAG}{}_{P63X}$, flhD::tet
MIB5126	*Salmonella enterica*	$PrgH^{FLAG}{}_{L52X}$, flhD::tet
MIB5128	*Salmonella enterica*	$PrgH^{FLAG}{}_{P53X}$, flhD::tet
MIB5176	*Salmonella enterica*	$OrgA^{FLAG}$, SipA-NL, *ΔprgH*, flhD::tet
MIB5178	*Salmonella enterica*	$PrgH^{FLAG}$, *ΔorgA*, flhD::tet
MIB5226	*Salmonella enterica*	$OrgA^{FLAG}$, SipA-NL, $PrgH_{L52X}$, flhD::tet
MIB5228	*Salmonella enterica*	$OrgA^{FLAG}$, SipA-NL, $PrgH_{F60X}$, flhD::tet
MIB5230	*Salmonella enterica*	$OrgA^{FLAG}$, SipA-NL, $PrgH_{P63X}$, flhD::tet
MIB5232	*Salmonella enterica*	$OrgA^{FLAG}$, SipA-NL, $PrgH_{T47X}$, flhD::tet

MIB5234	*Salmonella enterica*	$OrgA^{FLAG}$, SipA-NL, PrgH_control, flhD::tet
MIB5290	*Salmonella enterica*	$OrgA^{FLAG}$, SipA-NL, $PrgH_{F60X}$, *ΔinvC*, flhD::tet
MIB5312	*Salmonella enterica*	$OrgA^{FLAG}$, SipA-NL, $PrgH_{F60X}$, *ΔspaO*, flhD::tet
MIB5314	*Salmonella enterica*	$OrgA^{FLAG}$, SipA-NL, $PrgH_{F60X}$, *ΔinvA*, flhD::tet
MIB5316	*Salmonella enterica*	$OrgA^{FLAG}$, SipA-NL, $PrgH_{F60X}$, *ΔinvJ*, flhD::tet
MIB5318	*Salmonella enterica*	$OrgA^{FLAG}$, SipA-NL, $PrgH_{F60X}$, *ΔinvE*, flhD::tet
MIB5320	*Salmonella enterica*	$OrgA^{FLAG}$, SipA-NL, $PrgH_{P63X}$, *ΔinvC*, flhD::tet
MIB5322	*Salmonella enterica*	$OrgA^{FLAG}$, SipA-NL, $PrgH_{P63X}$, *ΔspaO*, flhD::tet
MIB5324	*Salmonella enterica*	$OrgA^{FLAG}$, SipA-NL, $PrgH_{P63X}$, *ΔinvA*, flhD::tet
MIB5326	*Salmonella enterica*	$OrgA^{FLAG}$, SipA-NL, $PrgH_{P63X}$, *ΔinvJ*, flhD::tet
MIB5328	*Salmonella enterica*	$OrgA^{FLAG}$, SipA-NL, $PrgH_{P63X}$, *ΔinvE*, flhD::tet
MIB5330	*Salmonella enterica*	$OrgA^{FLAG}$, SipA-NL, PrgH_control, *ΔinvC*, flhD::tet
MIB5332	*Salmonella enterica*	$OrgA^{FLAG}$, SipA-NL, PrgH_control, *ΔspaO*, flhD::tet
MIB5334	*Salmonella enterica*	$OrgA^{FLAG}$, SipA-NL, PrgH_control, *ΔinvA*, flhD::tet
MIB5336	*Salmonella enterica*	$OrgA^{FLAG}$, SipA-NL, PrgH_control, *ΔinvJ*, flhD::tet
MIB5338	*Salmonella enterica*	$OrgA^{FLAG}$, SipA-NL, PrgH_control, *ΔinvE*, flhD::tet
MIB3214	*Salmonella enterica*	*ΔprgH*, flhD::tet
MIB5144	*Salmonella enterica*	$OrgA^{FLAG}$,control (no *p*Bpa position), flhD::tet

MIB5172	*Salmonella enterica*	PrgH^{FLAG},control (no *p*Bpa position), flhD::tet
MIB3418	*Salmonella enterica*	*ΔorgA ΔprgH*, flhD::tet
MIB5224	*Salmonella enterica*	PrgH^{FLAG}, OrgA control, flhD::tet
MIB5226	*Salmonella enterica*	OrgA^{FLAG}, SipA-NL, PrgH$_{L52X}$, flhD::tet
MIB5228	*Salmonella enterica*	OrgA^{FLAG}, SipA-NL, PrgH$_{F60X}$, flhD::tet
MIB5230	*Salmonella enterica*	OrgA^{FLAG}, SipA-NL, PrgH$_{P63X}$, flhD::tet
MIB5232	*Salmonella enterica*	OrgA^{FLAG}, SipA-NL, PrgH$_{T47X}$, flhD::tet
MIB3426	*Salmonella enterica*	*ΔprgK ΔprgH*, flhD::tet
SB1881	*Salmonella enterica*	PrgH^{FLAG}, flhD::tet
MIB3902	*Salmonella enterica*	PrgH$^{FLAG}_{L20X}$, flhD::tet
MIB3904	*Salmonella enterica*	PrgH$^{FLAG}_{N25X}$, flhD::tet
MIB3906	*Salmonella enterica*	PrgH$^{FLAG}_{Q51X}$, flhD::tet
MIB3908	*Salmonella enterica*	PrgH$^{FLAG}_{D54X}$, flhD::tet
MIB3910	*Salmonella enterica*	PrgH$^{FLAG}_{Q104X}$, flhD::tet

Table 4: Plasmids used in this study

Plasmid name	Description	Resistance	Reference
pSB3292	pBAD24, *hilA*	Amp	Lara-Tejero *et al.* (2011)
pSup-pBpa	Amber suppressor plasmid (constitutive)	Cm	Ryu and Shultz (2006)
pMIB5022	pT10, SpaPQR^{FLAG}S	Kan	Tobias Dietsche (2016)
pMIB6693	pT10, SpaPQRS$_{A94X,N258A}^{FLAG}$	Kan	Sandra Bäurle
pMIB5534	pT10, SpaP$_{V170X}^{FLAG}$QRS	Kan	Tobias Dietsche (2016)
pMIB5250	pT10, SpaPQR$_{M209X}^{FLAG}$S	Kan	Tobias Dietsche (2016)
pMIB5544	pT10, SpaP$_{V203X}^{FLAG}$QRS	Kan	Tobias Dietsche (2016)
pMIB6089	pT10, SpaPQRS$_{N258A}^{FLAG}$	Kan	Tobias Dietsche (2016)
pSB3704	pT10, SpaP^{FLAG}QRS	Kan	Jorge E. Galán
pMIB5467	pSB890, SpaQ	Tet	Mehari T. Mebrhatu
pSB3539	pSB890, SpaR^{FLAG}	Tet	Wagner *et al.* (2010)
pMIB7558	pSB890, SpaRS	Tet	This study
pMIB7291	p890, SpaS$_{N258A}^{FLAG}$, +-1000 bp of SpaS	Tet	This study
pMIB7554	pSB890, SpaQ$_{E44D}$	Tet	This study

pMIB7555	pSB890, $SpaQ_{E44Q}$	Tet	This study
pMIB7556	pSB890, $SpaR_{R204A}^{FLAG}$	Tet	This study
pMIB7557	pSB890, $SpaR_{R204Q}^{FLAG}$	Tet	his study
pMIB7558	pSB890, SpaRS	Tet	This study
pMIB7559	pSB890, $SpaR_{R204A}$	Tet	This study
pMIB7560	pSB890, $SpaRR_{204Q}$	Tet	This study
pMIB6985	pT10, $SpaPQR_{R204A}^{FLAG}S$	Kan	This study
pMIB6986	pT10, $SpaPQR_{R204Q}^{FLAG}S$	Kan	This study
pMIB6987	pT10, $SpaPQ_{E44D}R^{FLAG}S$	Kan	This study
pMIB6988	pT10, $SpaPQ_{E44Q}R^{FLAG}S$	Kan	This study
pMIB6989	pT10, $SpaPQ_{K52A}R^{FLAG}S$	Kan	This study
pMIB6990	pT10, $SpaPQ_{K52Q}R^{FLAG}S$	Kan	This study
pMIB7147	pT10, $SpaPQR_{R204A}S_{A94X,N258A}^{FLAG}$	Kan	This study
pMIB7148	pT10, $SpaPQR_{R204Q}S_{A94X,N258A}^{FLAG}$	Kan	This study
pMIB7149	pT10, $SpaPQ_{E44D}RS_{A94X,N258A}^{FLAG}$	Kan	This study
pMIB7150	pT10, $SpaPQ_{E44Q}RS_{A94X,N258A}^{FLAG}$	Kan	This study
pMIB7151	pT10, $SpaPQ_{K52A}RS_{A94X,N258A}^{FLAG}$	Kan	This study
pMIB7152	pT10, $SpaPQ_{K52Q}RS_{A94X,N258A}^{FLAG}$	Kan	This study

pMIB7159	pT10, SpaP$_{V170X}^{FLAG}$QR$_{R204A}$S	Kan	This study
pMIB7160	pT10, SpaP$_{V170X}^{FLAG}$QR$_{R204Q}$S	Kan	This study
pMIB7167	pT10, SpaPQ$_{E44D}$R$_{M209X}^{FLAG}$S	Kan	This study
pMIB7168	pT10, SpaPQ$_{E44Q}$R$_{M209X}^{FLAG}$S	Kan	This study
pMIB7169	pT10, SpaPQ$_{K52A}$R$_{M209X}^{FLAG}$S	Kan	This study
pMIB7170	pT10, SpaPQ$_{K52Q}$R$_{M209X}^{FLAG}$S	Kan	This study
pMIB7175	pT10, SpaP$_{V203X}^{FLAG}$Q$_{E44D}$RS	Kan	This study
pMIB7176	pT10, SpaP$_{V203X}^{FLAG}$Q$_{E44Q}$RS	Kan	This study
pMIB7177	pT10, SpaP$_{V203X}^{FLAG}$Q$_{K52A}$RS	Kan	This study
pMIB7178	pT10, SpaP$_{V203X}^{FLAG}$Q$_{K52Q}$RS	Kan	This study
pMIB7406	pT10, SpaPQR$_{R204A}$S$_{N258A}^{FLAG}$	Kan	This study
pMIB7407	pT10, SpaPQR$_{R204Q}$S$_{N258A}^{FLAG}$	Kan	This study
pMIB7408	pT10, SpaPQ$_{E44D}$RS$_{N258A}^{FLAG}$	Kan	This study
pMIB7409	pT10, SpaPQ$_{E44Q}$RS$_{N258A}^{FLAG}$	Kan	This study
pMIB7410	pT10, SpaPQ$_{K52A}$RS$_{N258A}^{FLAG}$	Kan	This study
pMIB7411	pT10, SpaPQ$_{K52Q}$RS$_{N258A}^{FLAG}$	Kan	This study
pMIB7413	pT10, SpaPQRS^{FLAG}	Kan	This study
pMIB7320	pT10, SpaPQR$_{R204A}$S^{FLAG}	Kan	This study

pMIB7321	pT10, SpaPQR$_{R204Q}$S^{FLAG}	Kan	This study
pMIB7322	pT10, SpaPQ$_{E44D}$RS^{FLAG}	Kan	This study
pMIB7323	pT10, SpaPQ$_{E44Q}$RS^{FLAG}	Kan	This study
pMIB7324	pT10, SpaPQ$_{K52A}$RS^{FLAG}	Kan	This study
pMIB7325	pT10, SpaPQ$_{K52Q}$RS^{FLAG}	Kan	This study
pMIB7688	pT10, SpaPQR$_{K219A}$^{FLAG}S	Kan	This study
pMIB7689	pT10, SpaPQR$_{K219A}$S^{FLAG}	Kan	This study
pMIB7690	pT10, SpaPQR$_{K219A}$S$_{N258A}$^{FLAG}	Kan	This study
pMIB7669	pT10, SpaP$_{K198A}$^{FLAG}QRS	Kan	This study
pMIB7670	pT10, SpaP$_{K198A}$QR^{FLAG}S	Kan	This study
pMIB7179	pSB890, OrgA^{FLAG}	Tet	This study
pMIB7180	pSB890, PrgH^{FLAG}	Tet	This study
pMIB7301	pT10, PrgH$_{T47X}$^{FLAG}	Kan	This study
pMIB7302	pT10, PrgH$_{G50X}$^{FLAG}	Kan	This study
pMIB7303	pT10, PrgH$_{P53X}$^{FLAG}	Kan	This study
pMIB7304	pT10, PrgH$_{F60X}$^{FLAG}	Kan	This study
pMIB7305	pT10, PrgH$_{F61X}$^{FLAG}	Kan	This study
pMIB7306	pT10, PrgH$_{P63X}$^{FLAG}	Kan	This study
pMIB7313	pT10, PrgH$_{L52X}$^{FLAG}	Kan	This study

pMIB7315	pSB890, $PrgH_{T47X}^{FLAG}$	Tet	This study
pMIB7316	pSB890, $PrgH_{G50X}^{FLAG}$	Tet	This study
pMIB7317	pSB890, $PrgH_{F60X}^{FLAG}$	Tet	This study
pMIB7318	pSB890, $PrgH_{F61X}^{FLAG}$	Tet	This study
pMIB7319	pSB890, $PrgH_{P63X}^{FLAG}$	Tet	This study
pMIB7404	pSB890, $PrgH_{L52X}^{FLAG}$	Tet	This study
pMIB7405	pSB890, $PrgH_{P53X}^{FLAG}$	Tet	This study
pMIB7326	pSB890, $PrgH_{L52X}$	Tet	This study
pMIB7327	pSB890, $PrgH_{F60X}$	Tet	This study
pMIB7328	pSB890, $PrgH_{P63X}$	Tet	This study
pMIB7329	pSB890, $PrgH_{T47X}$	Tet	This study
pMIB7681	pSB890, $PrgH_{L20X}$	Tet	This study
pMIB7682	pSB890, $PrgH_{N25X}$	Tet	This study
pMIB7683	pSB890, $PrgH_{E89X}$	Tet	This study
pMIB7684	pSB890, $PrgH_{N91X}$	Tet	This study
pMIB7685	pSB890, $PrgH_{R95X}$	Tet	This study
pMIB5726	pT10, $PrgH^{FLAG}$	Kan	This study
pMIB6061	pT10, $PrgH_{L20X}^{FLAG}$	Kan	This study
pMIB6062	pT10, $PrgH_{N25X}^{FLAG}$	Kan	This study
pMIB6063	pT10, $PrgH_{F29X}^{FLAG}$	Kan	This study
pMIB6064	pT10, $PrgH_{L46X}^{FLAG}$	Kan	This study

pMIB6065	pT10, $PrgH_{Q51X}^{FLAG}$	Kan	This study
pMIB6066	pT10, $PrgH_{D54X}^{FLAG}$	Kan	This study
pMIB6067	pT10, $PrgH_{E89X}^{FLAG}$	Kan	This study
pMIB6068	pT10, $PrgH_{N91X}^{FLAG}$	Kan	This study
pMIB6069	pT10, $PrgH_{R95X}^{FLAG}$	Kan	This study
pMIB6070	pT10, $PrgH_{Q104X}^{FLAG}$	Kan	This study
pMIB6071	pT10, $PrgH_{R35X}^{FLAG}$	Kan	This study
pMIB6072	pT10, $PrgH_{H66X}^{FLAG}$	Kan	This study
pMIB6073	pT10, $PrgH_{W119X}^{FLAG}$	Kan	This study

Table 5: Primers used in this study

Primer name	**Sequence (5' to 3')**
SpaR_R204A_QC_f	GTATTCCTGGGTTTATTGTCGGCCTTTGCTCCGCAAATGAAC
SpaR_R204A_QC_r	GTTCATTTGCGGAGCAAAGGCCGACAATAAACCCAGGAATAC
SpaR_R204Q_QC_f	CCTGGGTTTATTGTCGCAATTTGCTCCGCAAATGAACG
SpaR_R204Q_QC_r	CGTTCATTTGCGGAGCAAATTGCGACAATAAACCCAGG
SpaQ_E44D_QC_f	CGGTAACGCAATTACAGGATCAGACGCTGCCTTTTG
SpaQ_E44D_QC_r	CAAAAGGCAGCGTCTGATCCTGTAATTGCGTTACCG
SpaQ_E44Q_QC_f	CGGTAACGCAATTACAGCAACAGACGCTGCCTTTTG
SpaQ_E44Q_QC_r	CAAAAGGCAGCGTCTGTTGCTGTAATTGCGTTACCG
SpaQ_K52A_QC_f	CGCTGCCTTTTGGCATTGCATTACTTGGCGTGTGTTTATG

SpaQ_K52A_QC_r	CATAAACACACGCCAAGTAATGCAATGCCAAAAGGCAGCG
SpaQ_K52Q_QC_f	GCTGCCTTTTGGCATTCAATTACTTGGCGTGTGTTTATG
SpaQ_K52Q_QC_r	CATAAACACACGCCAAGTAATTGAATGCCAAAAGGCAGC
SpaS_A258N_QC_f	CACGCCTGATTGTTGCCAACCCCACGCATATTACGATCG
SpaS_A258N_QC_r	CGATCGTAATATGCGTGGGGTTGGCAACAATCAGGCGTG
SpaR_K219A_QC_f	CTTTTGCGATTTCACTGACGGTAGCGAGCGGTATTGCCGTTTTAATTATGC
SpaR_K219A_QC_r	GCA TAA TTA AAA CGG CAA TAC CGC TCG CTA CCG TCA GTG AAA TCG CAA AAG
SpaP_K198A_QC_f	GAC GAT ATC TAC ACC TAT TGC CCT GGT GCT TTT TGT CGC GCT TG
SpaP_K198A_QC_r	CAA GCG CGA CAA AAA GCA CCA GGG CAA TAG GTG TAG ATA TCG TC
gib_uni_890_f2	CAAGCTCAATAAAAAGCCCCAC
gib_890_SpaS257_r	GTGGGGCTTTTTATTGAGCTTGGGCAACAATCAGGCGTGAG
prgH_W119X_QC_f	CGGAAAGCGAGCCGTAGGTGCCCGAGCAGCC
prgH_W119X_QC_r	GGC TGC TCG GGC ACC TAC GGC TCG CTT TCC G
prgH_L20X_QC_f	CAGGGCCATACATAGTTCGATTATAGAACAGCTCACTGAACGGC
prgH_L20X_QC_r	GCC GTT CAG TGA GCT GTT CTA TAA TCG AAC TAT GTA TGG CCC TG
prgH_N25X_QC_f	GTTCGATTACTTAACAGCTCACTGTAGGGCTGTGAGTTTCCATTGCTG
prgH_N25X_QC_r	CAG CAA TGG AAA CTC ACA GCC CTA CAG TGA GCT GTT AAG TAA TCG AAC
prgH_R35X_QC_f	G TTT CCA TTG CTG ACA GGC TAG ACA CTC TTT GTG GTA GGT CAG
prgH_R35X_QC_r	CTG ACC TAC CAC AAA GAG TGT CTA GCC TGT CAG CAA TGG AAA C
prgH_Q104X_QC_f	G GTG CAA TTA AAT ACG CCA ATA TAG GTC GGT GAA TTG CTT ATC

prgH_Q104X_QC_r	GAT AAG CAA TTC ACC GAC CTA TAT TGG CGT ATT TAA TTG CAC C
prgH_R95X_QC_f	GCT GAA AGA AGG AAA TTC TGA ATC TTA GTC GGT GCA ATT AAA TAC GCC AAT ACA G
prgH_R95X_QC_r	CTG TAT TGG CGT ATT TAA TTG CAC CGA CTA AGA TTC AGA ATT TCC TTC TTT CAG C
prgH_N91X_QC_f	TCC ATG AGC TGA AAG AAG GAT AGT CTG AAT CTC GTT CGG TGC
prgH_N91X_QC_r	GCA CCG AAC GAG ATT CAG ACT ATC CTT CTT TCA GCT CAT GGA
prgH_H66X_QC_f	GCT TTT TTA TCC CGC TGG ACT AGG GCG GAG TAA ATT TTG AAA TCC
prgH_H66X_QC_r	GGA TTT CAA AAT TTA CTC CGC CCT AGT CCA GCG GGA TAA AAA AGC
prgH_E89X_QC_f	CGA AAT TAT ACT CCA TGA GCT GAA ATA GGG AAA TTC TGA ATC TCG TTC G
prgH_E89X_QC_r	CGA ACG AGA TTC AGA ATT TCC CTA TTT CAG CTC ATG GAG TAT AAT TTC G
prgH_F29X_QC_f	TCA CTG AAC GGC TGT GAG TAG CCA TTG CTG ACA GGC
prgH_F29X_QC_r	GCC TGT CAG CAA TGG CTA CTC ACA GCC GTT CAG TGA
prgH_Q51X_QC_f	CGC TCA CTG CTT CAG GTT AGC TCC CTG ATA TAC CTG C
prgH_Q51X_QC_r	GCA GGT ATA TCA GGG AGC TAA CCT GAA GCA GTG AGC G
prgH_D54X_QC_f	CTT CAG GTC AAC TCC CTT AGA TAC CTG CCG ATA GCT TTT TTA TC
prgH_D54X_QC_r	GAT AAA AAA GCT ATC GGC AGG TAT CTA AGG GAG TTG ACC TGA AG
prgH_L46X_QC_f	GTA GGT CAG AGT GAT GCG TAG ACT GCT TCA GGT CAA CTC
prgH_L46X_QC_r	GAG TTG ACC TGA AGC AGT CTA CGC ATC ACT CTG ACC TAC
prgH_D44X_QC_f	CTC TTT GTG GTA GGT CAG AGT TAG GCG CTC ACT GCT TCA GG
prgH_D44X_QC_r	CCT GAA GCA GTG AGC GCC TAA CTC TGA CCT ACC ACA AAG AG

Parts of this result section (Part 1) have been published in:

- Conserved salt bridges facilitate assembly of the helical core export apparatus of a *Salmonella enterica* type III secretion system

  Nidhi Singh, Thales Kronenberger, Andrea Eipper, Felix Weichel, Mirita Franz, Boris Macek, Samuel Wagner (revision submitted)

4. Results

Part 1: Conserved salt bridges facilitate assembly of the helical core export apparatus of a *Salmonella* enterica type III secretion system

This study concentrates on exploring the role of the conserved charged residues in the assembly of T3SS and also in its function. The export apparatus of the T3SS arranges itself into a unique helical complex constituted by four hydrophobic proteins SctR, SctS, SctT, and SctU and these proteins contain numerous extremely conserved charged residues within their hydrophobic domains. These charged residues form several inter- and intramolecular salt bridges, which need to be broken to open the secretion pore of the injectisome. Mutagenesis of individual conserved residues in virulence-associated as well as related flagellar T3SS manifested either compromised assembly, or secretion. Nonetheless, the exact role of these conserved charged residues in the assembly and function of T3SS has remained elusive. Here, we performed an in-depth mutagenesis analysis of these residues in the T3SS of *Salmonella* Typhimurium, coupled with blue native PAGE, *in vivo* photocrosslinking, and luciferase-based secretion assays.

4.1 Functional analysis of mutants of $SctS_{E44}$, $SctS_{K52}$, and $SctT_{R204}$

$SctS_{E44}$, $SctS_{K52,}$ and $SctT_{R204}$ are the highly conserved charged positions in the respective proteins of the T3SS. In order to decipher their role in the assembly and function of the T3SS encoded by the SPI-1, the following replacements were done: $SctT_{R204}$ was either replaced by alanine (R204A) or by glutamine (R204Q). Similarly, the $SctS_{E44}$ position was replaced either by aspartic acid (E44D) or by glutamine (E44Q), while $SctS_{K52}$ was replaced either by alanine (K52A) or by glutamine (K52Q).

All of the SctS and SctT mutant variants mentioned above were expressed in an inducible manner by the addition of rhamnose with the help of the low copy number pT10-SctRSTU

plasmid. SctT was C-terminally tagged by 3x FLAG to enable its detection, whereas SctS, unfortunately, could not be tagged. As a substitute, we determined the accumulation levels of SctS along with the complex assembly of the autocleavage-deficient SctU mutant, which was C-terminally by 3x FLAG tag, since the assembly of SctU exclusively demands prior assembly of SctS. The sole objective behind using the autocleavage-deficient mutant of SctU was to observe the expression of full-length SctU. We used the *S.* Typhimurium *ΔsctRSTU* mutant strain, which further expressed a chromosomally encoded NanoLuc luciferase (NL)-tagged effector protein SipA (SipA-NL) as our background strain [177]. Together with all other derived mutagenized plasmids, the wild type was placed in the background strain mentioned above.

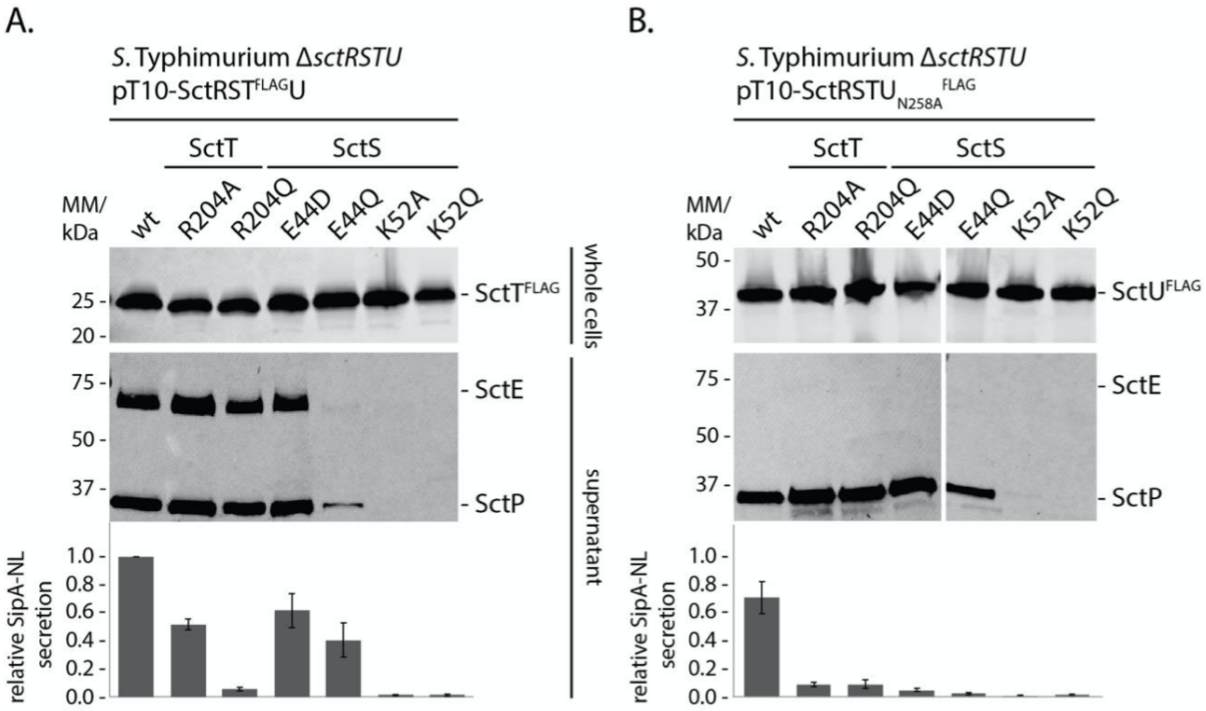

Figure 8: Functional analysis of mutants of $SctS_{E44}$, $SctS_{K52}$, and $SctT_{R204}$. A. Top: Immunodetection of $SctT^{FLAG}$ on Western blots of SDS PAGE-separated whole-cell samples of *S*. Typhimurium expressing the indicated plasmid-complemented SctT and SctS mutants. Middle: Immunodetection of the type III-secreted early substrate SctP and the intermediate substrate SctE on Western blots of SDS PAGE-separated culture supernatants of the indicated plasmid-complemented SctT and SctS mutants. Bottom: Luminescence of type III-secreted SipA-NL measured in the supernatant of cultures of the indicated plasmid-complemented SctT and SctS mutants. **B.** As in A. but expressing $SctU_{N258A}{}^{FLAG}$ instead of $SctT^{FLAG}$. These results are representative of n=3 independent experiments. Error bars show the standard deviation of a student's t-test.

In order to ascertain if any replacement or mutation of the conserved charged residues resulted in altered function of the T3SS, we determined secretion of the early substrate SctP (needle length regulator) along with the secretion of the intermediate substrate SctE (major

translocon component) in the culture supernatant by Western blotting. The detection of the late substrate SipA-NL (effector) was done by luminometry (Fig. 8).

On the one hand, for $SctT_{R204}$ mutants, we did not observe any persistent remarkable secretion defect in the $SctT^{FLAG}$ background for the early substrate SctP and the intermediate substrate SctE secretion. Notably, secretion of late substrate SipA-NL in case of $SctT_{R204Q}$ mutant seemed defective (Fig. 8A). While on the other hand, further reduction in the secretion of the late substrate SipA-NL was observed in the case of $SctT_{R204A}$ and autocleavage-deficient $SctU_{N258A}{}^{FLAG}$ double mutant background (Fig. 8B). This observation uncovered a potential synergistic effect of $SctT_{R204A/Q}$ and $SctU_{N258A}$ mutations on the secretion of the late substrates.

$SctS_{E44D}$ mutant exhibited comparable results (Fig. 8A,B) while the $SctS_{E44Q}$ mutant displayed even severe alarming defects in decreased secretion of the early and intermediate substrates in the $SctT^{FLAG}$ background also (Fig. 8A). All SctS mutants with replaced K52 positions consistently displayed enormous defects in secretion of all three screened substrates (Fig. 8A). This observation was independent of the backgrounds or FLAG tag positions as in the case of $SctT^{FLAG}$ (Fig. 8A) or for $SctU_{N258A}{}^{FLAG}$ (Fig. 8B).

Collectively, these results recommended that SctS positions E44 ($SctS_{E44}$) and K52 ($SctS_{K52}$) are paramount and crucial for the functional competence of the T3SS. However, the R204 position in SctT ($SctT_{R204}$) appeared to be playing a slightly less prominent role. In light of the synergistic effect on the secretion of the late substrates, $SctT_{R204}$ behaved like the $SctS_{E44D}$ mutant in the autocleavage-deficient SctU background (Fig. 8B).

4.2 Analysis of the assembly of mutants of $SctS_{E44}$, $SctS_{K52}$, and $SctT_{R204}$

The functional incompetence or the compromised and impeded secretion phenotype of the assessed mutants might potentially be an outcome of defective assembly of the export apparatus. Therefore, for evaluating the mutagenesis effects of the salt bridge forming SctS and SctT residues on the assembly of the helical $SctR_5S_4T_1U_1$ complex, blue native (BN) PAGE was performed for establishing the composition of the complex.

BN PAGE is an electrophoretic method for investigating the composition of membrane-bound protein complexes [178]. This method uses nonionic detergents for mild extraction of membrane proteins or membrane protein complexes that are expected to protect protein conformation in their native state. It is handy for a qualitative and quantitative assessment of needle complex assembly, including base and export apparatus components.

Crude membrane isolation of each complemented strain was done, followed by its solubilization with the help of non-ionic mild detergent lauryl maltose neopentyl glycol (LMNG). Compared with dodecyl maltopyranoside (DDM), LMNG efficiently solubilizes and stabilizes challenging membrane proteins [179] and is known to be able to maintain the integrity of the inner membrane SctRT, SctRST, and SctRSTU complexes both in flagellar as well as in injectisome homologs [43,83,180].

The results obtained from BN PAGE analysis of the strains co-expressing either of the two $SctS_{K52}$ mutant variants exposed the failure of the assembly process. Although the competence of forming SctRT complexes was unaltered, further successful integration of SctRST and SctRSTU complexes could not be achieved for the two $SctS_{K52}$ mutant variants (Fig. 9A,B). Additionally, $SctS_{E44Q}$ mutants displayed a substantial decrease in the potential of assembling SctRST and SctRSTU complexes. Assembly of SctRST and SctRSTU complexes remained unaltered in $SctT_{R204A/Q}$ and $SctS_{E44D}$ mutants (Fig. 9B).

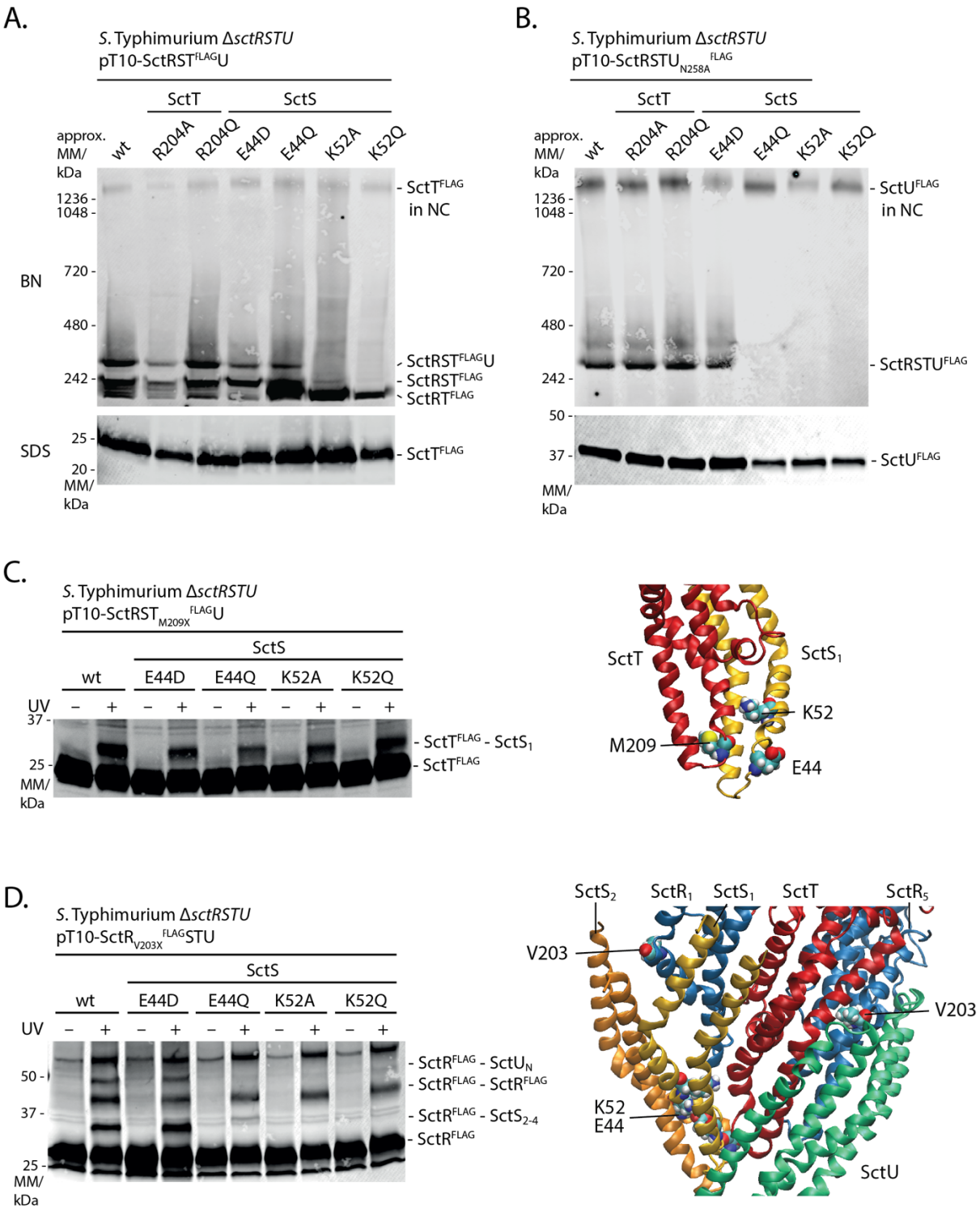

Figure 9: Analysis of the assembly of mutants of $SctS_{E44}$, $SctS_{K52}$, and $SctT_{R204}$. A. Top: Immunodetection of $SctT^{FLAG}$ on Western blots of BN PAGE-separated crude membrane samples of *S.* Typhimurium expressing the indicated plasmid-complemented SctT and SctS mutants. Indicated is also which band corresponds to which complex composition [3,9]. Bottom: Immunodetection of $SctT^{FLAG}$ on Western blots of SDS PAGE-separated crude membrane samples of *S.* Typhimurium expressing the indicated plasmid-complemented SctT and SctS mutants.

B. As in A. but expressing $SctU_{N258A}^{FLAG}$ instead of $SctT^{FLAG}$. **C.** Immunodetection of $SctT_{M209X}^{FLAG}$ on Western blots of SDS PAGE-separated crude membrane samples of *S*. Typhimurium expressing the indicated plasmid-complemented SctS mutants. Each sample is shown with (+) and without (-) UV-irradiation to induce photocrosslinking of *p*Bpa at position 209 of SctT to the first SctS ($SctS_1$). The structural position of $SctT_{M209}$ relative to the targeted $SctS_1$ and of the two mutated residues $SctS_{E44}$ and $SctS_{K52}$ is shown on the right. **D.** Immunodetection of $SctR_{V203X}^{FLAG}$ on Western blots of SDS PAGE-separated crude membrane samples of *S*. Typhimurium expressing the indicated plasmid-complemented SctS mutants. Each sample is shown with (+) and without (-) UV-irradiation to induce photocrosslinking of *p*Bpa at position 203 of SctR to $SctS_{2\text{-}4}$ and SctU, respectively. The structural position of $SctR_{V203}$ relative to the targeted $SctS_2$ and SctU, respectively, and of the two mutated residues $SctS_{E44}$ and $SctS_{K52}$ is shown on the right. Abbreviations: NC: needle complex. The results are representative of n=3 independent experiments.

Furthermore, the crude membrane isolates of $SctS_{E44Q}$, $SctS_{K52A}$, and $SctS_{K52Q}$ mutants exhibited diminished accumulation levels of $SctU_{N258A}^{FLAG}$. The failure in the assembly of SctRSTU complexes indicated decreased stability of SctU. Intriguingly, the presence of a band corresponding to >1248 kDa in size suggested a circumstantial assembly of $SctS_{E44Q}$, $SctS_{K52A}$, and $SctS_{K52Q}$ mutants into the injectisome. The sole plausible rationale behind this observation despite the presence of mutations in SctS is that a reasonably tiny share of SctU managed to get integrated into the SctRST complex and finally become a part of the protected base structure.

For the sake of checking the reliability of the results obtained from plasmid-based complementation, the same mutations for all of the six positions were introduced into the chromosomally encoded genes, too (Fig. 10). BN PAGE analysis of the crude membrane isolates from chromosomally encoded strains further validated our previous observations that the assembly process of the needle complex gets interrupted after the stage of SctRT complex formation in $SctS_{E44Q}$, $SctS_{K52A}$, and $SctS_{K52Q}$ mutants. Nevertheless, some complexes still manage to assemble, leading to the formation of the SctRSTU complexes and their successful integration into the needle complex (Fig. 10B,D). Moreover, chromosomally encoded $SctS_{E44D}$ mutation strikingly displayed a stronger predominance of the SctRST complex than that of the SctRT complex (Fig. 10B), thereby implying the stabilized and sustained assembly status of mutant $SctS_{E44D}$.

In the case of injectisomes, the BN PAGE protocol is limited to complexes and subcomplexes that are considerably stable and present in ample amounts in order to be determined. Not every assembly intermediate involved in the assembly process fulfills the given criteria. Even though BN PAGE provides concurrent information regarding the size and complex composition across the entire complex space of a given protein, yet it banks on detergent

extraction, which could fragment the protein complexes to a certain degree. Also, this method fails to offer structural information concerning specific pairwise interactions.

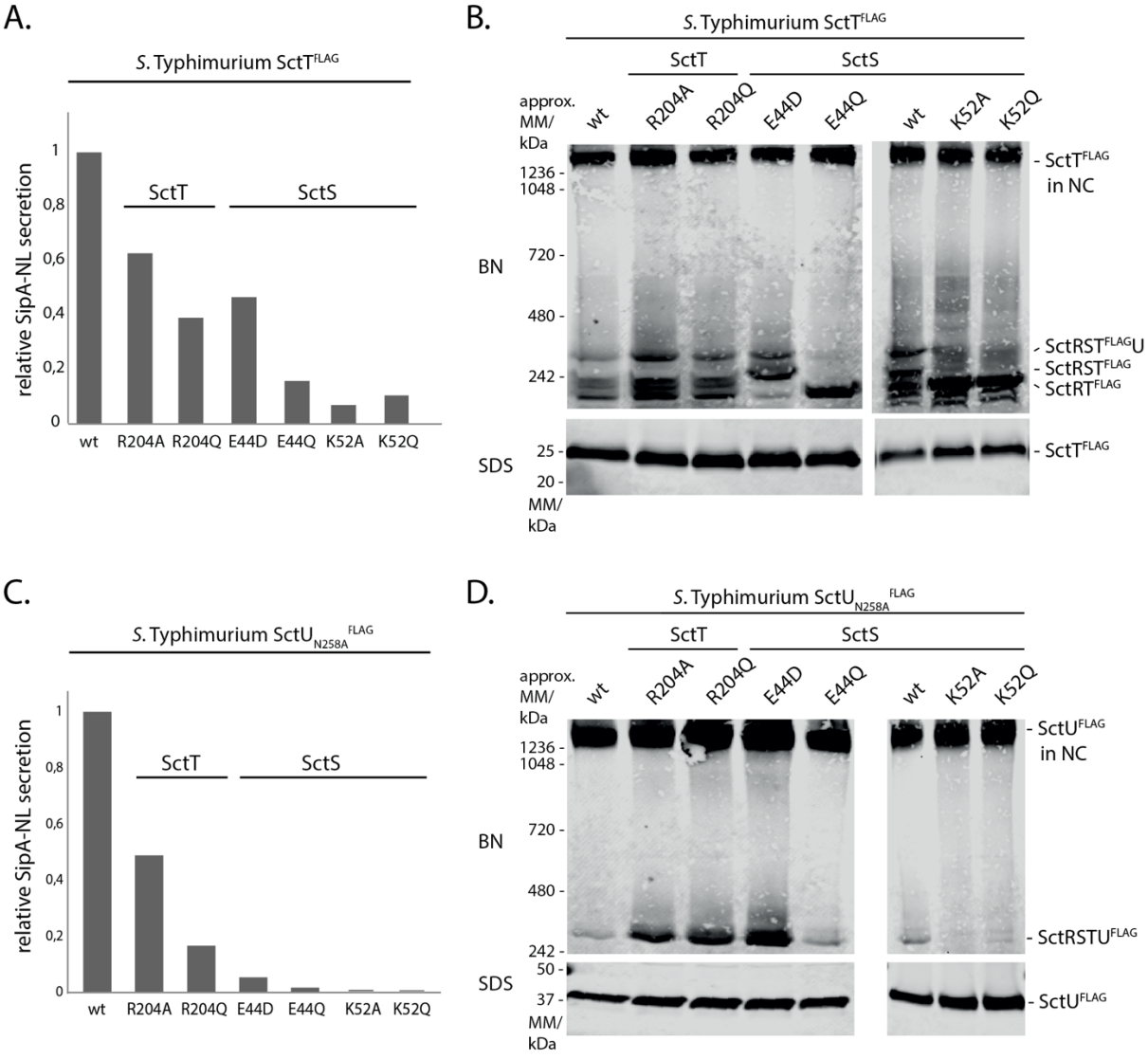

Figure 10: Analysis of function and assembly of chromosomal mutants of $SctS_{E44}$, $SctS_{K52}$, and $SctT_{R204}$. A. Luminescence of type III-secreted SipA-NanoLuc measured in the supernatant of cultures of the indicated chromosomal SctT and SctS mutants in a $SctT^{FLAG}$ background. **B.** Top: Immunodetection of $SctT^{FLAG}$ on Western blots of BN PAGE-separated crude membrane samples of *S*. Typhimurium expressing the indicated chromosomal SctT and SctS mutants. Indicated is which band corresponds to which complex composition [77,83]. Bottom: Immunodetection of $SctT^{FLAG}$ on Western blots of SDS PAGE-separated crude membrane samples of *S*. Typhimurium expressing the indicated chromosomal SctT and SctS mutants. **C. & D.** As in A. & B. but in a $SctU_{N258A}^{FLAG}$ strain background instead of $SctT^{FLAG}$. The results are representative of n=3 independent experiments.

In order to overcome the limitations of BN PAGE in assembly assessment of the hydrophobic export apparatus components and capture assembly intermediates, we extensively employed

in vivo photocrosslinking to complement the information obtained already from BN PAGE regarding the SctRSTU complex assembly in SctS E44 and K52 mutants.

In vivo photocrosslinking depends on the genetic encoding of the UV- reactive artificial crosslinking amino acid *para*- benzoyl- phenylalanine (*p*Bpa) with the assistance of the suppressed amber stop codons (UAG), which can be introduced by site-directed mutagenesis at any position of interest in a protein [45,175]. As a result of UV irradiation, free radicals are formed by *p*Bpa, which tend to crosslink with the nearby interacting proteins. This *p*Bpa crosslink evidences the occurrence of a specific protein-protein interaction that can be visualized by immunoblotting the crosslinked proteins. This method, since the incorporation of *p*Bpa already occurs during translation, makes remote or obscured positions within the membrane or positions enclosed within the core of the proteins or protein complexes more approachable. Together with genetics, this technique gives a chance to draw inferences and conclusions regarding the terms that need to be fulfilled to accomplish the assembly of any given protein complex.

Previous studies in our lab aiming to resolve the early assembly stages of the T3SS export apparatus probed for many specific pairwise protein interactions such as SctR-SctS, SctR-SctU, and SctT-SctS with the help of *in vivo* photocrosslinking. Extensive mapping of different protein-protein interactions of the export apparatus components SctR and SctS by probing amino acid positions within each predicted TMS was done [80]. Signature crosslinks establishing SctR-SctS and SctR-SctU interactions at $SctR_{V203X}$ position (X for *p*Bpa) were detected together with another interaction of SctT-SctS at $SctT_{M209X}$ position [80]. Based on these prior pieces of information, we encoded *p*Bpa at specific positions, which would permit the assembly assessment of the first SctS subunit with $SctT_{M209X}^{FLAG}$ and further assembly of the subsequent SctS subunits as well as the interaction of SctU with $SctR_{V203X}^{FLAG}$ (Fig. 9C,D) [80].

The *S*. Typhimurium *ΔsctRSTU*, SipA-NL background strain with respective SctS mutations at E44 and K52 positions and SctS wild type was used for crosslinking experiments. The pBpa mutants were additionally expressed from pT10-SctRSTU plasmid. Intact bacterial cells (whole cells) were irradiated with UV for crosslinking, followed by SDS PAGE of the crude membrane isolates. Consistent with our expectations, even in the presence of $SctS_{E44D/Q}$ and $SctS_{K52A/Q}$ mutations, we detected unaltered SctR-SctR interactions. The crosslinks obtained with $SctR_{V203X}^{FLAG}$ explicitly showed wild type comparable SctR-SctR interactions (Fig. 9D). The crosslinking results of $SctT_{M209X}^{FLAG}$ distinctly exhibited that $SctS_{E44D/Q}$ and $SctS_{K52A/Q}$ mutations apparently did not alter the assembly of the first SctS subunit onto the SctRT

complex (Fig. 9C). On the contrary, crosslinking results of $SctR_{V203X}^{FLAG}$ displayed impaired assembly of the $SctS_{2-4}$ subunits in addition to SctU as well in $SctS_{E44Q}$ and $SctS_{K52A/Q}$ mutations. However, this was not the case for $SctS_{E44D}$ mutants, and the assembly appeared comparable to that of the wild type strain (Fig. 9D).

Considering all the results together, eventually, SctS positions E44 and K52 appear to be pivotal for the assembly of $SctS_{2-4}$ subunits onto the SctRT complex, further affecting the assembly of SctU. However, recruitment of $SctS_1$ subunit appears to be uninfluenced in these mutants, inferring that their transmembrane topology or folding did not face any major deformity or flaws. Despite the introduced mutations, the assembly of the needle complex could still take place. This observation establishes that the detected secretion defects were not a consequence of impaired core export apparatus assembly, instead emphasizing a direct involvement of the mutated positions in the secretion function of the needle complex.

4.3 The conserved intramolecular salt bridge-forming residues $SctR_{K198/D173}$ and $SctT_{K219/E196}$ correspond to the $SctS_{K52/E44}$ pair in structure, assembly, and function

Until now, both $SctS_{K52}$ and $SctS_{E44}$ positions have been ascertained crucial for the assembly of the SctRSTU core export apparatus as well as for its function. However, the $SctS_{E44}$ mutant exhibited a considerably milder defect. On the other hand, $SctT_{R204}$ appeared to be insignificant concerning the assembly and function of the T3SS core export apparatus. Also, $SctT_{R204}$ did not correspond to $SctS_{K52}$ referring to the salt bridge formation with $SctS_{E44}$ as initially predicted at the project's conception.

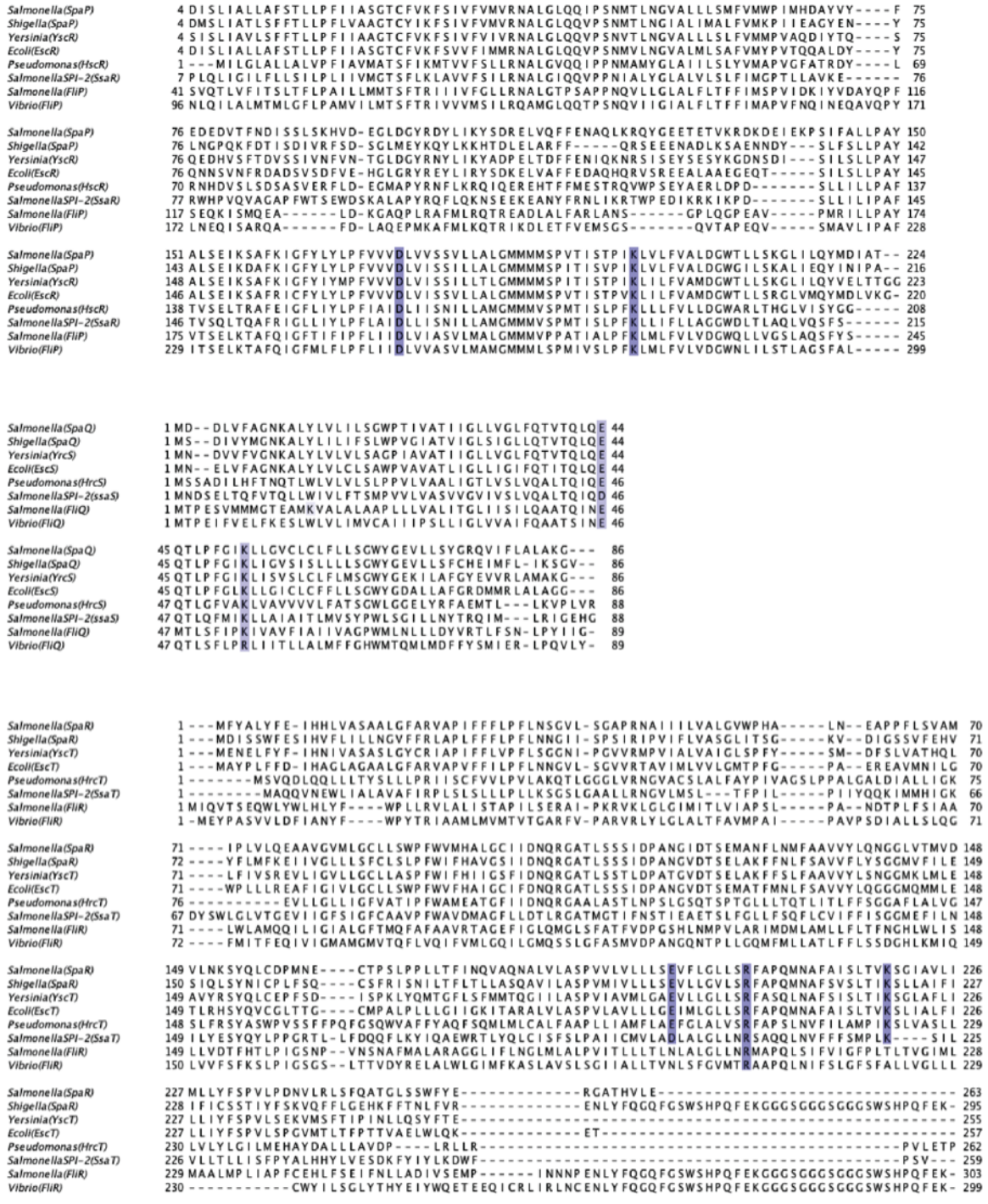

Figure 11: Amino acid sequence alignment of *S.* Typhimurium SctR (SpaP), SctS (SpaQ), and SctT (SpaR) and its homologs in type III secretion systems from other pathogenic bacteria as well as from flagellar systems. Included in the alignment are SpaP/SctR, SpaQ/SctS, SpaR/SctT from *S. typhimurium* (PDB number 6Q15), SpaP, SpaQ, SpaR from *Shigella flexneri* (PDB number 6R6B), YscR, YscS, YscT from *Yersinia enterocolitica*, EscR, EscS, EscT from *E. coli*, HrcR, HrcS, HrcT from *Pseudomonas aeruginosa*, SsaR, SsaS, SsaT from *S. typhimurium* SPI-2, FliP, FliQ, FliR from *Salmonella* flagellar type III secretion system (PDB number 6R69) and FliP, FliQ, FliR from *Vibrio mimicus* flagellar type III secretion system (PDB number 6S3S). Positions of

interest for this work have been highlighted in blue: SpaP$_{D173}$, SpaP$_{K198}$, SpaQ$_{E44}$, SpaQ$_{K52}$, SpaR$_{E196}$, SpaR$_{R204}$, SpaR$_{K219}$. MAFFT [181] was used with default settings to create multiple sequence alignments. Alignment visualization was done with Jalview [182].

In-depth exploration of SctRSTU structure informed that conserved lysine residue positions of SctR and SctT are structurally homologous to SctS$_{K52}$: SctR$_{K198}$ and SctT$_{K219}$ positions (Fig. 11, Fig. 12A). Intramolecular salt bridges are formed by SctR$_{K198}$ and SctT$_{K219}$ with SctR$_{D173}$ and SctT$_{E196,}$ respectively whereas, SctS$_{K52}$ forms intermolecular salt bridges with SctS$_{E44}$ (Fig. 12A).

After establishing that the SctS$_{K52}$ position plays a crucial role in integrating SctS$_{2-4}$ subunits with the SctRT complex. SctR$_{K198}$ and SctT$_{K219}$ positions became our next target because of their structural homology with SctS$_{K52}$. Therefore, to determine the role of SctR$_{K198}$ and SctT$_{K219}$ positions in the assembly, conserved lysine residues were replaced by alanine residues. The aftereffects of these modifications regarding the assembly and activity of the T3SS in SctR and SctT variants were investigated. Accordingly, the *S.* Typhimurium *ΔsctRSTU*, SipA-NL background strain was transformed with pT10 plasmid derivatives encoding either SctRST$_{K219A}$^{FLAG}U or SctR$_{K198A}$^{FLAG}STU. The functionality of the secretion system in the case of SctT$_{K219A}$ and SctR$_{K198A}$ mutants was evaluated after 5 h of culture growth by assessing type III- dependent secretion of various substrate proteins (SctP, SctE, and SipA-NL) in the culture supernatant by Western blot (SctP and SctE) and luminometry (SipA-NL) (Fig. 12B). The results obtained for the mutant strain expressing SctT$_{K219A}$ exhibited failed secretion of the intermediate substrate SctE and extreme depletion in the secretion levels of the early substrate protein SctP and late effector protein SipA in comparison to the wild type strain (Fig. 12B). Based on these results, the SctT$_{K219}$ position appeared to be crucial for maintaining the secretion system's functional competence. Meanwhile, the mutant strain expressing SctR$_{K198A}$ continued secretion of the early substrate protein SctP but exhibited a decline in the secretion levels of the intermediate substrate SctE and late effector protein SipA-NL (Fig. 12B). Although, expression of FLAG-tagged SctR$_{K198A}$ was poorly detectable in whole cell lysates (Fig. 12C), suggesting that K198A mutation leaves SctR unstable. Consequently, the functionality of the T3SS gets compromised.

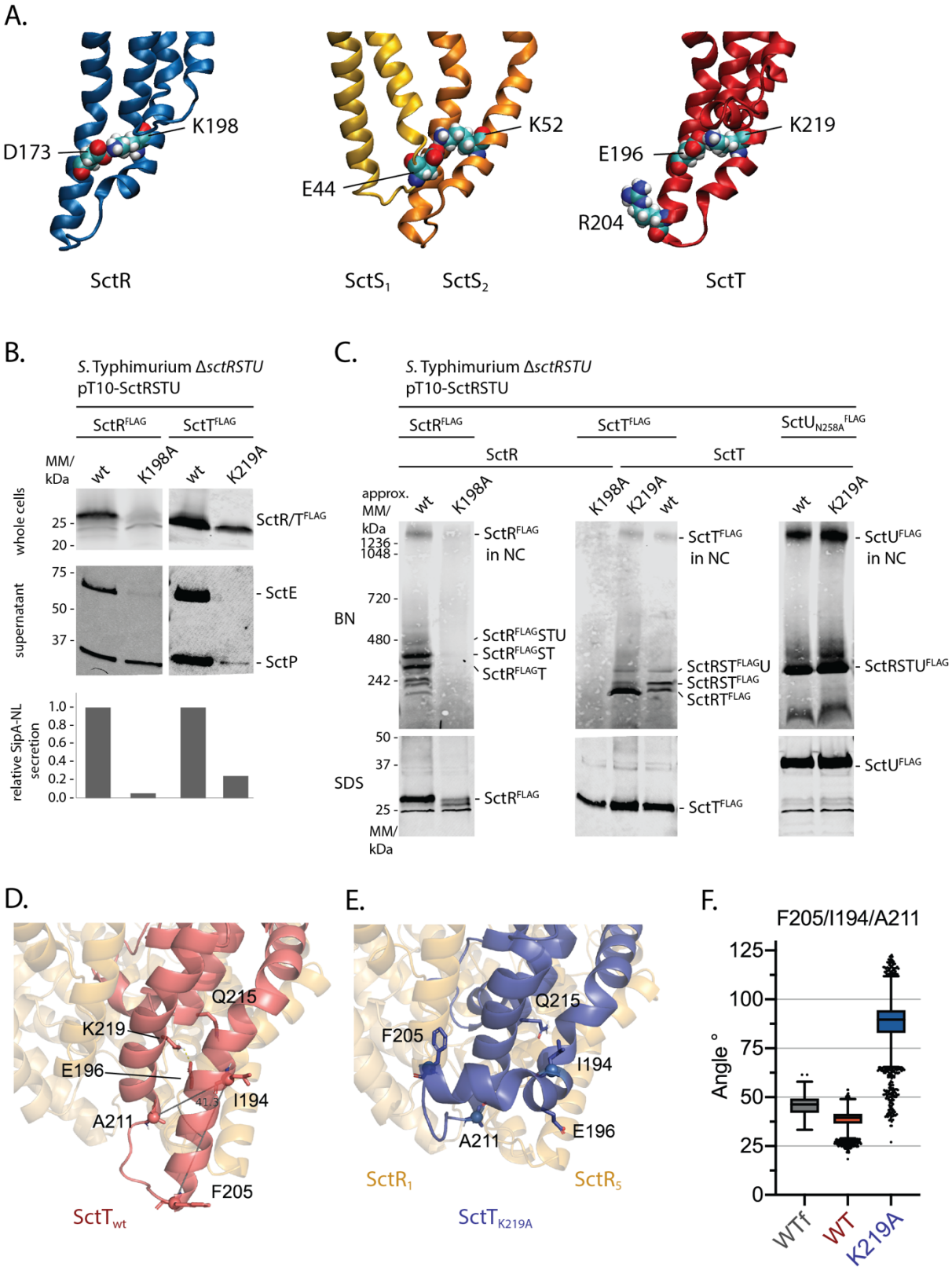

Figure 12: Analysis of function and assembly of mutants of $SctR_{K198}$ and $SctT_{K219}$. A. Structures showing the positions of the indicated residues and the intermolecular and intramolecular salt bridges they form. Note the similar structural location of $SctR_{K198}$, $SctS_{K52}$, and $SctT_{K219}$. **B.** Top: Immunodetection of $SctR^{FLAG}$ and $SctT^{FLAG}$,

respectively, on Western blots of SDS PAGE-separated whole cell samples of *S*. Typhimurium expressing the indicated plasmid-complemented SctR and SctT mutants. Middle: Immunodetection of the type III-secreted early substrate SctP and the intermediate substrate SctE on Western blots of SDS PAGE-separated culture supernatants of the indicated plasmid-complemented SctR and SctT mutants. Bottom: Luminescence of type III-secreted SipA-NanoLuc measured in the supernatant of cultures of the indicated plasmid-complemented SctR and SctT mutants. **C.** Top: Immunodetection of $SctR^{FLAG}$, $SctT^{FLAG}$, and $SctU_{N258A}{}^{FLAG}$, respectively, on Western blots of BN PAGE-separated crude membrane samples of *S*. Typhimurium expressing the indicated plasmid-complemented SctR and SctT mutants. Indicated is also which band corresponds to which complex composition [77,83]. Bottom: Immunodetection of $SctR^{FLAG}$, $SctT^{FLAG}$, and $SctU_{N258A}{}^{FLAG}$, respectively, on Western blots of SDS PAGE-separated crude membrane samples of *S*. Typhimurium expressing the indicated plasmid-complemented SctR and SctT mutants. The results represent n=3 independent experiments. **D.** and **E.** Representative structures derived from molecular dynamics simulations for the $SctT_{wt}$ (D.) and $SctT_{K219A}$ (E.). Both images (D, E.) highlight as sticks residues the mutation site and residues involved in stabilization (K219, E196, and Q215), as well as residues utilized as coordinate references for angle calculation (I194, A211, and F205). **F.** Boxplot represents observed angle values in the different simulated systems, the central box line represents the average, and the points represent TukTukey'sermined outliers. The reference angle of 41.3° is depicted in (**D**).

Following the same approach as before, we intended to analyze the effect of $SctR_{K198}$ and $SctT_{K219}$ mutations on assembly of the SctRSTU complex and the injectisome by BN PAGE, Western blotting, and immunodetection of $SctR^{FLAG}$, $SctT^{FLAG,}$ or $SctU_{N258A}{}^{FLAG}$, respectively. Substitution of $SctT_{K219}$ position with alanine distinctly disturbed the progression of the $SctR_5T_1$ complex stage to the successive $SctR_5S_4T_1$ complex stage while $SctR_5S_4T_1U_1$ complex levels, as well as the injectisome levels, remained identical to the wild type (Fig. 12C). On the contrary, $SctR_{K198A}$ mutation led to a severe assembly defect with no detectable levels of SctRSTU precursor complex (Fig. 12C).

All-inclusive, these data suggest that omission of these charged residues surprisingly does not affect the assembly of the mutated subunit itself, instead leads to the failure of assembly of the following subsequent subunits in the assembly process:

(1) The $SctR_{K198A}$ mutation destroyed the assembly of the SctRSTU subcomplex, presumably by impairing the interactions between the first and the second SctR. Therefore, $SctR_{K198A}$ was extremely unstable and degraded.

(2) The $SctT_{K219A}$ mutation exhibited efficient assembly of SctRT complexes, but its progression to the following assembly stage of SctS addition was hindered, as concluded from BN PAGE analysis.

(3) The $SctS_{E44Q}$ and $SctS_{K52A/Q}$ mutations did not impede the assembly up to the $SctR_5T_1SctS_1$ complex stage, but after that, further addition of the remaining SctS subunits as well as SctU could not take place, leading to a destabilized SctU in these mutants.

Further analysis of $SctR_{K198}$ and $SctT_{K219}$ positions revealed that they form intramolecular salt bridges with $SctR_{D173}$ and $SctT_{E196}$, respectively. In order to comprehend the way by which salt bridges assist in the assembly of the SctRSTU complex, a molecular dynamics simulation was run by our collaborating colleague for comparing the flexibility of complexes containing the wild type SctT and the $SctT_{K219A}$ mutant, respectively. The assessment was accomplished with an integrated model of the SctFIRSTU complex based on the reported *Salmonella* Typhimurium T3SS-1 SctFIRST and the *Vibrio mimicus* FliPQR-$FlhB_N$ structures [83,163]. This simulation study indicated that the $SctT_{K219A}$ mutant goes through conformational changes in the Ile194-Ala211 helix-loop region (Fig. 12D-F), leading to a compromised SctS assembly interface. Particularly, the $SctT_{K219A}$ mutation not only appeared to be preventing the interaction with $SctT_{E196A}$ but also disturbed the interaction network with $SctT_{S215}$ and $SctT_{Q105}$. Lack of this particular salt bridge has exceeding conformational effects, thereby accentuating the flexibility of the Ile194-Ala211 region, which could contribute to the detected defects in the assembly of the SctRST complex.

In summary, molecular dynamics simulations of the $SctRST_{K219A}$ mutant complex also further consolidated that these conserved salt bridges are not critical for the assembly of the respective protein but rather facilitate the assembly of the following subunit by stabilizing the last helical hairpin of the respective protein (Fig. 12A). Therefore, owing to the conserved structural positions of $SctS_{K52}$, $SctR_{K198,}$ and $SctT_{K219,}$ it is plausible that the conformational changes simulated for $SctT_{K219}$ underlie the assembly defects of the $SctS_{K52A/Q}$, $SctR_{K198A}$ mutants too. Our results additionally indicate that these conserved charged residues are also indispensable for type III secretion and exhibit a functional link between $SctS_{E44}$ and $SctT_{R204}$ and the cytoplasmic domain of SctU in gating the T3SS injectisome. Overall, the presented results impart an unprecedented insight into the delicate requirements for the assembly and function of the unique hydrophobic helical core export apparatus of the T3SS.

This result section (Part 2) is in preparation:

- Interaction of SctD with SctK in *Salmonella enterica* type III secretion system

Nidhi Singh, Thales Kronenberger, Sam Ulrich, Iwan Grin, Samuel Wagner

Part 2: Interaction of SctD with SctK in *Salmonella* enterica type III secretion system (in preparation)

T3SS comprises many different proteins, and the exact interactions amongst constituent proteins are not fully understood, with numerous open questions about the intricate details of the assembly process still being left open. A dynamic cytoplasmic sorting platform with a rigidly anchored basal body and a needle filament conjointly constitute the injectisome (see section 1.5). The inner membrane ring (IR) protein SctD has its periplasmic and cytoplasmic domains linked by a single-pass transmembrane helix. The sorting platform exists underneath the basal body and is formed by centrally placed ATPase SctN linked to six radially spoked SctQ 'pods' by SctL proteins. Adaptor protein SctK mutually interacts and bridges the SctQ pods of the sorting platform to the cytosolic domain of SctD [62,63].

Although the interaction amidst IR and the sorting platform components is critical for the principal activity of type III secretion systems (see section 1.3.1, 1.3.2, and 1.5), our grasp and comprehension regarding these interactions are particularly limited. In the beginning of this study, the high-resolution structure of the adaptor protein SctK was not known, therefore, we started with exploring the interactions between cytoplasmic components SctK and its interacting partner SctD in the inner membrane. Here, we performed an in-depth analysis of the interacting positions in the T3SS of *Salmonella* Typhimurium, coupled with *in vivo* photocrosslinking, luciferase-based secretion assays, and different functional assays. In particular, since there is no structure of the SctD-SctK complex known yet, we set out to acquire the information suggesting the correct orientation of the IR in the T3SS, highlighting the interacting interface of SctD-SctK. Additionally, motivated by the findings of Wimmi et al. in the T3SS of *Yersinia*, where they suggested that an adaptive regulatory interface is established by the cytosolic components of the secretion system in response to change in environmental conditions such as a change in pH [161]. Therefore, we also aimed to obtain experimental support representing the effect of pH change on SctD-SctK interaction. Also, the T3SS is fundamentally a PMF-driven system executing protein export [183–186]. The associated ATPase complex is not exclusively required for protein export, and it has a facilitating role in recognizing and unfolding the substrates and in energy transduction [65]. In

order to analyze and confirm the effect of PMF change on the SctD-SctK interaction, we customized a methodology to monitor the resulting changes both in the presence and absence of compounds such as CCCP which has an inhibitory effect on the PMF.

Since this study involves the characterization of the key components of a functionally competent injectisome, the results obtained are expected to improve our understanding of the entire structure and function of the T3SS.

4.4 Identification of novel molecular interaction sites of SctD-SctK and acquisition of plausible orientation of the SctD monomers in the inner ring of the T3SS

Previous cryo-ET studies of SctD have already established its N-terminus is located in the cytoplasm and links the needle complex to the sorting platform [63]. Therefore, in order to identify via *in vivo* photocrosslinking different amino acid residues that might play a role in the interaction of the cytoplasmic domain of SctD with SctK, we randomly selected different amino acid positions in the N-terminus of SctD where protein-protein interactions with the cytoplasmic components were most likely to occur based on the information obtained from modeling of SctD protein by VMD program (Fig. 13). Thirteen positions in SctD were chosen (L20, N25, F29, D44, L46, Q51, D54, H66, E89, N91, R95, Q104, W119) and were replaced by an amber mutation 'X' encoding the UV- reactive artificial crosslinking amino acid *para*- benzoyl-phenylalanine (*p*Bpa) (see Section 4: Part 1 for experimental details). The amber mutations on SctD were expressed with the help of rhamnose-inducible low copy number derivatives of plasmid pT10-SctD. Detection of SctD was performed by utilizing a C-terminal 3xFLAG tag. The wild type and all derived mutagenized plasmids were introduced in an *S.* Typhimurium *ΔsctD* mutant strain. In order to determine whether any amber mutation at the chosen residual position altered the functional competence of the T3SS, we assessed secretion of the intermediate substrate SctE into the culture supernatant by Western blotting (Fig. 14).

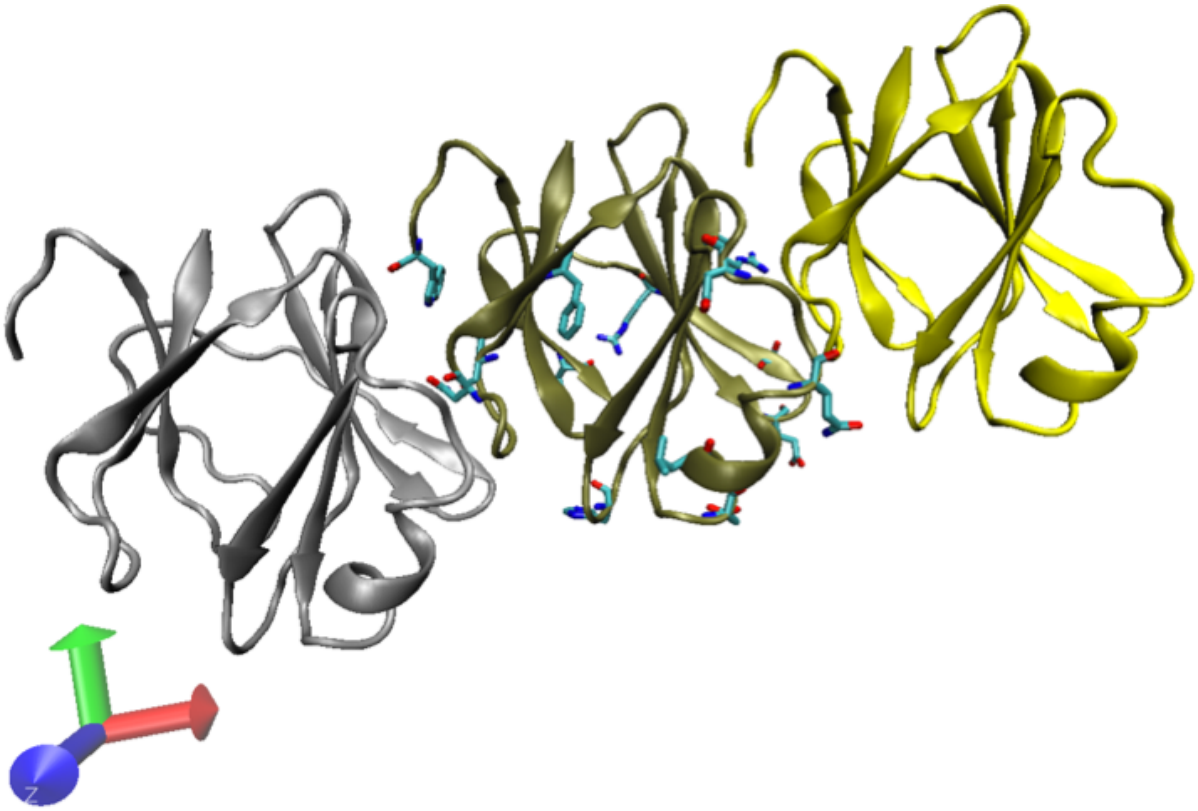

Figure 13: VMD illustration of SctD protein. *p*Bpa mutants used in this study are mapped to the structure of SctD (PDB file PrgHn3J1W.pdb). Amber mutations were introduced in SctD at different positions highlighted by stick representations to identify new interacting cytoplasmic protein partners of SctD using *in vivo* photo-crosslinking. VMD program designed for modeling, visualization, and analysis of proteins, etc., is used to display the structureof SctD protein from the respective PDB files.

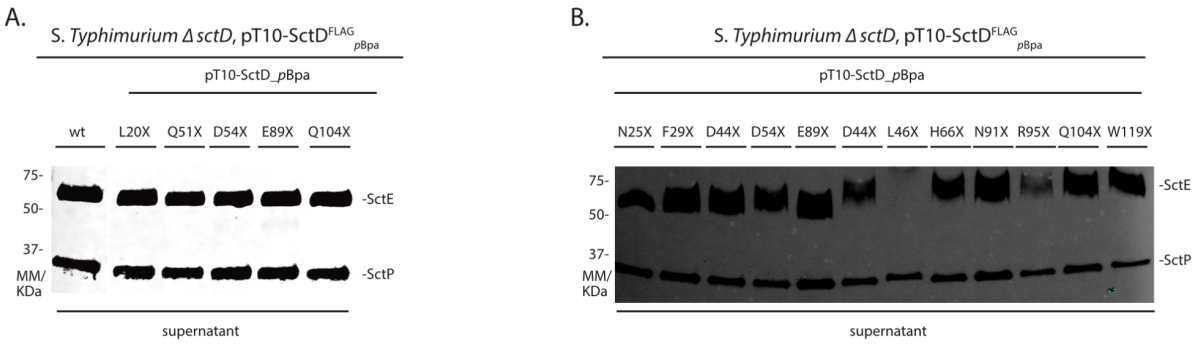

Figure 14: Functional analysis of the T3SS in the different pBpa mutants used in this study. A. Immunodetection of the type III-secreted early substrate SctP and the intermediate substrate SctE on Western blots of SDS PAGE-separated culture supernatants of the indicated *p*Bpa mutants. **B.** As in (A) for more *p*Bpa positions. The results are representative of n=3 independent experiments. Abbreviations: *p*Bpa, *para*- benzoyl-phenylalanine.

While almost all of the *p*Bpa mutants did not show any secretion defect in the secretion of the early substrate secretion of SctP as well in the secretion of the intermediate substrate secretion of SctE (Fig. 14A, B), L46X and R95X *p*Bpa positions failed to secrete intermediate substrate SctE (Fig. 14B). Altogether, these results suggest that, except for L46X and R95X, which might be critical for the functionality of the secretion system, the chosen *p*Bpa positions did not alter the functional competence of the T3SS.

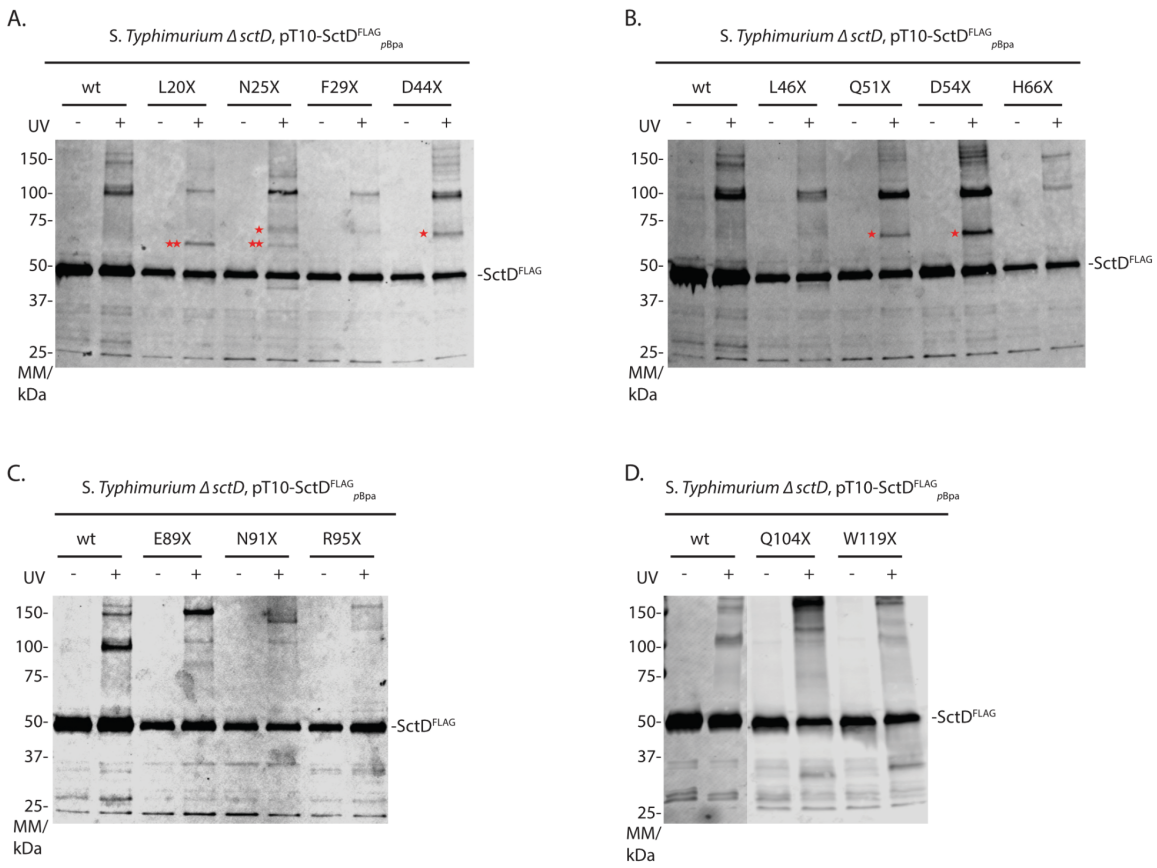

Figure 15: *In vivo* photocrosslinking of different *p*Bpa positions in SctD. A. Immunodetection of all different *p*Bpa positions in SctD^{FLAG} on Western blots of SDS PAGE-separated crude membrane samples of *S*. Typhimurium *sctD* null mutants carrying the indicated derivatives of plasmid pT10- SctD^{FLAG}. Each sample is shown with (+) and without (-) UV-irradiation, which was used to induce photocrosslinking of *p*Bpa at positions L20X, N25X, F29X, D44X of SctD. **B.** Same as in (A) with more *p*Bpa at positions L46X, Q51X, D54X, H66X of SctD. **C.** Same as in (A) with more *p*Bpa at positions E89X, N91X, R95X of SctD. **D.** Same as in (A) with more *p*Bpa at positions Q104X, W119X of SctD. Abbreviations: *p*Bpa, *para*- benzoyl- phenylalanine. The results are representative of n=3 independent experiments.

Next, *in vivo* photo-crosslinking was induced by UV irradiation of intact bacterial cells, and crosslinking was analyzed by SDS PAGE of isolated crude membranes. Among all the tested *p*Bpa mutants N25X, D44X, Q51X, and D54X were the positions that strikingly captured a

protein-protein interaction with a significant crosslink approximately 70 KDa in size highlighted with single red asterisks (Fig. 15A,B).

Given the molecular mass of the other cytoplasmic proteins that might interact and sum up to this size, it was evident that this interaction was of SctD with SctK. Interestingly, *p*Bpa mutants L20X, N25X also exhibited another crosslink of approximately 60 KDa (highlighted with double red asterisks) in size which remains unidentified (Fig. 15A).

In summary, the analysis of the acquired crosslinks showed that we were successful in the acquisition of potential interactions of IR protein SctD with the most likely cytoplasmic component SctK along with some interesting positions which might enlighten our understanding of the SctD-SctK interacting interface and could also provide some useful information regarding the orientation of SctD monomers in the needle complex.

Henceforth, we moved on with four chosen promising positions (L20X, N25X, Q51X, D54X) in order to derive detailed information.

4.5 Investigating the interactions of SctD with other potential interacting partner proteins and analyzing the role of SctJ protein in assembly of SctD subunits and on SctD-SctK interaction

Twenty four copies of SctD and SctJ in a concentrically arranged fashion form the IRs of the needle complex [55], and the interactions of these ring structures are envisioned to be associated with the sorting platform [55] (see section 1.3.1). Additionally, following the observations made in *Yersinia, the outside-in assembly model* already established that SctD gets associated with the secretin ring at the OM independent of SctJ [145,151] (see section 1.4.1). Hence, in terms of assembly, it is unclear if SctD and SctJ form dimers first and then the 24mer ring assembly takes place or if SctJ first interacts with the export apparatus and then recruits SctD. So, it became essential to further investigate the acquired crosslinks (Fig. 15) in different mutant backgrounds for their identification and examine the effects of the mutant backgrounds on the crosslinks (Fig. 16).

We narrowed down the thirteen *p*Bpa positions to four *p*Bpa positions in SctD (L20X, N25X, Q51X, and D54X). Along with the deletion mutant background of *ΔsctD ΔsctK*, we tested the crosslinks in *ΔsctDΔsctJ* background strain as well because we did not expect to achieve SctD-SctD assembly in absence of SctJ and hence clearly no further SctD-SctK interaction. For this, we expressed from plasmid pT10- either SctD wild type or the respective *p*Bpa mutant variants in an *S*. Typhimurium wild type, *ΔsctD*, *ΔsctD ΔsctK*, and in *ΔsctD ΔsctJ* background

strain. *In vivo* photo-crosslinking was induced by UV irradiation of intact bacterial cells, and crosslinking was analyzed by SDS PAGE of isolated crude membranes.

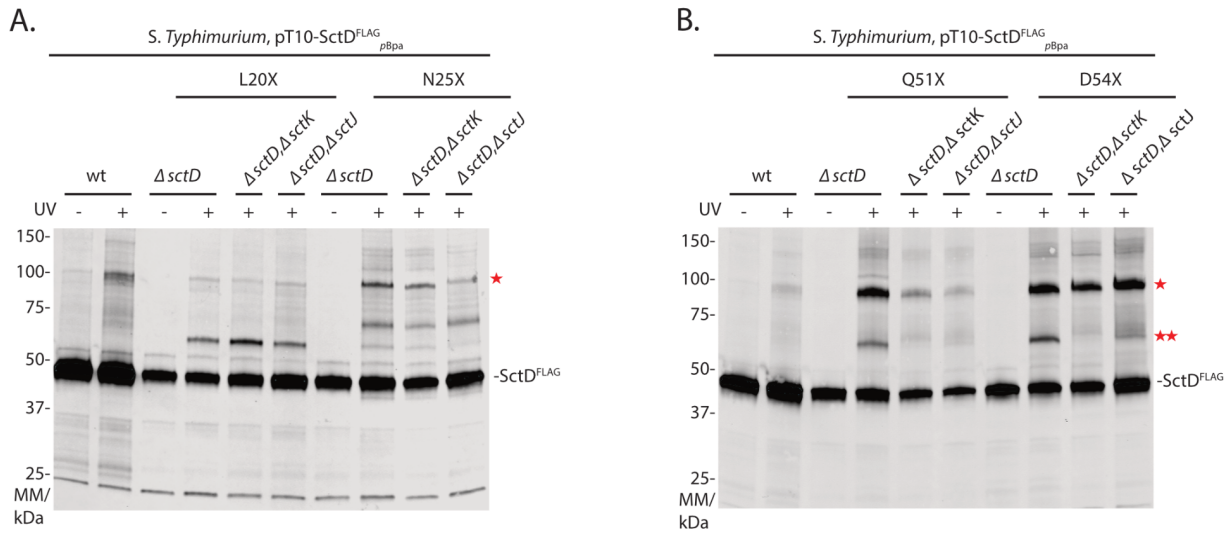

Figure 16: *In vivo* photocrosslinking of selected four *p*Bpa positions of SctD in different deletion backgrounds. A. Immunodetection of SctD^{FLAG} on `Western blots of SDS PAGE-separated crude membrane samples of *S*. Typhimurium wild type, *ΔsctD, ΔsctDΔsctK* and *ΔsctDΔsctJ* mutant strains carrying the plasmids with either L20X or N25X *p*Bpa SctD mutant variants. Each sample is shown with (+) and without (-) UV-irradiation, which induces photocrosslinking. **B.** Immunodetection of SctD^{FLAG} on Western blots of SDS PAGE-separated crude membrane samples of *S*. Typhimurium wild type, *ΔsctD, ΔsctDΔsctK* and *ΔsctDΔsctJ* mutant strains carrying the plasmids with either Q51X or D54X *p*Bpa SctD mutant variants. Abbreviations: QC, quick change position or *p*Bpa position; No del, wild type without any deletion.

As shown in Figure 16, the SctD-SctD interactions corresponding to the band size of approximately 100 KDa (highlighted in the figure with a single red star) seemed to be unaffected in the absence of SctJ for L20X and D54X *p*Bpa positions. In the *ΔsctD ΔsctJ* double mutant background strain for Q51X and D54X *p*Bpa positions, we observed that SctD-SctK interaction was affected by removing SctJ (Fig. 16B). This suggested that removing SctJ might interfere with SctD-SctK interactions and that these positions are very likely at the interaction site of SctD and SctK. Also, for N25X and Q51X *p*Bpa positions, we observed only a slight decrease in the intensity of the crosslink corresponding to SctD-SctD interaction (Fig. 16A,B). Hence, we can conclude that N25X and especially D54X SctD *p*Bpa positions apparently do not affect SctD-SctJ interaction as such while, decrease in the intensity of the SctD-SctD crosslink for Q51X *p*Bpa position might just be an outcome of some conformational changes that take place which also affect the downstream interaction of SctD-SctK corresponding to 70 kDa in size. The decrease in intensity of the 70 kDa crosslink of SctD-SctK for Q51X *p*Bpa position in the *ΔsctD ΔsctJ* double mutant background points out to the

fact that possibly absence of SctJ leads to some conformational changes which still allow assembly to take place (that is why we see some residual intensity) but not completely or in correct fashion. Additionally, we know that in absence of SctJ there is no secretion taking place and hence, the effect seen here can just be another outcome of absence of secretion. Based on the results obtained for D54X *p*Bpa position in the *ΔsctD ΔsctJ* double mutant background (highlighted with two red stars), the 70 kDa crosslink points out to the fact that SctJ ring formation is still taking place or possible for this position. Hence, we can conclude that SctJ does not solely play a role in SctD-SctD assembly. Conceivably, there might be other unknown assembly factors in the membrane or chaperones that affect the SctD-SctD assembly process, thereby explaining the decrease in the crosslink intensity of N25X and Q51X *p*Bpa positions. Additionally, with respect to the potential SctD-SctK interaction corresponding to approximately 70 KDa in size (highlighted by double red stars) for Q51X and D54X *p*Bpa positions (Fig. 16B), we could authenticate the SctD-SctK interaction by examining it in the *ΔsctD ΔsctK* double mutant background strain where we lost the signature crosslink and hence confirmed SctK as the interacting partner of SctD.

Consequently, based on the positioning of Q51X and D54X *p*Bpa positions, we selected additional *p*Bpa positions adjacent to the given interacting site to capture more potential interactions.

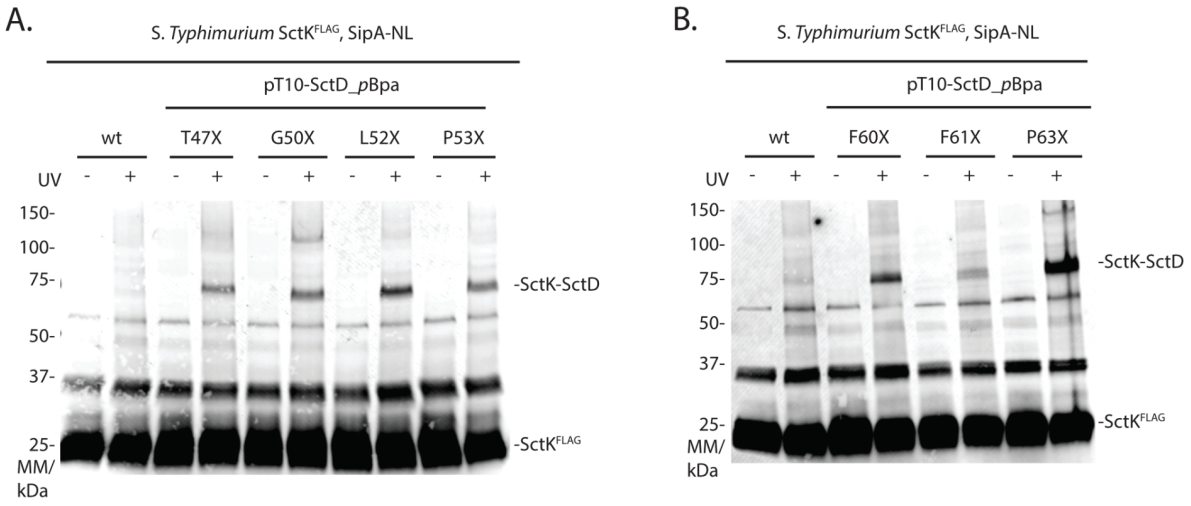

Figure 17: *In vivo* photocrosslinking of different *p*Bpa positions in SctK^{FLAG} *S. Typhimurium*. A. Immunodetection of 3XFLAG tagged SctK on Western blots of SDS PAGE-separated crude membrane samples of *S*. Typhimurium carrying plasmids with the indicated *p*Bpa SctD mutant variants. Each sample is shown with (+) and without (-) UV-irradiation, which induces photocrosslinking of *p*Bpa at position T47X, G50X, L52X, P53X of SctD. **B.** Same as in (A) with more *p*Bpa at positions F60X, F61X, P63X of SctD. The results represent n=3 independent experiments. Abbreviations: *p*Bpa, *para*- benzoyl- phenylalanine; NL, nanoLuc luciferase.

Here, in order to substantiate and confirm the SctD-SctK interactions, we reciprocally tagged SctK C-terminally by 3x FLAG tag to enable its detection. This reciprocal FLAG tagging of SctK with simultaneous placement of the *p*Bpa positions on SctD protein gave us confirmation of the occurring SctD-SctK interactions observed in the previous results for the first time, because in this case we can only detect a significant crosslink based on the FLAG tag when SctK is the only interacting partner of SctD. We used the *S.* Typhimurium $SctK^{FLAG}$ variant of the T3SS, which further expressed a chromosomally encoded NL-tagged effector protein SipA (SipA-NL) as our background strain [177] to express the *p*Bpa mutant variants (T47X, G50X, L52X, P53X, F60X, F61X, P63X) of SctD (Fig. 17A, B). All of the *p*Bpa SctD mutants were expressed with the help of the low copy number pT10-SctD plasmid, which gets induced by the addition of rhamnose (Fig. 17A, B). As shown in Figure 17, we could verify the occurring SctD-SctK interactions with the signature crosslinks corresponding to approximately 70 KDa in size (Fig. 17A,B).

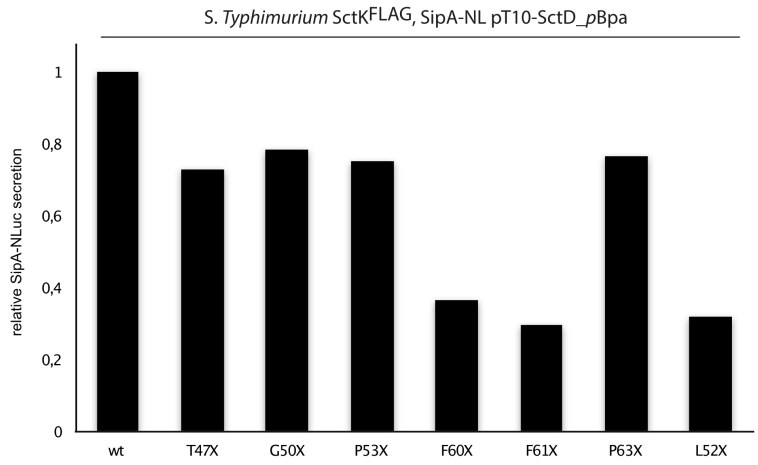

Figure 18: Functional analysis of the T3SS in the different pBpa mutants used in this study. (related to the mutants mentioned in figure 17). Luminescence of type III-secreted SipA-NL measured in the supernatant cultures of the indicated SctD *p*Bpa mutants in a $SctK^{FLAG}$ background. The results are representative of n=3 independent experiments. Abbreviations: *p*Bpa, *para*- benzoyl- phenylalanine; NL, nanoLuc luciferase.

In order to ascertain if any mutation of the given residues resulted in altered function of the T3SS, we also detected secretion of the late substrate SipA (SipA-NL) in the culture supernatant by luminometry (Fig. 18). While most of the *p*Bpa mutants (T47X, G50X, P53X, P63X) exhibited comparable levels of late substrate SipA secretion with the wild type secretion, few *p*Bpa mutants (F60X, F61X, and L52X) did show a mild decrease in their secretion levels (Fig.18). This might indicate that F60X, F61X, and L52X *p*Bpa mutants involve positions crucial for the system's secretion competence and should not be altered. Unfortunately, we miss a negative control here in this experiment, but typically negative

controls amount to approximately 6 to 10 % of SipA-NL secretion levels when compared to the wild type. Hence, in light of this information, the overall secretion levels of all the *p*Bpa mutants are quite good.

4.6 Effect of pH on SctD-SctK interaction: Dissociation and reassociation of the cytosolic components with the inner ring

A recent fluorescence microscopic study conducted in gastrointestinal pathogens such as *Yersinia enterocolitica* and *Shigella flexneri* reported that the cytosolic injectisome components set loose at low external pH transiently from the proximal end of the injectisome [161]. As a result, protein secretion in acidic environments such as the 'stomach' gets hampered [161]. Therefore, based on these findings, we aimed to investigate the effects of pH in *Salmonella*. Additionally, the previous studies only had fluorescence microscopy-based data, but no particular molecular interaction was investigated. So, after establishing the connection between the cytosolic component SctK and the IR protein SctD (Fig. 17), we tested the effect of different pH on SctD-SctK interaction.

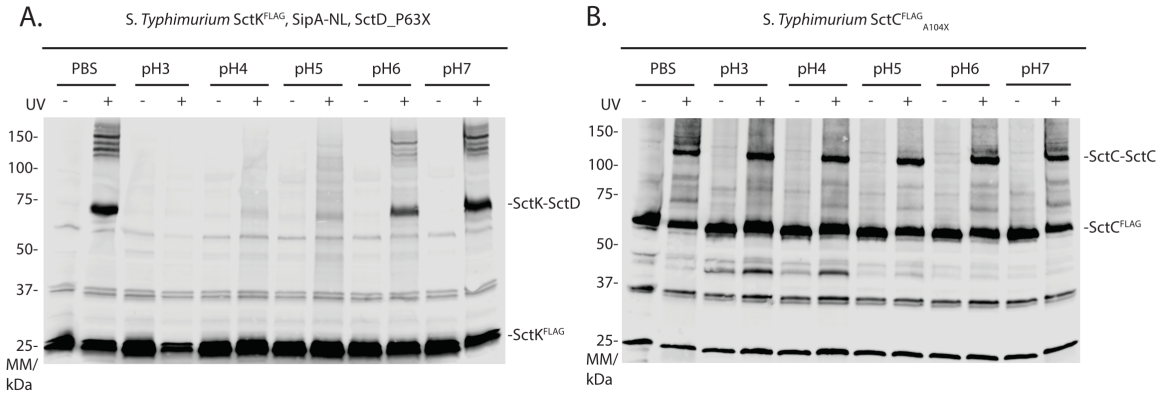

Figure 19: pH effect on SctD-SctK interaction. A. Immunodetection of chromosomally encoded 3XFLAG tagged SctK in pH-adjusted media with different pH values (pH 3 to 7) on Western blots of SDS PAGE-separated crude membrane samples of *S*. Typhimurium chromosomally expressing the SctD *p*Bpa P63X mutant variant. Each sample is shown with (+) and without (-) UV-irradiation, which serves to induce photocrosslinking. **B.** Same as in (A) with A104X *p*Bpa position in 3XFLAG tagged SctC. Abbreviations: *p*Bpa, *para*- benzoyl- phenylalanine; NL, nanoLuc luciferase. The results are representative of n=3 independent experiments.

For this, we used *S.* Typhimurium SctK^{FLAG} with chromosomally encoded P63X *p*Bpa position on SctD variant of the T3SS together with chromosomally encoded NL-tagged effector protein SipA (SipA-NL) too as our background strain [177] (Fig. 19A). Chromosomally placed *p*Bpa position (A104X) in the outer membrane protein SctC with *S.* Typhimurium SctC^{FLAG} was used

as the control because firstly, the outer membrane secretin complex is very stable and expected to remain unaffected by any pH change, secondly, to be able to show that change in pH does not affect the crosslinking capabilities and the chemistry of the *in vivo* photocrosslinker. Hence, photocrosslinking is possible even at low pH levels. Supernatant from the bacterial cultures was collected and resuspended in a range of pH-adjusted media (pH 3 to pH 7) buffered with 50 mM HEPES, 50 mM glycine, and 50 mM MES. The bacterial cultures were incubated for 20 min in the indicated pH with PBS incubation as a control. *In vivo* photo-crosslinking was then induced by UV irradiation of intact bacterial cells, and crosslinking was analyzed by SDS PAGE of isolated crude membranes. Our findings clearly show that the secretin interactions remained unaffected by any pH change whatsoever. The SctC-SctC interactions for the A104X *p*Bpa position represented by the signature crosslink corresponding to approximately 120 KDa in size were comparable with the PBS control as well (Fig. 19B). In comparison, the SctD-SctK interactions for P63X *p*Bpa position in SctD were lost over the pH range of 3 to 5 and resumed at pH6 with comparable intensities at pH7 (Fig. 19A). These findings are in accordance with those made in *Yersinia enterocolitica* [161] and suggest that such low external pH (pH 3 to pH 5) in the periplasm possibly induces partial dissociation of the IR protein SctD thereby triggering the dissociation of the cytosolic components. At neutral pH values, the SctD-SctK interaction is unaltered, indicating that perhaps the cytosolic components devise an adaptive regulatory interface responsible for regulating the activity of T3SS in response to change in environmental conditions.

4.7 PMF-dependence of type III secretion and assessment of effects of PMF inhibitor CCCP on SctD-SctK interaction

So far, several different models have been proposed in order to explain how the export of effector proteins into the host cell is energized. Thus, the underlined mechanism empowering the export of effector proteins has been the prime subject of a significant debate. As formerly known, ATP hydrolysis by the ATPase of the secretion system and the proton motive force (PMF) are primarily the two energy sources on which the type III secretion relies [64,187,188]. Recent advancements indicate that PMF is the chief source of energy in type III secretion. Both in fT3SS and vT3SS, it has been shown that obstruction of PMF terminates the secretion of the effector proteins hence asserting and proclaiming the crucial and indispensable role of PMF in protein export [183–186]. PMF comprises of two components: the gradient of proton concentration across the membrane (ΔpH), and second is the electrical potential difference between the cytoplasm and periplasm (ΔΨ).

Since the proton motive force is one of the driving forces of the T3SS and the dynamics of the cytoplasmic components might be important for secretion, we asked the question: does the disruption of the proton gradient somehow affect these dynamics, which in the end are required to recruit and stabilize the SctD-SctK interaction? The contribution of the two PMF components in the functioning of T3SS can be analyzed with the help of specific inhibitors such as Carbonyl cyanide 3-chlorophenylhydrazone (CCCP) [184]. CCCP is a chemical inhibitor (protonophore) that uncouples the proton gradient and is known as PMF uncoupler. It operates as a proton carrier and thereby discharges the concentration (ΔpH) along with the electric potential (ΔΨ) components of the PMF by transferring protons across the membrane.

For this, we again used the strain with chromosomally encoded P63X *p*Bpa on SctD and $SctK^{FLAG}$ for analyzing the effect of CCCP on the SctD-SctK interaction (Fig. 20A). The control strain carried the A104X *p*Bpa position on $SctC^{FLAG}$ since the outer membrane secretin complex is relatively stable and expected to remain unaffected by any change in the PMF (Fig. 20C). Five µM CCCP were added to the bacterial culture, 4.5 hrs after induction of SPI-1 for only 15 minutes.

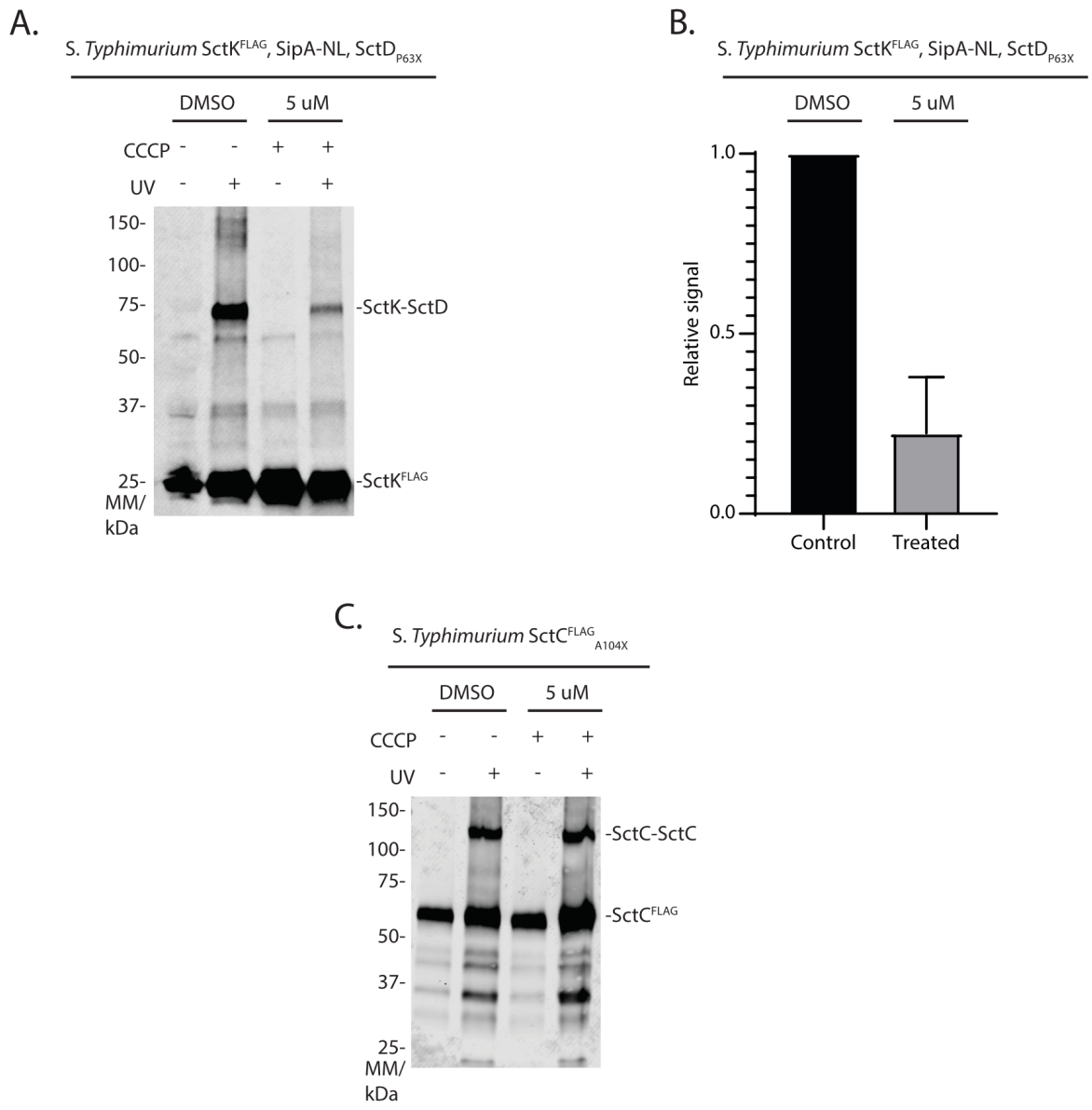

Figure 20: CCCP effect on SctD-SctK interaction. A. Immunodetection of chromosomally encoded 3XFLAG tagged SctK in presence or absence of 5 µM CCCP and DMSO as a negative control on Western blots of SDS PAGE-separated crude membrane samples of *S*. Typhimurium chromosomally expressing the SctD *p*Bpa P63X mutant variant. Each sample is shown with (+) and without (-) UV-irradiation, which induces photocrosslinking. **B.** Comparison of the CCCP-treated SctD-SctK crosslink intensities with DMSO treated negative control from the results obtained in (A). The relative signal of the CCCP treated is presented. **C.** Same as in (A) with A104X *p*Bpa position in 3XFLAG tagged SctC. Abbreviations: *p*Bpa, *para*- benzoyl- phenylalanine; NL, nanoLuc luciferase; PMF, proton motive force. The results are representative of n=3 independent experiments.

After that, the culture supernatants were collected, *in vivo* photo-crosslinking was then induced by UV irradiation of intact bacterial cells, and crosslinking was analyzed by SDS PAGE of

isolated crude membranes. We observed a substantial decrease in the intensity of the SctD-SctK interaction in the CCCP treated P63X *p*Bpa position compared to the DMSO control (Fig. 20A). When quantified, the relative decrease in the signal intensity amounted to even less than 50 percent compared to the DMSO control (Fig. 20B). In terms of molecular interaction, this is the first time one could show what happens when we disrupt the PMF or block the secretion. We could successfully show that disruption of the PMF negatively affected the interaction of SctD with SctK. Somehow disruption of the proton gradient possibly affected the dynamics of the cytosolic components, which perhaps is required for stabilizing the SctD-SctK interaction or even in recruiting the cytosolic components. Additional experiments in line with this argument should be performed.

4.8 Effect of Spheroplasting on SctD-SctK interaction

As shown in previous experiments, pH change (section 4.6) and CCCP treatment (section 4.7) had significant effects on the interaction of SctD-SctK. Changes in pH triggered dissociation of the cytosolic components, thereby affecting SctD-SctK interaction (Fig. 19). CCCP treatment to the bacterial cells disturbed the proton gradient leading to unprecedented changes in the dynamics of the cytosolic components and destabilized the SctD-SctK interaction (Fig. 20). Next, we examined whether the system could cope with rather substantial physical changes such as removing the outer membrane framework, which provides rigidity and stability to the needle complex. For this, we performed spheroplasting of the whole bacterial cells. We again used the same strain as explained in section 4.6 with P63X *p*Bpa position on SctD and a wild type strain without any *p*Bpa position.

Spheroplasts are spherical-shaped, osmotically fragile derivatives of Gram-negative bacteria from which the outer membrane is completely removed. This can be achieved by “enzymatic disruption of the outer membrane in which incubation of the bacterial cells in a hypertonic solution of sucrose in the presence of lysozyme, protease inhibitor and EDTA (ethylene diamine tetra-acetic acid) leads to the formation of spheroplasts.

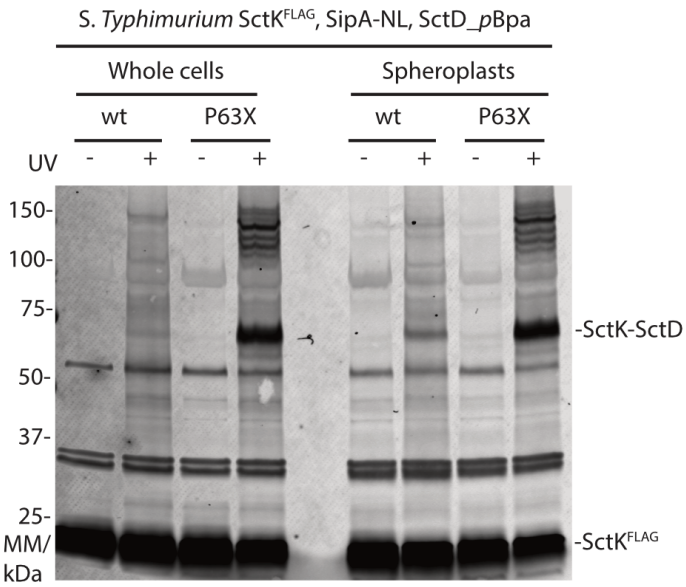

Figure 21: Effect of spheroplasting on SctD-SctK interaction. Immunodetection of chromosomally encoded 3XFLAG tagged SctK on Western blots of SDS PAGE-separated crude membrane samples of *S*. Typhimurium chromosomally expressing the SctD *p*Bpa P63X mutant following different treatments. Each sample is shown with (+) and without (-) UV-irradiation, which induces photocrosslinking. Different treatments include using whole cells for crosslinking and spheroplasting of the bacterial cells for removing the outer membrane before crosslinking. Abbreviations: *p*Bpa, *para*- benzoyl- phenylalanine; NL, nanoLuc luciferase.

The spheroplasts and untreated whole cells were collected, *in vivo* photo-crosslinking was then induced by UV irradiation, and crosslinking was analyzed by SDS PAGE of isolated crude membranes (Fig. 21). As shown in Figure 21, the SctD-SctK interaction seemed relatively stable and was not affected by such extensive physical changes. Most importantly, there was no visible difference in the intensity of the signature crosslink corresponding to SctD-SctK interaction between the whole cells and spheroplasts, which also authenticates the findings of our functional assays such as the CCCP experiment by establishing the fact that this pBpa site (P63X) is not an interacting site that easily falls apart. In fact, the results obtained from functional assays such as CCCP treatment are more reliable and specific (section 4.7).

4.9 Analyzing SctD-SctK interaction in different deletion backgrounds

The large multi-protein cytoplasmic complex known as sorting platform in *Salmonella* comprises five proteins SctQ, SctK, SctL, SctO, and the hexameric ATPase SctN [59] (see section 1.3.2). A ring-shaped, nonameric inner membrane protein SctV (known as the export gate) engages other inner membrane proteins SctR, SctS, SctT, and SctU, forming the export apparatus [63]. The sorting platform connects the inner membrane complex to the ATPase [61,69]. In previous studies, the absence of ATPase has already been shown to affect the overall stability of the sorting platform in *Salmonella* [63]. Nevertheless, the substantially reduced densities of the sorting platform in the study done by Hu et al. prompted us to look at the effects of removing ATPase on the molecular SctD-SctK interaction. Therefore, we chromosomally expressed two chosen *p*Bpa positions, P63X and F60X *p*Bpa SctD mutants in a wild type strain or single-gene deletion mutant strains such as Δ*sctN* for a comprehensive analysis. As a further control, we used the wild type strain with no *p*Bpa mutations (Fig. 22A). *In vivo* photo-crosslinking was induced by UV irradiation of intact bacterial cells with desired *p*Bpa positions, and crosslinking was analyzed by SDS PAGE of isolated crude membranes. As exhibited by our result for single gene deletion mutants of Δ*sctN*, removal of ATPase did not have a drastic effect on the SctD-SctK interaction (Fig. 22A). In comparison to the wild type, the intensity of the band corresponding to the SctD-SctK interaction only displayed mild reduction for both of the *p*Bpa positions (Fig. 22A), which leads to the conclusion that by removal of the ATPase (SctN), the complete cytoplasmic complex is instead not falling apart. It points out that for the chosen interacting *p*Bpa positions (P63X, F60X), the effect of removing SctN is not that drastic as it is more likely to be held up firmly with the help of static interactions in a default state of the secretion system. Additionally, as we know that in *Salmonella*, SctN is not considered crucial for the recruitment of the cytoplasmic components [59–61] (see section 1.4), our findings stand in corroboration with this fact and explain why no effect on the interaction of the IR and the cytoplasmic component is observed in our results (Fig. 22A).

The export apparatus consists of five hydrophobic proteins SctR, SctS, SctT, SctU, and SctV [76] (see section 1.3.3). SctV is considered loosely connected with the needle complex and assumed to execute specialized functions concerning the arrangements in the secretion of the T3S substrates [77,86]. It has been already reported that deployment of any membrane proteins (e.g., Δ*sctV*) results in significant local reorganization of the inner membrane [63]. Therefore, in order to analyze the effect of the deletion of *sctV* (export apparatus component) on the SctD-SctK interaction, we tested both P63X and F60X *p*Bpa positions on SctD in *sctV* single gene deletion background (Δ*sctV)* (Fig. 22B).

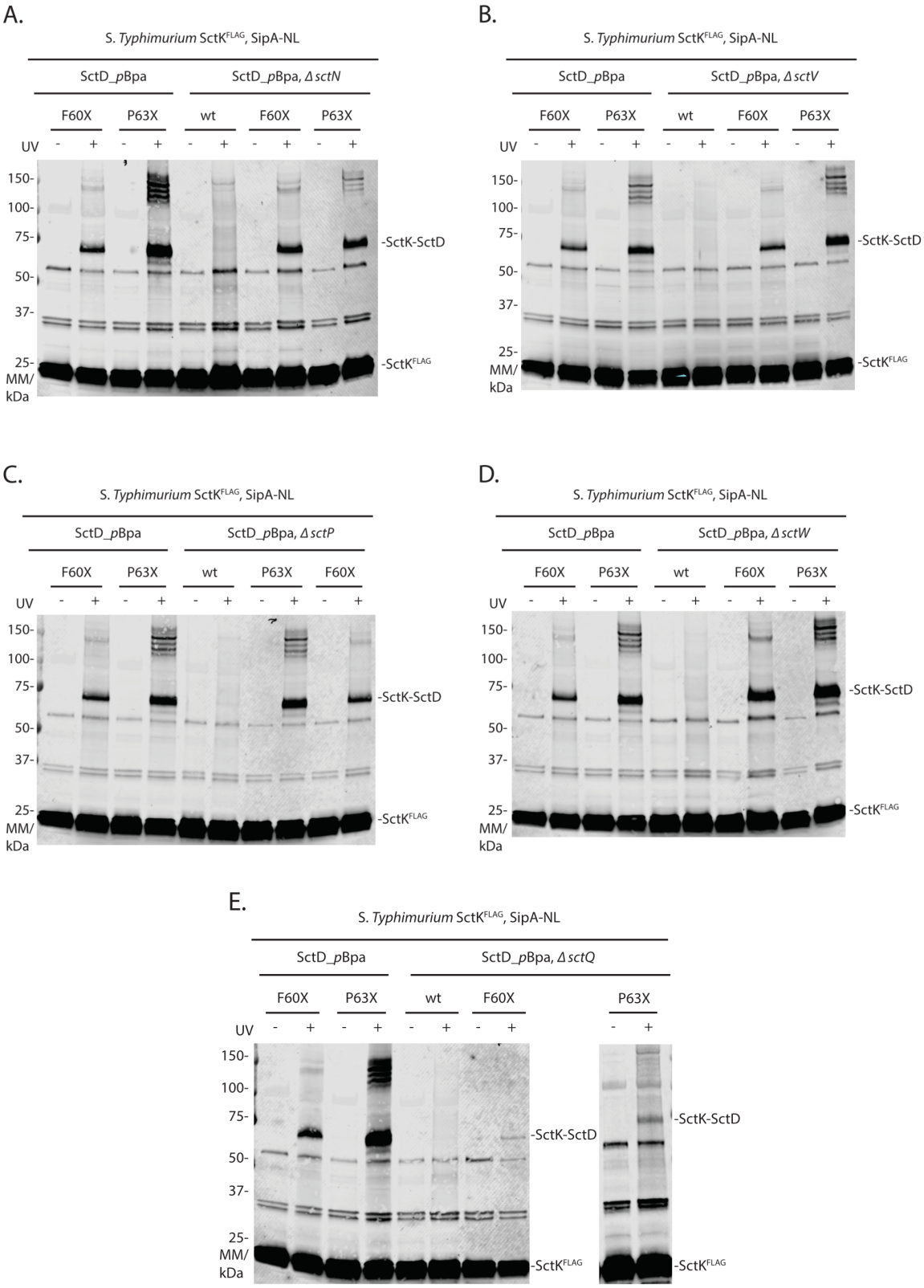

Figure 22: SctD-SctK interaction in different single gene deletion mutant backgrounds. A. Immunodetection of 3XFLAG tagged SctK on Western blots of SDS PAGE-separated crude membrane samples of *S*. Typhimurium wild type and *sctN* null mutant strain chromosomally encoding either F60X or P63X *p*Bpa mutant variants of SctD.

Each sample is shown with (+) and without (-) UV-irradiation, which induced photocrosslinking. **B.** Same as in (A) but in the Δ*sctV* deletion background strain. **C.** Same as in (A) but in the Δ*sctP* deletion background strain. **D.** Same as in (A) but in the Δ*sctW* deletion background strain. **E.** Same as in (A) but the Δ*sctQ* deletion background strain. The results are representative of n=3 independent experiments. Abbreviations: *p*Bpa, *para*- benzoyl-phenylalanine; NL, nanoLuc luciferase.

In vivo photo-crosslinking was induced by UV irradiation of intact bacterial cells with desired *p*Bpa positions, and crosslinking was analyzed by SDS PAGE of isolated crude membranes. Here too, we did not see any substantial change or effect on the SctD-SctK interaction for both the *p*Bpa positions in comparison to the wild type (Fig. 22B). This observation indicates that the absence of secretion has no direct effect on the SctD-SctK interaction.

Another explicit aspect of the T3SS is the ordered hierarchical export of substrate proteins (see section 1.3.5). The non-structural needle length control protein SctP is one of the early substrates of T3SS [125,126]. Switch protein SctU together with SctP induces switching of early substrates to intermediate substrate secretion [128]. A single gene deletion Δ*sctP* mutant is expected to secrete only early substrates. Therefore, to analyze whether the mode of secretion or state of secretion affects the SctD-SctK interaction, we tested both P63X and F60X *p*Bpa positions on SctD in single gene deletion Δ*sctP* strain (Fig. 22C). *In vivo* photo-crosslinking was induced by UV irradiation of intact bacterial cells with our desired *p*Bpa positions, and crosslinking was analyzed by SDS PAGE of isolated crude membranes. Our results indicated no effect on the SctD-SctK interaction in the Δ*sctP* mutants compared to the wild type. Furthermore, the cytoplasmic gatekeeper protein SctW is involved in the second switch step of substrate specificity switching, i.e., from intermediate effectors to late effector protein secretion [131–133] (see section 1.3.5 and 1.3.7). It has been already shown in previous studies that deletion of the gatekeeper protein concludes in discontinuation of the secretion of translocators and hypersecretion of the late effectors [131,137,138]. Therefore, to analyze whether the second secretion switch step affects the SctD-SctK interaction, we tested both P63X and F60X *p*Bpa positions on SctD in the single gene deletion Δ*sctW* strain (Fig. 22D). *In vivo* photo-crosslinking was induced by UV irradiation of intact bacterial cells with desired *p*Bpa positions, and crosslinking was analyzed by SDS PAGE of isolated crude membranes. Our results for Δ*sctW* (Fig. 22D), in addition to the results obtained from Δ*sctP* deletion (Fig. 22C), suggested that in these functional mutants, the SctD-SctK interaction did not depend on different states of secretion. Together, we could show that the SctD-SctK interaction for P63X and F60X *p*Bpa positions in SctD did neither depend on the different states of secretion nor the major export apparatus component ATPase (Fig. 22A, B, C, D). Unfortunately, the SctK protein is the least explored among the soluble T3SS cytoplasmic

components, hence its precise role still remains unknown. Strikingly, changes in pH and PMF lead to changes in this relatively stable interaction. So, this potentially points out the fact that the SctD-SctK interaction is not only already established in the default state of the complete system but is also stable rather than being dynamic. These changes possibly trigger the activation of the T3SS thereby directly influencing the cytosolic complexes, perhaps through essential components such as SctK.

In *Salmonella*, the interaction of SctK to SctQ is already established [61], and hence we also wanted to test a functional mutant with single gene deletion *sctQ* on the SctD-SctK interaction for both P63X and F60X *p*Bpa positions on SctD (Fig. 22E). *In vivo* photo-crosslinking was induced by UV irradiation of intact bacterial cells with desired *p*Bpa positions, and crosslinking was analyzed by SDS PAGE of isolated crude membranes. The results exhibited quite a strong effect on the SctD-SctK interaction for both P63X and F60X *p*Bpa positions. Interestingly, the effect on F60X *p*Bpa position was more pronounced as compared to P63X. It appears as if the interaction with SctD is more prominent compared to SctK, i.e., the stability of the SctK-SctQ interaction only mildly affects the SctD-SctK interaction. Additionally, this also implies that the cytoplasmic complex is probably not acting as a unit and is not completely falling apart by such discrete changes in different cytoplasmic components. Although the determination of precise roles and effects needs exhaustive study of all these components concerning other *p*Bpa positions as well, these results, to some extent, could provide an insight into the SctD-SctK molecular interaction when analyzed in different functional mutants and broaden our understanding of the action mechanism of T3SS and its components.

Parts of this discussion section (Part 1) have been published in:

- Conserved salt bridges facilitate assembly of the helical core export apparatus of a *Salmonella enterica* type III secretion system

  Nidhi Singh, Thales Kronenberger, Andrea Eipper, Felix Weichel, Mirita Franz, Boris Macek, Samuel Wagner (revision submitted)

5. Discussion

Part 1: Conserved salt bridges facilitate assembly of the helical core export apparatus of a *Salmonella enterica* type III secretion system

The export apparatus of T3SS spans the inner membrane and is a homolog of the flagella-associated T3SS [36]. SctR, SctS, SctT, SctU, and SctV together constitute the injectisomes, while FliP, FliQ, FliR, FlhB, and FlhA constitute the flagellar system (Fig. 7A). Protein export through T3SSs is quite crucial for motility and the virulence of numerous major bacterial pathogens. SPI-1 encoded T3SSs delivering a cohort of varied virulence effector proteins directly into the target host cells have been the subject of extensive research over the past few years, with export apparatus components as its principal focus. Kuhlen et al. illustrated how the SctRST export gate complex establishes itself as a core component of the basal body and is seated above the anticipated position of the bacterial inner membrane. Their findings also suggested that the pathway for the export of secreted substrates was across the center of this export gate complex. While much has been elucidated regarding the characterization of the export apparatus components, their contributions to the helical complex formation and its stabilization are multi-faceted and need to be explored for better understanding. We set out to gather new information about minute requirements for the assembly and function of the machinery at the core of T3SS.

Until now, several high-resolution structures of both flagella as well as injectisome T3SS core export apparatus have been revealed. This includes structures of isolated FliPQR/SctRST and FliPQR-FlhB complexes as well as the structure of SctRST while being a part of the assembled injectisome [43,81,83,163,189]. All of these structures at our disposal affirm that the SctRSTU complex assembles into an unpredicted pseudo-hexameric helical structure. In particular, SctR and SctS core components jointly structurally mimic SctT [43]. Additionally, the core stoichiometry of the export apparatus was shown to be conserved across both flagellar and

injectisome T3SS [43]. Apposition of the SctRST structure into reconstructions of an intact secretion system in conjunction with crosslinking studies localized the export apparatus as the core component of the periplasmic section of the needle complex [43]. Structures of the FliPQR/SctRST and FliPQR-FlhB complexes also exhibited a closed state of the export apparatus instituted by an outstretched loop between the third and fourth helixes of SctT, by the last helix-loop-helix substructure of each SctR, SctT, and SctS subunits, respectively, and by most of the hydrophobic domain of SctU, including an extended loop that runs along the SctS-formed edge of the complex. Strikingly, the helix-loop-helix substructures of SctR, SctT, and SctS were noticeably stabilized by extremely conserved inter- and intramolecular salt bridges within the hydrophobic domains of these proteins. In this study, we could establish that these conserved salt bridges are critical for the assembly and function of the SctRSTU core export apparatus.

5.1 Conserved charged residues are critical for the functionality and assembly of the T3SS

Our investigation for interpreting the role of the conserved charged residues $SctS_{E44}$, $SctS_{K52}$, $SctR_{K198,}$ and $SctT_{R204}$ in terms of assembly and function of the T3SS was carried out by substituting $SctS_{E44}$, $SctS_{K52}$, $SctR_{K198}$, and $SctT_{K219}$ positions with alanine and/or glutamine. These mutations resulted in severe impairment of the assembly of SctRSTU complexes. Remarkably, the absence of charged residues at the given positions in a subunit did not lead to its failure or incompetence in getting assembled. Instead, it hampered the assembly of the following subunit in the assembly process. Additionally, mutation of the charged residues apparently did not hinder their membrane integration and protein topogenesis since assembly of the mutated subunits themselves was still functional.

Ensuring tight closure of the SctRST complex so that it does not infringe the cell membrane before finishing up with a complete assembly of the basal body is seemingly critical for maintaining bacterial viability. The molecular dynamics simulation study of the $SctT_{K219A}$ mutant conducted by our collaborating colleague, illustrated that the final helix-loop-helix substructure of each subunit of the core export apparatus needs to be stabilized by salt bridges to form a tight helical complex.

Studies analyzing the interacting surfaces based on helicity and hydrophobicity pattern of the export gate complex revealed that the interfaces involving residue pairs were held together by homo-typic interactions, where the interacting interfaces between individual subunits appeared to be governed by hydrophobic residues, thereby suggesting that standard

localization of the export apparatus within the inner membrane was not feasible [43]. This stood in corroboration with our findings too, where we could also strongly suggest that the ionic interactions potentially stabilized the subunits involved, which might be needed to compensate for the comparably low hydrophobicity of these helical segments, consequently facilitating the upliftment of the assembled SctRSTU complex from the inner membrane to its final supra-membranous position in the injectisome base. The strength of the ionic interactions seems to be finely tuned for supporting assembly on the one hand and allowing export gate opening on the other. The subtle $SctS_{E44D}$ mutation resulted in a stabilized SctRST complex formation with a reduction in secretion efficiency for late substrates, particularly when combined with an autocleavage-deficient $SctU_{N258A}$ mutation.

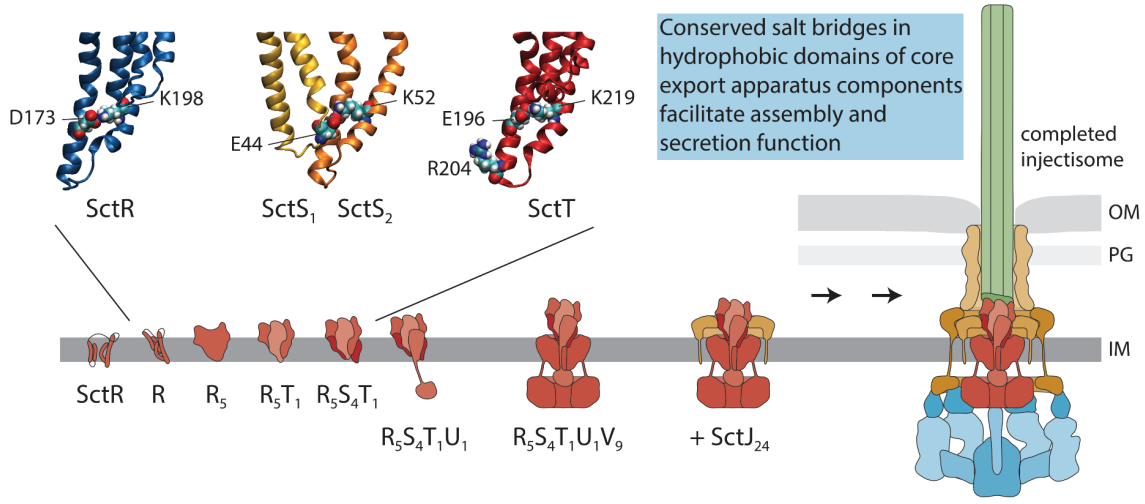

Figure 23: Conserved salt bridges are critical for the assembly and function of the SctRSTU core export apparatus. Top: The helix-loop-helix substructures of SctR, SctS, and SctT are stabilized by extremely conserved inter- and intramolecular salt bridges within the hydrophobic domains of these proteins. **Bottom:** Assembly of T3SS commences with integrating export apparatus components SctR, SctT, and SctS at the inner membrane with subsequent integration of SctU and SctV. Further oligomerization of IR proteins SctD and SctJ encompass the export apparatus. Thereafter, cytoplasmic components join the assembly process authorizing the secretion of SctI. The PG lytic enzyme gets activated by the secretion of SctI. Secretins then assemble into the secretin complex, and secretion of SctF and SctP begins. Polymerization of the needle leads to the opening of the periplasmic gate. Modified from [79]. **Abbreviations:** T3SS, TypeIII secretion system; OM, outer membrane; PG, Peptidoglycan; IM, inner membrane; IR, inner ring; Sct, secretion and cellular translocation.

5.2 Potential role of the conserved charged residues in the gating mechanism

It has already been revealed in flagella that a network of salt bridges in FliQ provides stability to the secretion pore, and the delicate role of the glutamate at this position for the functioning of the export apparatus was also shown in flagella, where a $FliQ_{E46D}$ mutant displayed a slight

reduction in motility and an altered gating phenotype when combined with mutations in the gasket formed by a string of conserved methionines in FliP. Apparently, the unique combination of physicochemical features provided by the string of conserved methionines in this gasket area supports the gating function and leads to the requisite conformational changes for protein substrate secretion [168]. In our study, while the effect of the $SctS_{E44D}$ mutation on secretion function was comparably mild, $SctS_{K52A/Q}$ and $SctT_{K219A}$ mutants displayed strong general secretion defects, and the $SctS_{E44Q}$ mutant could only secrete the early substrate SctP. These defects cannot be inferred due to impaired SctRSTU complexes assembly because a fraction of them could still assemble and successfully integrate into the injectisome base. Therefore, it is conceivable that these residues are positioned very close to the entrance of the SctRSTU secretion pore and interfere with the gating mechanism of the injectisome. The observation supports this notion that mutations in $SctT_{R204}$ and $SctS_{E44,}$ which are in direct contact with the N-terminal domain of the switch protein SctU, showed differential secretion defects for early and intermediate/late substrates that, at least in part, depend on the autocleavage proficiency of the C-terminal domain of SctU. This synthetic effect implies a functional link between the substrate secretion and the switching-relevant cytoplasmic domain of SctU and the gating-relevant SctT and SctS subunits. $SctS_{4\ E44}$ and $SctT_{R204}$ interact with SctU, and the mutants may result in subtle conformational changes at the interface of SctS/T and SctU that influence signal transduction from SctU to SctS relevant for gate opening.

In conclusion, our study identifies and supports the role of the salt bridge-forming residues in stabilizing the assembling helical core export apparatus complex and in the gating of the system during active secretion. Future experiments will be required to reveal the gating mechanism and its regulation by the switch protein SctU.

This discussion section (Part 2) is in preparation:

- Interaction of SctD with SctK in *Salmonella enterica* type III secretion system

Nidhi Singh,Thales Kronenberger, Sam Ulrich, Iwan Grin, Samuel Wagner

Part 2: Interaction of SctD with SctK in *Salmonella enterica* type III secretion system (in preparation)

5.3 Novel molecular interaction sites of SctD-SctK and correct orientation of the SctD monomers in the inner ring of the T3SS

The sorting platform with a rigidly anchored basal body and a needle filament conjointly constitute the injectisome (see section 1.5). VMD visualization of the N-terminus of the IR protein SctD assisted in identifying amino acid residues that might play a role in the interaction between these proteins.

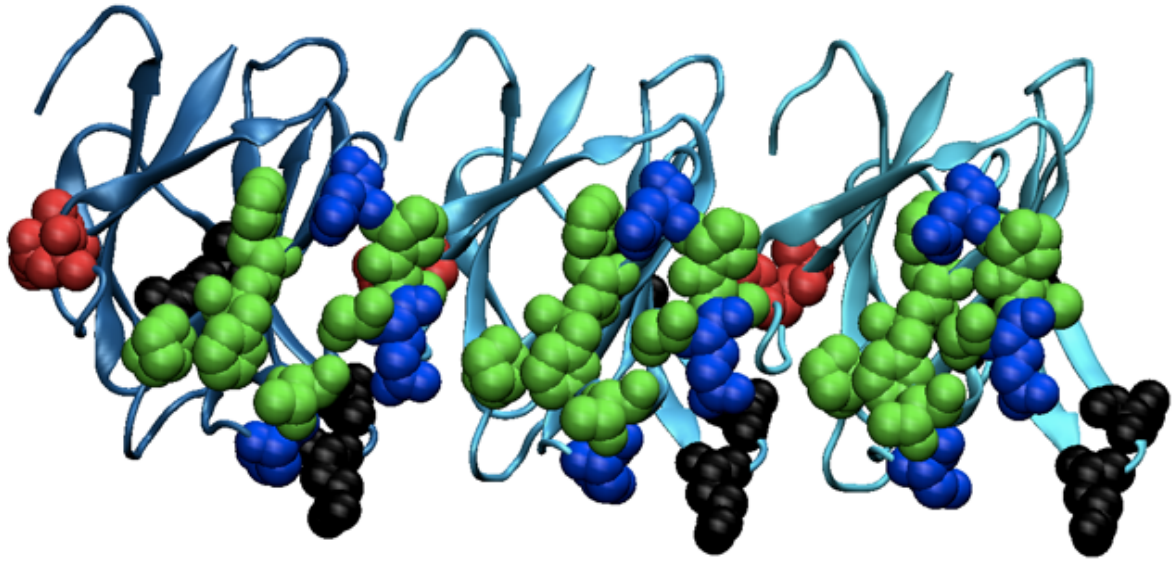

Figure 24: Expected orientation of SctD protein in the ring structure. All *p*Bpa mutants used in this study are mapped to the structure of SctD (PDB file PrgHn3J1W.pdb). Amber mutations were introduced in different positions of SctD to identify new interaction cytoplasmic protein partners of SctD using *in vivo* photo-crosslinking. VMD program designed for modeling, visualization, and analysis of proteins, etc., is used to display the structure of SctD protein from respective PDB files. Identified crosslinks of SctD to SctD, SctK, and other irrelevant interactions are mapped to the VMD structure of SctD in different colors. Blue & Green: SctD-SctK, red: weak SctD-SctD, black: irrelevant interactions towards outside.

In-depth analysis of various potentially interacting positions of SctD in the T3SS of *Salmonella* coupled with *in vivo* photocrosslinking could establish the cytoplasmic component SctK as the interacting partner SctD in the inner membrane (Fig.24).

Besides reporting the verified novel molecular interaction sites of the ring protein SctD with SctK for Q51X and D54X *p*Bpa positions in SctD, we also acquired sufficient information suggesting the orientation of the IR in the T3SS highlighting the interacting interface of SctD-SctK (Fig. 25) and mutagenesis of these key residues confirmed their importance in driving this interaction. All crosslinking results, when put together as illustrated (Fig. 25), presented a clear picture about the various interactions taking place: blue and green colored residues represent the crosslinking positions that distinctly interacted with the cytoplasmic protein SctK, red-colored residues represent weak SctD-SctD interactions, black colored residues represent those positions which did not give any relevant crosslinking information.

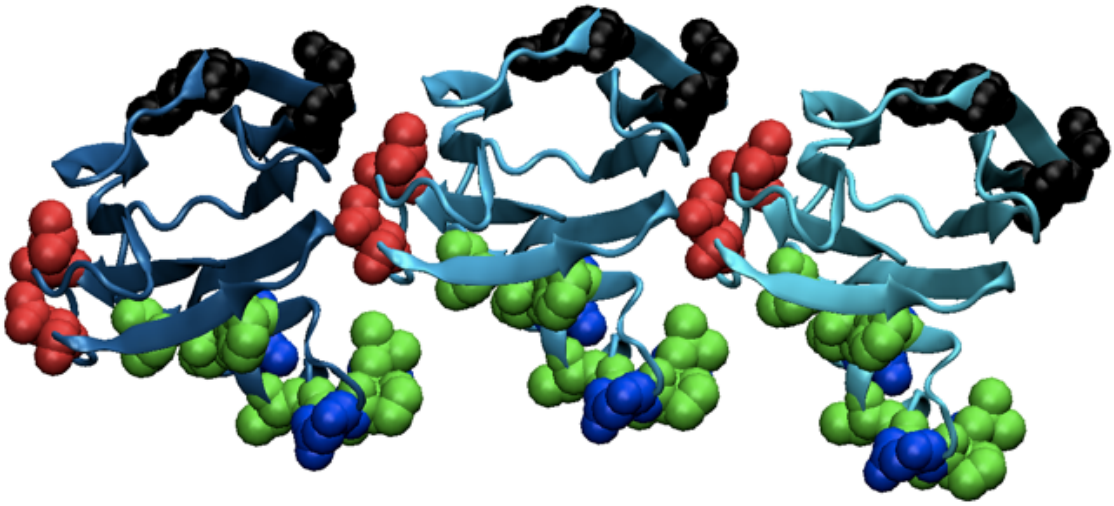

Figure 25: Correct orientation of the SctD protein in the ring structure (PDB file). All *p*Bpa mutants used in this study are mapped to the structure of SctD (PDB file PrgHn3J1W.pdb). Amber mutations were introduced in different positions of SctD to identify new interaction cytoplasmic protein partners of SctD using *in vivo* photo-crosslinking. VMD program designed for modeling, visualization, and analysis of proteins, etc., is used to display the structure of SctD protein from respective PDB files. Identified crosslinks of SctD to SctD, SctK, and other irrelevant interactions are mapped to the VMD structure of SctD in different colors. Blue & Green: SctD-SctK, red: weak SctD-SctD, black: irrelevant interactions towards outside.

Conceivably, the blue-green surface faces down, while the surface with black residues faces upwards in its orientation. The red residues capturing interaction amongst the SctD protomers also seem plausible. Interestingly, the residues present in the blue-green interface also

capture interactions amongst SctD subunits, suggesting that the preferred orientation is upside down and slightly tilted on its side. An insight into the plausible mechanistic interface between SctD and SctK could be established with L20X, N25X, D44X, T47X, G50X, Q51X, D54X, L52X, P53X, F60X, F61X, P63X, E89X, N91X, R95X *p*Bpa positions.

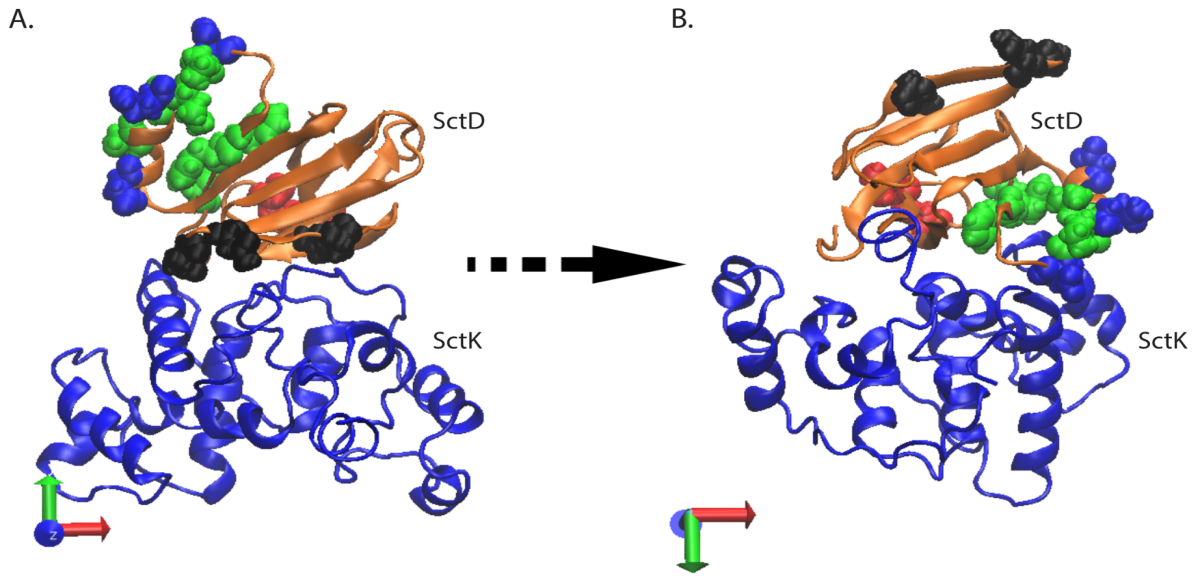

Figure 26: Computational docking of SctD with SctK showing two probable states of SctD-SctK interaction surfaces. All *p*Bpa mutants used in this study are mapped to the structure of SctD. Identified crosslinks of SctD to SctD, SctK, and other irrelevant interactions are mapped to the VMD structure of SctD in different colors. Blue & Green: SctD-SctK, red: weak SctD-SctD, black: irrelevant interactions towards outside. **A.** Docked complex of SctD (orange) protein with SctK (blue) according to the recently proposed crystal structure of SctK homolog in *Pseudomonas aeruginosa [158]*. **B.** The modeled interface between SctD and SctK is not in agreement with our crosslinking data, indicating another orientation of the SctD and SctK proteins.

Recent advancements regarding the newly reported structure of the SctK homolog PscK from *Pseudomonas* extended an opportunistic window for us to discuss our results in light of this structure. Additionally, the same study computationally modeled the interacting surface between the SctD homolog, PscD, and the cytosolic component PscK [158]. The model of the docked SctD-SctK complex as proposed by Muthuramalingam et al. (Fig. 26A) does not fit with our crosslinking results as highlighted in different colors on SctD (Fig. 26A) [158]. The investigated positions that yielded positive SctD-SctK interaction represented in blue and green do not fit with the reported interface. Since the black color-coded residues yielded no positive crosslinking results and also failed to capture any other meaningful interaction, we speculate that this orientation of SctD is rather upside down, as shown in our proposed model in Figure 26B. Since Muthuramalingam et al. were not successful in crystallizing the

PscK/PscD$_C$ complex, its accurate structure is still not fully known. They concluded and made assumptions based on the structures of the involved proteins (PscK, PscD) for characterizing the interaction surface of SctD/SctK [158]. Since the discrete structure of the PscK-PscD$_C$ complex is not resolute, our molecular interaction data which do not stand in agreement with the published study, provide a novel insight into the SctD/SctK interface. Further studies can fine-tune our understanding and assist in the dissection and comprehension of this mechanistic interface between these T3SS components.

5.4 Role of SctJ in the assembly of SctD subunits and SctD-SctK interaction

As per the findings in *Yersinia,* the outside-in assembly model suggested no particular role of SctJ in the association of SctD with SctC during the assembly of the T3SS [145,151]. Since the *Yersinia* study was primarily based on co-immunoprecipitation assays and fluorescence microscopic techniques, we wanted to gather accurate molecular data to support this notion. While, the results obtained from our study displayed the negative effect of removal of SctJ for Q51X and D54X *p*Bpa positions on SctD-SctK interaction, suggesting its involvement and also pointing out to the crucial placement of these positions, which most likely is at the interaction interface of SctD and SctK, we could also establish that SctJ does not play a role in SctD-SctD assembly. A noticeable decrease in the crosslink intensity of SctD-SctD interaction for N25X and Q51X *p*Bpa positions could be an outcome of significant conformational changes.

Overall, our results could show that SctJ is involved in establishing SctD-SctK interaction and very likely not in SctD-SctD interaction. Although these results are not sufficient to decide if SctD and SctJ form dimers first and then the 24mer ring assembly takes place or if SctJ first interacts with the export apparatus and then recruits SctD, they open the door to decipher this intricate step of assembly by unraveling residual positions playing a vital role in SctD-SctK interaction to take place.

5.5 Temporary dissociation of the cytosolic components from T3SS at low external pH

The cytosolic T3SS components devise a dynamic network, where protein exchange is coupled with the functionality of the injectisome [60,68]. Hence, we were intrigued if this dynamic environment in the cytoplasm could affect our established SctD-SctK interaction at low pH. Regarding molecular machines such as flagella, it has been shown that a dynamic exchange amongst the involved structural components exists, further suggesting that the structural and functional roles of a multimeric complex and the dynamic protein exchange are

not mutually exclusive [190]. SctD is a rather sturdy component of the basal body in the injectisome. Therefore, dissociation of such a stable core protein upon external changes such as pH is entirely unreasonable. Nonetheless, our results suggest that low external pH in the periplasm possibly induces partial dissociation of the IR protein SctD thereby triggering the dissociation of the cytosolic components, and hence the SctD-SctK interaction is lost at low pH levels. Nevertheless, stable SctD-SctK interaction at neutral pH points out to the adaptability of T3SS assembly, which potentially benefits from the dynamic exchange of the cytoplasmic components in response to changed environmental conditions by establishing an adaptive regulatory interface. Our results recommend that protein dynamics of T3SS is quite well adapted to the unique environment of the given bacteria and stand in close agreement to the findings made in *Yersinia [161]* too, but not much can be derived out of this functional assay at this given stage of our study. Remarkably, the observed disengagement of SctD and SctK in response to low pH might or might not impact the functionality of the complex, which needs to be further investigated with the help of secretion assays.

5.6 Change in PMF affects the dynamics of the cytosolic components in T3SS

PMF has been reported as the chief energy source by many studies showing that the ATPase complex is not necessary for protein export [65,185]. We wondered if disruption of the proton gradient caused any changes in the dynamics of the cytosolic components required for recruitment and stabilization of the SctK protein for SctD-SctK interaction to take place. This functional assay exhibited a substantial decrease in the intensity of the SctD-SctK interaction in the presence of CCCP, which is a PMF uncoupler. In our study, we could successfully display the effects of PMF disruption on SctD-SctK interaction and though this we could provide an indirect indication of how it might affect the dynamics of the cytosolic components, which are eventually required for stabilizing the SctD-SctK interaction or in recruiting the cytosolic components. Considering our spheroplasting results which verified the stability of the SctD-SctK interaction, these also corroborate the findings of our CCCP experiment by establishing the fact that P63X in SctD is not an interacting site that easily falls apart or is prone to any random physical changes. Hence, our functional assays gain a secondary confirmation of their reliability and support the notion that these are not random results obtained from different treatments given to the respective bacterial system, rather very specific effects reflecting events in the secretion process.

Even though the SctC is an outer membrane protein and hence relatively stable to any PMF changes, still to clearly identify and distinguish the effects of PMF on SctD-SctK interaction, it

would have been better if we used another inner membrane protein such as SctJ as a control. Additionally, secretion assay after CCCP treatment is also missing, which could have imparted an insight into the functional aspect of the T3SS after the CCCP treatment.

5.7 Characterization of the cytosolic components in different deletion backgrounds

A previous study proved that the needle complex structures which were acquired from only single gene deletion mutants of either of the components of the sorting platform (Δ*sctK*, Δ*sctL*, or Δ*sctQ*) restricted its assembly and hence the sorting platform was missing in the structures obtained from these mutants [63,157]. Owing to technical limitations, the cytosolic components cannot be copurified with the complete needle complex. Hence, the six pod structural arrangement of the cytosolic components could only recently be revealed by in situ cryo-electron tomographic study [62,63]. The connection linking these pod structures with the ring protein of the basal body in the needle complex is SctK. In SPI-1 encoded T3SS of *Salmonella,* the cytosolic domains of SctD rearrange themselves in the presence of SctK and form six discrete patches comprising four SctD each. These patches individually interact with SctK, which in turn associates with SctQ, SctL, and SctN [63,157,158]. We wanted to see if the cytosolic interaction with the ring protein depended on the different secretion states and other major constituent proteins.

Substantially reduced densities of the sorting platform in a single gene deletion mutant Δ*sctN* was reported earlier, indicating the potential role of the ATPase in the stability of the sorting platform [63]. Nevertheless, our results did not show any substantial effect of ATPase removal on the SctD-SctK interaction. Additionally, in agreement with other findings, our results also suggest that, most likely, SctN is not crucial in *Salmonella* for recruitment of the cytoplasmic components [59–61], and hence it has no downstream effect on SctD-SctK interaction. No effect on the SctD-SctK interaction after deletion of the major export apparatus membrane protein SctV indicated that absence of secretion has no direct effect on the cytoplasmic interactions with the rest of the needle complex. Probably the local reorganization of the inner membrane caused by the removal of membrane proteins [63] has no remarkable effect on the cytosolic interactions. Also, the membrane rings of the basal body are quite stable. The analysis of the interactions in the sorting platform mutant indicated the possibility that SctK might rather belong more to the base of the complex instead of the cytoplasm and hence imparts stability to the SctD-SctK interaction. Having said this, the determination of precise roles and effects of all these components still needs to be exhaustively studied, and structural

characterization of cytoplasmic components, namely SctK, etc., would help in addressing these questions.

In summary, our results reveal that the initially visualized model for the arrangement of N-terminus of SctD that we had was wrong. Most likely, based on all the information obtained through this study, the interacting interface of SctD-SctK is facing upside down in the correct orientation of the N-terminus of SctD. Additionally, the interaction of the membrane ring with the cytosolic component does neither depend on the different states of secretion nor on the major export apparatus component and the ATPase, but is affected by changes in pH and PMF. Strikingly, based on the spheroplasting experiment, we could establish that the positions examined in our functional assays were remarkably strong, and the SctD-SctK interactions were not lost even under harsh physical changes such as removal of the outer membrane. The results obtained from the PMF blockage become more prominent and further strengthened now, as they agree with the gene deletion experiment of SctV, which also revealed that the absence of secretion did not affect the SctD-SctK interaction. Normally, we would expect that the complete sorting platform falls apart in case of SctQ deletion which we also could show through our results where we noticed a quite strong decrease in the intensity of SctD-SctK interaction. This might be because of two reasons: firstly, it might be possible that the default state of the whole system is having SctK stably associated to the needle base rather than being dynamically associated with the cytosolic components and secondly, it might be that the interaction of SctK with SctD is more prominent than the interaction between SctK with SctQ and hence there is some residual interaction still seen for P63X *p*Bpa position as compared to F60X where the interaction is lost. Considering the fact that both F60X and P63X are *p*Bpa mutations, and we have these mutations additionally in another gene deletion mutant background, which makes it a double mutant, which is not the best-suited scenario for analysis. Additionally, it might be that F60X is a much stronger *p*Bpa mutation in itself or a critical residue with respect to the positioning of the P63X residue, which might also be inferred from the nanoluc secretion assay shown in Figure 18. While the P63X *p*Bpa mutant exhibited comparable levels of late substrate SipA secretion with the wild type secretion, F60X *p*Bpa mutant was not at par and exhibited slightly decreased secretion levels for the same.

6. Conclusion and outlook

Ultimately, our data attest that conserved residues establishing the salt bridges are essential for stabilizing the assembling core export apparatus and the gating mechanism of the injectisome during active secretion. Nonetheless, we could not characterize the mechanism of gating and its regulation by the switch protein SctU; hence future experiments are required to further our knowledge in this direction.

We have successfully established novel molecular interactions between the ring protein SctD and the cytosolic protein SctK and obtained some perspective into the plausible orientation of the N-terminus of SctD protein by *in vivo* photocrosslinking. This technique has yielded deep insight into discrete steps of assembly of the T3SS components, proteins that are otherwise inaccessible by other techniques. It may be beneficial to investigate more *p*Bpa positions in the SctD protein and try to capture signature crosslinks from the SctK side by placing *p*Bpa positions on SctK and a FLAG tag in SctD. In addition, the *p*Bpa positions chosen for identifying protein-protein interactions need authentication from mass spectrometry, which by exact mapping of the crosslinking sites will enable a clearer understanding of the mechanism of assembly.

The position of an individual component in a multimeric protein complex is often influenced by the presence or absence of the other constituents, which makes the evaluation of these types of correlations challenging. Delineation of assembly steps from deletion mutant analysis is one of the drawbacks of this study because the deletion of structural components from the needle complex can disturb the assembly pathway. Hence, we run into the grey zone of over-interpretation of obtained results. The existing knowledge about the functionality of the complex at low external pH is tenuous. Thus, for functional assays of pH effect on the SctD-SctK interaction, it can be worthwhile to look at the secretion profile of the treated *p*Bpa mutant over a different pH range. Additionally, we could have chosen a better control for the PMF experiment, such as another inner membrane protein SctJ, to compare our observations and draw more robust conclusions. Although, we successfully show that PMF disruption negatively affects the interaction of SctD with SctK, we still need additional experiments to show how this PMF disruption affects the dynamics of the cytosolic components which perhaps is required for stabilizing the SctD-SctK interaction or even in recruiting the cytosolic components.

Investigating the kinetics of assembly at the molecular level by synchronizing the assembly process would be another way to approach the goal of exploring the assembly process. Pulse-

chase labelling in conjunction with *in vivo* photocrosslinking would help track occurrences of subsequent crosslinks over the time of the assembly process.

7. List of abbreviations

Abbreviations	Description
ACA	aminocaproic acid
Amp	ampicillin
ATP	adenosine triphosphate
BN	blue native
CCCP	carbonyl cyanide 3-chlorophenylhydrazone
Cm	chloramphenicol
Cryo-EM	cryo-electron microscopy
DAP	diaminopimelic acid
DDM	n-dodecyl-β-D-malto-pyranoside
DTT	dithiothreitol
E. coli	*Escherichia coli*
EDTA	ethylenediaminetetraacetate
EPEC	enteropathogenic *Escherichia coli*
et al.	and others
FHA	forkhead associated domain

IM	inner membrane
IR	inner membrane concentric rings
Kan	kanamycin
Kda	kilodalton
LB	lysogeny broth
LMNG	lauryl maltose neopentyl glycol
MM	molecular mass
NC	needle complex
NL	NanoLuc luciferase
NPTH	letters refer to amino acids (asparagine, proline, threonine, hisitdine)
OD600	optical density at a wavelength of 600 nm
ODU	optical density per millilitre
OM	outer membrane
o/n	over night
OR	outer membrane secretin complex (outer ring)
PAGE	polyacrylamide gel electrophoresis
*p*Bpa	para-benzoyl-L-phenylalanine

PBS	phosphate-buffered saline
PCR	polymerase chain reaction
pT10	pTACO10
PEG	polyethylene glycol
PMF	proton motive force
PVDF	polyvinylidene difluoride
QC	QuikChange site-directed mutagenesis
rpm	revolutions per minute
RT	room temperature
S. Typhimurium	Salmonella enterica subspecies enterica serovar Typhimurium
SCV	Salmonella - containing vacuole
Sct	secretion and cellular translocation
SDS	sodium dodecylsulfate
SN	Supernatant
SPI-1	Salmonella pathogenicity island 1
Strep	Streptomycin
T3SS	Type III secretion system

TAE	Tris-acetate buffer supplemented with EDTA
Taq	*Thermus aquaticus*
TBS	Tris-buffered saline
TBS-T	Tris-buffered saline supplemented with Tween 20
TCA	trichloroacetic acid
TEA	triethanolamine
TEMED	N,N,N,N-tetramethylethane-1,2-diamine
Tet	tetracycline
TMH	transmembrane helices
Tris	tris(hydroxymethyl)aminomethane
UV	ultraviolet light
v/v	volume per volume
w/v	weight per volume
WC	whole cells
wt	wild-type

8. References

1. Flemming H-C, Wuertz S. Bacteria and archaea on Earth and their abundance in biofilms. Nat Rev Microbiol. 2019;17: 247–260.

2. Mueller EA, Levin PA. Bacterial Cell Wall Quality Control during Environmental Stress. MBio. 2020;11. doi:10.1128/mBio.02456-20

3. Yadav AK, Espaillat A, Cava F. Bacterial Strategies to Preserve Cell Wall Integrity Against Environmental Threats. Front Microbiol. 2018;9: 2064.

4. Silhavy TJ, Kahne D, Walker S. The bacterial cell envelope. Cold Spring Harb Perspect Biol. 2010;2: a000414.

5. Majowicz SE, Musto J, Scallan E, Angulo FJ, Kirk M, O'Brien SJ, et al. The global burden of nontyphoidal Salmonella gastroenteritis. Clin Infect Dis. 2010;50: 882–889.

6. Haraga A, Ohlson MB, Miller SI. Salmonellae interplay with host cells. Nat Rev Microbiol. 2008;6: 53–66.

7. Fàbrega A, Vila J. Salmonella enterica serovar Typhimurium skills to succeed in the host: virulence and regulation. Clin Microbiol Rev. 2013;26: 308–341.

8. Coburn B, Grassl GA, Finlay BB. Salmonella, the host and disease: a brief review. Immunol Cell Biol. 2007;85: 112–118.

9. Guibourdenche M, Roggentin P, Mikoleit M, Fields PI, Bockemühl J, Grimont PAD, et al. Supplement 2003-2007 (No. 47) to the White-Kauffmann-Le Minor scheme. Res Microbiol. 2010;161: 26–29.

10. McClelland M, Sanderson KE, Spieth J, Clifton SW, Latreille P, Courtney L, et al. Complete genome sequence of Salmonella enterica serovar Typhimurium LT2. Nature. 2001;413: 852–856.

11. Bhunia AK. Foodborne Microbial Pathogens: Mechanisms and Pathogenesis. Springer; 2018.

12. Garcia-del Portillo F, Foster JW, Finlay BB. Role of acid tolerance response genes in Salmonella typhimurium virulence. Infect Immun. 1993;61: 4489–4492.

13. Foster JW, Hall HK. Inducible pH homeostasis and the acid tolerance response of Salmonella typhimurium. J Bacteriol. 1991;173: 5129–5135.

14. Bäumler AJ, Tsolis RM, Heffron F. Contribution of fimbrial operons to attachment to and invasion of epithelial cell lines by Salmonella typhimurium. Infect Immun. 1996;64: 1862–1865.

15. Jones BD, Ghori N, Falkow S. Salmonella typhimurium initiates murine infection by penetrating and destroying the specialized epithelial M cells of the Peyer's patches. J Exp Med. 1994;180: 15–23.

16. Francis CL, Starnbach MN, Falkow S. Morphological and cytoskeletal changes in

epithelial cells occur immediately upon interaction with Salmonella typhimurium grown under low-oxygen conditions. Mol Microbiol. 1992;6: 3077–3087.

17. Galán JE, Wolf-Watz H. Protein delivery into eukaryotic cells by type III secretion machines. Nature. 2006;444: 567–573.

18. Hansen-Wester I, Hensel M. Salmonella pathogenicity islands encoding type III secretion systems. Microbes Infect. 2001;3: 549–559.

19. Prouty AM, Gunn JS. Salmonella enterica serovar typhimurium invasion is repressed in the presence of bile. Infect Immun. 2000;68: 6763–6769.

20. Bajaj V, Hwang C, Lee CA. hilA is a novel ompR/toxR family member that activates the expression of Salmonella typhimurium invasion genes. Mol Microbiol. 1995;18: 715–727.

21. Humphreys D, Davidson A, Hume PJ, Koronakis V. Salmonella virulence effector SopE and Host GEF ARNO cooperate to recruit and activate WAVE to trigger bacterial invasion. Cell Host Microbe. 2012;11: 129–139.

22. Cirillo DM, Valdivia RH, Monack DM, Falkow S. Macrophage-dependent induction of the Salmonella pathogenicity island 2 type III secretion system and its role in intracellular survival. Mol Microbiol. 1998;30: 175–188.

23. Hensel M, Shea JE, Waterman SR, Mundy R, Nikolaus T, Banks G, et al. Genes encoding putative effector proteins of the type III secretion system of Salmonella pathogenicity island 2 are required for bacterial virulence and proliferation in macrophages. Mol Microbiol. 1998;30: 163–174.

24. Alpuche-Aranda CM, Racoosin EL, Swanson JA, Miller SI. Salmonella stimulate macrophage macropinocytosis and persist within spacious phagosomes. J Exp Med. 1994;179: 601–608.

25. Ochman H, Groisman EA. Distribution of pathogenicity islands in Salmonella spp. Infect Immun. 1996;64: 5410–5412.

26. Erhardt M, Dersch P. Regulatory principles governing Salmonella and Yersinia virulence. Front Microbiol. 2015;6: 949.

27. Worley MJ, Nieman GS, Geddes K, Heffron F. Salmonella typhimurium disseminates within its host by manipulating the motility of infected cells. Proc Natl Acad Sci U S A. 2006;103: 17915–17920.

28. Green ER, Mecsas J. Bacterial Secretion Systems: An Overview. Virulence Mechanisms of Bacterial Pathogens. 2016. pp. 213–239. doi:10.1128/9781555819286.ch8

29. Hamed MB, Anné J, Karamanou S, Economou A. Streptomyces protein secretion and its application in biotechnology. FEMS Microbiol Lett. 2018;365. doi:10.1093/femsle/fny250

30. Costa TRD, Felisberto-Rodrigues C, Meir A, Prevost MS, Redzej A, Trokter M, et al. Secretion systems in Gram-negative bacteria: structural and mechanistic insights. Nature Reviews Microbiology. 2015. pp. 343–359. doi:10.1038/nrmicro3456

31. Galán JE, Waksman G. Protein-Injection Machines in Bacteria. Cell. 2018;172: 1306–1318.

32. Gu L, Zhou S, Zhu L, Liang C, Chen X. Small-Molecule Inhibitors of the Type III Secretion System. Molecules. 2015;20: 17659–17674.

33. Anantharajah A, Mingeot-Leclercq M-P, Van Bambeke F. Targeting the Type Three Secretion System in Pseudomonas aeruginosa. Trends Pharmacol Sci. 2016;37: 734–749.

34. Büttner D. Protein export according to schedule: architecture, assembly, and regulation of type III secretion systems from plant- and animal-pathogenic bacteria. Microbiol Mol Biol Rev. 2012;76: 262–310.

35. Galán JE, Collmer A. Type III secretion machines: bacterial devices for protein delivery into host cells. Science. 1999;284: 1322–1328.

36. Abby SS, Rocha EPC. The non-flagellar type III secretion system evolved from the bacterial flagellum and diversified into host-cell adapted systems. PLoS Genet. 2012;8: e1002983.

37. Macnab RM. How bacteria assemble flagella. Annu Rev Microbiol. 2003;57: 77–100.

38. Galán JE. SnapShot: effector proteins of type III secretion systems. Cell. 2007;130: 192.

39. Collazo CM, Galán JE. The invasion-associated type III system of Salmonella typhimurium directs the translocation of Sip proteins into the host cell. Mol Microbiol. 1997;24: 747–756.

40. Park D, Lara-Tejero M, Waxham MN, Li W, Hu B, Galán JE, et al. Visualization of the type III secretion mediated -host cell interface using cryo-electron tomography. Elife. 2018;7. doi:10.7554/eLife.39514

41. Zilkenat S, Franz-Wachtel M, Stierhof Y-D, Galán JE, Macek B, Wagner S. Determination of the Stoichiometry of the Complete Bacterial Type III Secretion Needle Complex Using a Combined Quantitative Proteomic Approach. Mol Cell Proteomics. 2016;15: 1598–1609.

42. Kubori T, Matsushima Y, Nakamura D, Uralil J, Lara-Tejero M, Sukhan A, et al. Supramolecular structure of the Salmonella typhimurium type III protein secretion system. Science. 1998;280: 602–605.

43. Kuhlen L, Abrusci P, Johnson S, Gault J, Deme J, Caesar J, et al. Structure of the core of the type III secretion system export apparatus. Nat Struct Mol Biol. 2018;25: 583–590.

44. Hueck CJ. Type III protein secretion systems in bacterial pathogens of animals and plants. Microbiol Mol Biol Rev. 1998;62: 379–433.

45. Singh N, Wagner S. Investigating the assembly of the bacterial type III secretion system injectisome by in vivo photocrosslinking. Int J Med Microbiol. 2019;309: 151331.

46. Galán JE. Common themes in the design and function of bacterial effectors. Cell Host Microbe. 2009;5: 571–579.

47. Portaliou AG, Tsolis KC, Loos MS, Zorzini V, Economou A. Type III Secretion: Building and Operating a Remarkable Nanomachine. Trends Biochem Sci. 2016;41: 175–189.

48. Worrall LJ, Hu J, Strynadka NCJ. Aligning the Symmetry of the Type III Secretion System Needle Complex. J Chem Inf Model. 2020;60: 2430–2435.

49. Hu J, Worrall LJ, Strynadka NC. Towards capture of dynamic assembly and action of the T3SS at near atomic resolution. Curr Opin Struct Biol. 2020;61: 71–78.

50. Schraidt O, Marlovits TC. Three-dimensional model of Salmonella's needle complex at subnanometer resolution. Science. 2011;331: 1192–1195.

51. Worrall LJ, Hong C, Vuckovic M, Deng W, Bergeron JRC, Majewski DD, et al. Near-atomic-resolution cryo-EM analysis of the Salmonella T3S injectisome basal body. Nature. 2016;540: 597–601.

52. Kowal J, Chami M, Ringler P, Müller SA, Kudryashev M, Castaño-Díez D, et al. Structure of the dodecameric Yersinia enterocolitica secretin YscC and its trypsin-resistant core. Structure. 2013;21: 2152–2161.

53. Filloux A, Voulhoux R. Multiple Structures Disclose the Secretins' Secrets. J Bacteriol. 2018;200. doi:10.1128/JB.00702-17

54. Hu J, Worrall LJ, Hong C, Vuckovic M, Atkinson CE, Caveney N, et al. Cryo-EM analysis of the T3S injectisome reveals the structure of the needle and open secretin. Nat Commun. 2018;9: 3840.

55. Schraidt O, Lefebre MD, Brunner MJ, Schmied WH, Schmidt A, Radics J, et al. Topology and organization of the Salmonella typhimurium type III secretion needle complex components. PLoS Pathog. 2010;6: e1000824.

56. Koo J, Burrows LL, Howell PL. Decoding the roles of pilotins and accessory proteins in secretin escort services. FEMS Microbiol Lett. 2012;328: 1–12.

57. Spreter T, Yip CK, Sanowar S, André I, Kimbrough TG, Vuckovic M, et al. A conserved structural motif mediates formation of the periplasmic rings in the type III secretion system. Nat Struct Mol Biol. 2009;16: 468–476.

58. Yip CK, Kimbrough TG, Felise HB, Vuckovic M, Thomas NA, Pfuetzner RA, et al. Structural characterization of the molecular platform for type III secretion system assembly. Nature. 2005;435: 702–707.

59. Lara-Tejero M, Kato J, Wagner S, Liu X, Galán JE. A sorting platform determines the order of protein secretion in bacterial type III systems. Science. 2011;331: 1188–1191.

60. Diepold A, Sezgin E, Huseyin M, Mortimer T, Eggeling C, Armitage JP. A dynamic and adaptive network of cytosolic interactions governs protein export by the T3SS injectisome. Nat Commun. 2017;8: 15940.

61. Zhang Y, Lara-Tejero M, Bewersdorf J, Galán JE. Visualization and characterization of individual type III protein secretion machines in live bacteria. Proc Natl Acad Sci U S A. 2017;114: 6098–6103.

62. Hu B, Morado DR, Margolin W, Rohde JR, Arizmendi O, Picking WL, et al. Visualization

of the type III secretion sorting platform of Shigella flexneri. Proc Natl Acad Sci U S A. 2015;112: 1047–1052.

63. Hu B, Lara-Tejero M, Kong Q, Galán JE, Liu J. In Situ Molecular Architecture of the Salmonella Type III Secretion Machine. Cell. 2017;168: 1065–1074.e10.

64. Akeda Y, Galán JE. Chaperone release and unfolding of substrates in type III secretion. Nature. 2005;437: 911–915.

65. Erhardt M, Mertens ME, Fabiani FD, Hughes KT. ATPase-independent type-III protein secretion in Salmonella enterica. PLoS Genet. 2014;10: e1004800.

66. Majewski DD, Worrall LJ, Hong C, Atkinson CE, Vuckovic M, Watanabe N, et al. Cryo-EM structure of the homohexameric T3SS ATPase-central stalk complex reveals rotary ATPase-like asymmetry. Nat Commun. 2019;10: 626.

67. Bzymek KP, Hamaoka BY, Ghosh P. Two Translation Products ofYersinia yscQAssemble To Form a Complex Essential to Type III Secretion. Biochemistry. 2012. pp. 1669–1677. doi:10.1021/bi201792p

68. Diepold A, Kudryashev M, Delalez NJ, Berry RM, Armitage JP. Composition, formation, and regulation of the cytosolic c-ring, a dynamic component of the type III secretion injectisome. PLoS Biol. 2015;13: e1002039.

69. Lara-Tejero M, Qin Z, Hu B, Butan C, Liu J, Galán JE. Role of SpaO in the assembly of the sorting platform of a Salmonella type III secretion system. PLoS Pathog. 2019;15: e1007565.

70. McDowell MA, Marcoux J, McVicker G, Johnson S, Fong YH, Stevens R, et al. Characterisation of Shigella Spa33 and Thermotoga FliM/N reveals a new model for C-ring assembly in T3SS. Mol Microbiol. 2016;99: 749–766.

71. Song M, Sukovich DJ, Ciccarelli L, Mayr J, Fernandez-Rodriguez J, Mirsky EA, et al. Control of type III protein secretion using a minimal genetic system. Nat Commun. 2017;8: 14737.

72. Yu X-J, Liu M, Matthews S, Holden DW. Tandem translation generates a chaperone for the Salmonella type III secretion system protein SsaQ. J Biol Chem. 2011;286: 36098–36107.

73. Carroll BL, Nishikino T, Guo W, Zhu S, Kojima S, Homma M, et al. The flagellar motor of undergoes major structural remodeling during rotational switching. Elife. 2020;9. doi:10.7554/eLife.61446

74. Notti RQ, Bhattacharya S, Lilic M, Stebbins CE. A common assembly module in injectisome and flagellar type III secretion sorting platforms. Nat Commun. 2015;6: 7125.

75. Milne-Davies B, Wimmi S, Diepold A. Adaptivity and dynamics in type III secretion systems. Mol Microbiol. 2021;115: 395–411.

76. Galán JE, Lara-Tejero M, Marlovits TC, Wagner S. Bacterial type III secretion systems: specialized nanomachines for protein delivery into target cells. Annu Rev Microbiol. 2014;68: 415–438.

77. Wagner S, Königsmaier L, Lara-Tejero M, Lefebre M, Marlovits TC, Galán JE. Organization and coordinated assembly of the type III secretion export apparatus. Proc Natl Acad Sci U S A. 2010;107: 17745–17750.

78. Diepold A, Wagner S. Assembly of the bacterial type III secretion machinery. FEMS Microbiol Rev. 2014;38: 802–822.

79. Wagner S, Grin I, Malmsheimer S, Singh N, Torres-Vargas CE, Westerhausen S. Bacterial type III secretion systems: a complex device for the delivery of bacterial effector proteins into eukaryotic host cells. FEMS Microbiol Lett. 2018;365. doi:10.1093/femsle/fny201

80. Dietsche T, Tesfazgi Mebrhatu M, Brunner MJ, Abrusci P, Yan J, Franz-Wachtel M, et al. Structural and Functional Characterization of the Bacterial Type III Secretion Export Apparatus. PLoS Pathog. 2016;12: e1006071.

81. Johnson S, Kuhlen L, Deme JC, Abrusci P, Lea SM. The Structure of an Injectisome Export Gate Demonstrates Conservation of Architecture in the Core Export Gate between Flagellar and Virulence Type III Secretion Systems. MBio. 2019;10. doi:10.1128/mBio.00818-19

82. Kuhlen L, Abrusci P, Johnson S, Gault J, Deme J, Caesar J, et al. Author Correction: Structure of the core of the type III secretion system export apparatus. Nat Struct Mol Biol. 2018;25: 743.

83. Kuhlen L, Johnson S, Zeitler A, Bäurle S, Deme JC, Caesar JJE, et al. The substrate specificity switch FlhB assembles onto the export gate to regulate type three secretion. Nat Commun. 2020;11: 1296.

84. Berger C, Robin GP, Bonas U, Koebnik R. Membrane topology of conserved components of the type III secretion system from the plant pathogen Xanthomonas campestris pv. vesicatoria. Microbiology. 2010;156: 1963–1974.

85. Zarivach R, Deng W, Vuckovic M, Felise HB, Nguyen HV, Miller SI, et al. Structural analysis of the essential self-cleaving type III secretion proteins EscU and SpaS. Nature. 2008;453: 124–127.

86. Abrusci P, Vergara-Irigaray M, Johnson S, Beeby MD, Hendrixson DR, Roversi P, et al. Architecture of the major component of the type III secretion system export apparatus. Nat Struct Mol Biol. 2013;20: 99–104.

87. Edqvist PJ, Olsson J, Lavander M, Sundberg L, Forsberg A, Wolf-Watz H, et al. YscP and YscU regulate substrate specificity of the Yersinia type III secretion system. J Bacteriol. 2003;185: 2259–2266.

88. Magdalena J, Hachani A, Chamekh M, Jouihri N, Gounon P, Blocker A, et al. Spa32 regulates a switch in substrate specificity of the type III secreton of Shigella flexneri from needle components to Ipa proteins. J Bacteriol. 2002;184: 3433–3441.

89. Ferris HU, Furukawa Y, Minamino T, Kroetz MB, Kihara M, Namba K, et al. FlhB regulates ordered export of flagellar components via autocleavage mechanism. J Biol Chem. 2005;280: 41236–41242.

90. Minamino T, Macnab RM. Domain structure of Salmonella FlhB, a flagellar export

component responsible for substrate specificity switching. J Bacteriol. 2000;182: 4906–4914.

91. Monjarás Feria JV, Lefebre MD, Stierhof Y-D, Galán JE, Wagner S. Role of autocleavage in the function of a type III secretion specificity switch protein in Salmonella enterica serovar Typhimurium. MBio. 2015;6: e01459–15.

92. Allaoui A, Woestyn S, Sluiters C, Cornelis GR. YscU, a Yersinia enterocolitica inner membrane protein involved in Yop secretion. J Bacteriol. 1994;176: 4534–4542.

93. Deane JE, Graham SC, Mitchell EP, Flot D, Johnson S, Lea SM. Crystal structure of Spa40, the specificity switch for the Shigella flexneri type III secretion system. Mol Microbiol. 2008;69: 267–276.

94. Lountos GT, Austin BP, Nallamsetty S, Waugh DS. Atomic resolution structure of the cytoplasmic domain of Yersinia pestis YscU, a regulatory switch involved in type III secretion. Protein Sci. 2009;18: 467–474.

95. Wiesand U, Sorg I, Amstutz M, Wagner S, van den Heuvel J, Lührs T, et al. Structure of the type III secretion recognition protein YscU from Yersinia enterocolitica. J Mol Biol. 2009;385: 854–866.

96. Büttner D, Lorenz C, Weber E, Bonas U. Targeting of two effector protein classes to the type III secretion system by a HpaC- and HpaB-dependent protein complex from Xanthomonas campestris pv. vesicatoria. Mol Microbiol. 2006;59: 513–527.

97. Kinoshita M, Hara N, Imada K, Namba K, Minamino T. Interactions of bacterial flagellar chaperone-substrate complexes with FlhA contribute to co-ordinating assembly of the flagellar filament. Mol Microbiol. 2013;90: 1249–1261.

98. Khanra N, Rossi P, Economou A, Kalodimos CG. Recognition and targeting mechanisms by chaperones in flagellum assembly and operation. Proc Natl Acad Sci U S A. 2016;113: 9798–9803.

99. Barker CS, Inoue T, Meshcheryakova IV, Kitanobo S, Samatey FA. Function of the conserved FHIPEP domain of the flagellar type III export apparatus, protein FlhA. Mol Microbiol. 2016;100: 278–288.

100. Erhardt M, Wheatley P, Kim EA, Hirano T, Zhang Y, Sarkar MK, et al. Mechanism of type-III protein secretion: Regulation of FlhA conformation by a functionally critical charged-residue cluster. Mol Microbiol. 2017;104: 234–249.

101. Diepold A, Wiesand U, Amstutz M, Cornelis GR. Assembly of the Yersinia injectisome: the missing pieces. Mol Microbiol. 2012;85: 878–892.

102. Portaliou AG, Tsolis KC, Loos MS, Balabanidou V, Rayo J, Tsirigotaki A, et al. Hierarchical protein targeting and secretion is controlled by an affinity switch in the type III secretion system of enteropathogenic. EMBO J. 2017;36: 3517–3531.

103. Gaytán MO, Monjarás Feria J, Soto E, Espinosa N, Benítez JM, Georgellis D, et al. Novel insights into the mechanism of SepL-mediated control of effector secretion in enteropathogenic Escherichia coli. Microbiologyopen. 2018;7: e00571.

104. Yu X-J, Grabe GJ, Liu M, Mota LJ, Holden DW. SsaV Interacts with SsaL to Control

the Translocon-to-Effector Switch in the SPI-2 Type Three Secretion System. MBio. 2018;9. doi:10.1128/mBio.01149-18

105. Mohammad-Khani S, Otremba B, Klein R, Capelle HH, Logemann F, Bange FC, et al. A fatal case of AIDS-defining meningoencephalitis by C. neoformans, sensitive to antifungal therapy. Eur J Med Res. 2010;15: 504–506.

106. Bange G, Kümmerer N, Engel C, Bozkurt G, Wild K, Sinning I. FlhA provides the adaptor for coordinated delivery of late flagella building blocks to the type III secretion system. Proc Natl Acad Sci U S A. 2010;107: 11295–11300.

107. Sukhan A, Kubori T, Wilson J, Galán JE. Genetic analysis of assembly of the Salmonella enterica serovar Typhimurium type III secretion-associated needle complex. J Bacteriol. 2001;183: 1159–1167.

108. Wang Y, Ouellette AN, Egan CW, Rathinavelan T, Im W, De Guzman RN. Differences in the electrostatic surfaces of the type III secretion needle proteins PrgI, BsaL, and MxiH. J Mol Biol. 2007;371: 1304–1314.

109. Loquet A, Sgourakis NG, Gupta R, Giller K, Riedel D, Goosmann C, et al. Atomic model of the type III secretion system needle. Nature. 2012;486: 276–279.

110. Demers J-P, Sgourakis NG, Gupta R, Loquet A, Giller K, Riedel D, et al. The common structural architecture of Shigella flexneri and Salmonella typhimurium type three secretion needles. PLoS Pathog. 2013;9: e1003245.

111. Demers J-P, Habenstein B, Loquet A, Kumar Vasa S, Giller K, Becker S, et al. High-resolution structure of the Shigella type-III secretion needle by solid-state NMR and cryo-electron microscopy. Nat Commun. 2014;5: 4976.

112. Broz P, Mueller CA, Müller SA, Philippsen A, Sorg I, Engel A, et al. Function and molecular architecture of the Yersinia injectisome tip complex. Mol Microbiol. 2007;65: 1311–1320.

113. Marlovits TC, Kubori T, Lara-Tejero M, Thomas D, Unger VM, Galán JE. Assembly of the inner rod determines needle length in the type III secretion injectisome. Nature. 2006;441: 637–640.

114. Torres-Vargas CE, Kronenberger T, Roos N, Dietsche T, Poso A, Wagner S. The inner rod of virulence-associated type III secretion systems constitutes a needle adapter of one helical turn that is deeply integrated into the system's export apparatus. Mol Microbiol. 2019;112: 918–931.

115. Mueller CA, Broz P, Müller SA, Ringler P, Erne-Brand F, Sorg I, et al. The V-antigen of Yersinia forms a distinct structure at the tip of injectisome needles. Science. 2005;310: 674–676.

116. Epler CR, Dickenson NE, Bullitt E, Picking WL. Ultrastructural analysis of IpaD at the tip of the nascent MxiH type III secretion apparatus of Shigella flexneri. J Mol Biol. 2012;420: 29–39.

117. Hayward RD, Koronakis V. Direct nucleation and bundling of actin by the SipC protein of invasive Salmonella. EMBO J. 1999;18: 4926–4934.

118. Myeni SK, Wang L, Zhou D. SipB-SipC complex is essential for translocon formation. PLoS One. 2013;8: e60499.

119. Romano FB, Tang Y, Rossi KC, Monopoli KR, Ross JL, Heuck AP. Type 3 Secretion Translocators Spontaneously Assemble a Hexadecameric Transmembrane Complex. J Biol Chem. 2016;291: 6304–6315.

120. Dickenson NE, Choudhari SP, Adam PR, Kramer RM, Joshi SB, Middaugh CR, et al. Oligomeric states of the Shigella translocator protein IpaB provide structural insights into formation of the type III secretion translocon. Protein Sci. 2013;22: 614–627.

121. Montagner C, Arquint C, Cornelis GR. Translocators YopB and YopD from Yersinia enterocolitica form a multimeric integral membrane complex in eukaryotic cell membranes. J Bacteriol. 2011;193: 6923–6928.

122. Marenne M-N, Journet L, Mota LJ, Cornelis GR. Genetic analysis of the formation of the Ysc-Yop translocation pore in macrophages by Yersinia enterocolitica: role of LcrV, YscF and YopN. Microb Pathog. 2003;35: 243–258.

123. Kaniga K, Trollinger D, Galán JE. Identification of two targets of the type III protein secretion system encoded by the inv and spa loci of Salmonella typhimurium that have homology to the Shigella IpaD and IpaA proteins. J Bacteriol. 1995;177: 7078–7085.

124. Ménard R, Sansonetti P, Parsot C. The secretion of the Shigella flexneri Ipa invasins is activated by epithelial cells and controlled by IpaB and IpaD. EMBO J. 1994;13: 5293–5302.

125. Kimbrough TG, Miller SI. Contribution of Salmonella typhimurium type III secretion components to needle complex formation. Proc Natl Acad Sci U S A. 2000;97: 11008–11013.

126. Kubori T, Sukhan A, Aizawa SI, Galán JE. Molecular characterization and assembly of the needle complex of the Salmonella typhimurium type III protein secretion system. Proc Natl Acad Sci U S A. 2000;97: 10225–10230.

127. Kato J, Dey S, Soto JE, Butan C, Wilkinson MC, De Guzman RN, et al. A protein secreted by the type III secretion system controls needle filament assembly. Elife. 2018;7. doi:10.7554/eLife.35886

128. Wee DH, Hughes KT. Molecular ruler determines needle length for the Salmonella Spi-1 injectisome. Proc Natl Acad Sci U S A. 2015;112: 4098–4103.

129. Lara-Tejero M, Galán JE. Salmonella enterica serovar typhimurium pathogenicity island 1-encoded type III secretion system translocases mediate intimate attachment to nonphagocytic cells. Infect Immun. 2009;77: 2635–2642.

130. Mueller CA, Broz P, Cornelis GR. The type III secretion system tip complex and translocon. Mol Microbiol. 2008;68: 1085–1095.

131. Kubori T, Galán JE. Salmonella type III secretion-associated protein InvE controls translocation of effector proteins into host cells. J Bacteriol. 2002;184: 4699–4708.

132. Kim JS, Jang JI, Eom JS, Oh CH, Kim HG, Kim BH, et al. Molecular characterization of the InvE regulator in the secretion of type III secretion translocases in Salmonella

enterica serovar Typhimurium. Microbiology. 2013;159: 446–461.

133. Roehrich AD, Bordignon E, Mode S, Shen D-K, Liu X, Pain M, et al. Steps for Shigella Gatekeeper Protein MxiC Function in Hierarchical Type III Secretion Regulation. J Biol Chem. 2017;292: 1705–1723.

134. Lavander M, Sundberg L, Edqvist PJ, Lloyd SA, Wolf-Watz H, Forsberg A. Proteolytic cleavage of the FlhB homologue YscU of Yersinia pseudotuberculosis is essential for bacterial survival but not for type III secretion. J Bacteriol. 2002;184: 4500–4509.

135. Sorg I, Wagner S, Amstutz M, Müller SA, Broz P, Lussi Y, et al. YscU recognizes translocators as export substrates of the Yersinia injectisome. EMBO J. 2007;26: 3015–3024.

136. Shen D-K, Moriya N, Martinez-Argudo I, Blocker AJ. Needle length control and the secretion substrate specificity switch are only loosely coupled in the type III secretion apparatus of Shigella. Microbiology. 2012;158: 1884–1896.

137. Forsberg A, Viitanen AM, Skurnik M, Wolf-Watz H. The surface-located YopN protein is involved in calcium signal transduction in Yersinia pseudotuberculosis. Mol Microbiol. 1991;5: 977–986.

138. Botteaux A, Sory MP, Biskri L, Parsot C, Allaoui A. MxiC is secreted by and controls the substrate specificity of the Shigella flexneri type III secretion apparatus. Mol Microbiol. 2009;71: 449–460.

139. Bahrani FK, Sansonetti PJ, Parsot C. Secretion of Ipa proteins by Shigella flexneri: inducer molecules and kinetics of activation. Infect Immun. 1997;65: 4005–4010.

140. Lee VT, Mazmanian SK, Schneewind O. A program of Yersinia enterocolitica type III secretion reactions is activated by specific signals. J Bacteriol. 2001;183: 4970–4978.

141. Blocker AJ, Deane JE, Veenendaal AKJ, Roversi P, Hodgkinson JL, Johnson S, et al. What's the point of the type III secretion system needle? Proc Natl Acad Sci U S A. 2008;105: 6507–6513.

142. Cheng LW, Kay O, Schneewind O. Regulated secretion of YopN by the type III machinery of Yersinia enterocolitica. J Bacteriol. 2001;183: 5293–5301.

143. Yu X-J, McGourty K, Liu M, Unsworth KE, Holden DW. pH sensing by intracellular Salmonella induces effector translocation. Science. 2010;328: 1040–1043.

144. Park D, Lara-Tejero M, Neal Waxham M, Li W, Hu B, Galán JE, et al. Visualization of the type III secretion mediated Salmonella–host cell interface using cryo-electron tomography. eLife. 2018. doi:10.7554/elife.39514

145. Diepold A, Amstutz M, Abel S, Sorg I, Jenal U, Cornelis GR. Deciphering the assembly of the Yersinia type III secretion injectisome. EMBO J. 2010;29: 1928–1940.

146. Burghout P, Beckers F, de Wit E, van Boxtel R, Cornelis GR, Tommassen J, et al. Role of the pilot protein YscW in the biogenesis of the YscC secretin in Yersinia enterocolitica. J Bacteriol. 2004;186: 5366–5375.

147. Collin S, Guilvout I, Nickerson NN, Pugsley AP. Sorting of an integral outer

membrane protein via the lipoprotein-specific Lol pathway and a dedicated lipoprotein pilotin. Mol Microbiol. 2011;80: 655–665.

148. Crago AM, Koronakis V. Salmonella InvG forms a ring-like multimer that requires the InvH lipoprotein for outer membrane localization. Mol Microbiol. 1998;30: 47–56.

149. Daefler S, Russel M. The Salmonella typhimurium InvH protein is an outer membrane lipoprotein required for the proper localization of InvG. Mol Microbiol. 1998;28: 1367–1380.

150. Okon M, Moraes TF, Lario PI, Creagh AL, Haynes CA, Strynadka NCJ, et al. Structural characterization of the type-III pilot-secretin complex from Shigella flexneri. Structure. 2008;16: 1544–1554.

151. García-Gómez E, Espinosa N, de la Mora J, Dreyfus G, González-Pedrajo B. The muramidase EtgA from enteropathogenic Escherichia coli is required for efficient type III secretion. Microbiology. 2011;157: 1145–1160.

152. Hoang HH, Nickerson NN, Lee VT, Kazimirova A, Chami M, Pugsley AP, et al. Outer membrane targeting of Pseudomonas aeruginosa proteins shows variable dependence on the components of Bam and Lol machineries. MBio. 2011;2. doi:10.1128/mBio.00246-11

153. Burkinshaw BJ, Deng W, Lameignère E, Wasney GA, Zhu H, Worrall LJ, et al. Structural analysis of a specialized type III secretion system peptidoglycan-cleaving enzyme. J Biol Chem. 2015;290: 10406–10417.

154. Deng W, Marshall NC, Rowland JL, McCoy JM, Worrall LJ, Santos AS, et al. Assembly, structure, function and regulation of type III secretion systems. Nat Rev Microbiol. 2017;15: 323–337.

155. Jackson MW, Plano GV. Interactions between type III secretion apparatus components from Yersinia pestis detected using the yeast two-hybrid system. FEMS Microbiol Lett. 2000;186: 85–90.

156. Thomas D, Morgan DG, DeRosier DJ. Structures of bacterial flagellar motors from two FliF-FliG gene fusion mutants. J Bacteriol. 2001;183: 6404–6412.

157. Tachiyama S, Chang Y, Muthuramalingam M, Hu B, Barta ML, Picking WL, et al. The cytoplasmic domain of MxiG interacts with MxiK and directs assembly of the sorting platform in the type III secretion system. J Biol Chem. 2019;294: 19184–19196.

158. Muthuramalingam M, Whittier SK, Lovell S, Battaile KP, Tachiyama S, Johnson DK, et al. The Structures of SctK and SctD from Pseudomonas aeruginosa Reveal the Interface of the Type III Secretion System Basal Body and Sorting Platform. J Mol Biol. 2020;432: 166693.

159. Rocha JM, Richardson CJ, Zhang M, Darch CM, Cai E, Diepold A, et al. Single-molecule tracking in live Yersinia enterocolitica reveals distinct cytosolic complexes of injectisome subunits. Int Bio (Cam). 2018;10: 502–515.

160. Bernal I, Börnicke J, Heidemann J, Svergun D, Horstmann JA, Erhardt M, et al. Molecular Organization of Soluble Type III Secretion System Sorting Platform Complexes. J Mol Biol. 2019;431: 3787–3803.

161. Wimmi S, Balinovic A, Jeckel H, Selinger L, Lampaki D, Eisemann E, et al. Dynamic relocalization of cytosolic type III secretion system components prevents premature protein secretion at low external pH. Nat Commun. 2021;12: 1625.

162. Wagner S, Diepold A. A Unified Nomenclature for Injectisome-Type Type III Secretion Systems. Curr Top Microbiol Immunol. 2020;427: 1–10.

163. Hu J, Worrall LJ, Vuckovic M, Hong C, Deng W, Atkinson CE, et al. T3S injectisome needle complex structures in four distinct states reveal the basis of membrane coupling and assembly. Nat Microbiol. 2019;4: 2010–2019.

164. Hara N, Namba K, Minamino T. Genetic characterization of conserved charged residues in the bacterial flagellar type III export protein FlhA. PLoS One. 2011;6: e22417.

165. Tseytin I, Madar A, Mitrovic B, Deng W, Finlay BB, Sal-Man N. The Third Transmembrane Domain of EscR Is Critical for Function of the Enteropathogenic Type III Secretion System. mSphere. 2018;3. doi:10.1128/mSphere.00162-18

166. Tseytin I, Mitrovic B, David N, Langenfeld K, Zarivach R, Diepold A, et al. The Role of the Small Export Apparatus Protein, SctS, in the Activity of the Type III Secretion System. Front Microbiol. 2019;10: 2551.

167. Miletic S, Fahrenkamp D, Goessweiner-Mohr N, Wald J, Pantel M, Vesper O, et al. Substrate-engaged type III secretion system structures reveal gating mechanism for unfolded protein translocation. Nat Commun. 2021;12: 1546.

168. Hüsing S, van Look U, Guse A, Gálvez EJC, Charpentier E, Blair DF, et al. Controlling membrane barrier during bacterial type-III protein secretion. bioRxiv. bioRxiv; 2020. doi:10.1101/2020.11.25.397760

169. Hoiseth SK, Stocker BA. Aromatic-dependent Salmonella typhimurium are non-virulent and effective as live vaccines. Nature. 1981;291: 238–239.

170. Kaniga K, Bossio JC, Galán JE. The Salmonella typhimurium invasion genes invF and invG encode homologues of the AraC and PulD family of proteins. Mol Microbiol. 1994;13: 555–568.

171. Website. [cited 2 May 2021]. Available: Agilent, QuikChange II Site-Directed Mutagenesis Kit, http://www.chem.agilent.com/ library/usermanuals/Public/200523.pdf

172. Gibson DG, Young L, Chuang R-Y, Venter JC, Hutchison CA 3rd, Smith HO. Enzymatic assembly of DNA molecules up to several hundred kilobases. Nat Methods. 2009;6: 343–345.

173. Dower WJ, Miller JF, Ragsdale CW. High efficiency transformation of E. coli by high voltage electroporation. Nucleic Acids Res. 1988;16: 6127–6145.

174. Babic A, Guérout A-M, Mazel D. Construction of an improved RP4 (RK2)-based conjugative system. Res Microbiol. 2008;159: 545–549.

175. Farrell IS, Toroney R, Hazen JL, Mehl RA, Chin JW. Photo-cross-linking interacting proteins with a genetically encoded benzophenone. Nat Methods. 2005;2: 377–384.

176. Zilkenat S, Dietsche T, Monjarás Feria JV, Torres-Vargas CE, Mebrhatu MT, Wagner S. Blue Native PAGE Analysis of Bacterial Secretion Complexes. Methods Mol Biol. 2017;1615: 321–351.

177. Westerhausen S, Nowak M, Torres-Vargas CE, Bilitewski U, Bohn E, Grin I, et al. A NanoLuc luciferase-based assay enabling the real-time analysis of protein secretion and injection by bacterial type III secretion systems. Mol Microbiol. 2020;113: 1240–1254.

178. Schägger H, von Jagow G. Blue native electrophoresis for isolation of membrane protein complexes in enzymatically active form. Anal Biochem. 1991;199: 223–231.

179. Hauer F, Gerle C, Fischer N, Oshima A, Shinzawa-Itoh K, Shimada S, et al. GraDeR: Membrane Protein Complex Preparation for Single-Particle Cryo-EM. Structure. 2015;23: 1769–1775.

180. Fukumura T, Makino F, Dietsche T, Kinoshita M, Kato T, Wagner S, et al. Assembly and stoichiometry of the core structure of the bacterial flagellar type III export gate complex. PLoS Biol. 2017;15: e2002281.

181. Katoh K, Standley DM. MAFFT multiple sequence alignment software version 7: improvements in performance and usability. Mol Biol Evol. 2013;30: 772–780.

182. Waterhouse AM, Procter JB, Martin DMA, Clamp M, Barton GJ. Jalview Version 2--a multiple sequence alignment editor and analysis workbench. Bioinformatics. 2009;25: 1189–1191.

183. Wilharm G, Lehmann V, Krauss K, Lehnert B, Richter S, Ruckdeschel K, et al. Yersinia enterocolitica type III secretion depends on the proton motive force but not on the flagellar motor components MotA and MotB. Infect Immun. 2004;72: 4004–4009.

184. Paul K, Erhardt M, Hirano T, Blair DF, Hughes KT. Energy source of flagellar type III secretion. Nature. 2008;451: 489–492.

185. Minamino T, Namba K. Distinct roles of the FliI ATPase and proton motive force in bacterial flagellar protein export. Nature. 2008;451: 485–488.

186. Lee P-C, Zmina SE, Stopford CM, Toska J, Rietsch A. Control of type III secretion activity and substrate specificity by the cytoplasmic regulator PcrG. Proc Natl Acad Sci U S A. 2014;111: E2027–36.

187. Lee P-C, Rietsch A. Fueling type III secretion. Trends Microbiol. 2015;23: 296–300.

188. Minamino T, Kinoshita M, Imada K, Namba K. Interaction between FliI ATPase and a flagellar chaperone FliT during bacterial flagellar protein export. Mol Microbiol. 2012;83: 168–178.

189. Goessweiner-Mohr N, Kotov V, Brunner MJ, Mayr J, Wald J, Kuhlen L, et al. Structural control for the coordinated assembly into functional pathogenic type-3 secretion systems. Cold Spring Harbor Laboratory. 2019. p. 714097. doi:10.1101/714097

190. Delalez NJ, Berry RM, Armitage JP. Stoichiometry and turnover of the bacterial flagellar switch protein FliN. MBio. 2014;5: e01216–14.

9. Acknowledgements

My deepest thanks to,

- My supervisor, **Prof. Samuel Wagner** for his mentoring and guidance.
I express deepest gratitude for providing me with the opportunity and freedom to learn from and explore the larger scientific community through various conferences and workshops that I had the privilege to attend. Thank you for encouraging and nurturing my interest in different aspects of my projects and methods by our fruitful discussions. I will always be mesmerized with your positive take on even the worst of the scenarios. Thank you for entertaining me with my questions and doubts whenever I knocked at your door.

- My second supervisor **PD Dr. Evi Stegmann** for taking out your valuable time to review my work.

- **Dr. Libera Lo Presti** for the critical review of my thesis and your valuable inputs.

- **Andrea** and **Melanie** for your constant support and help with my experiments. **Andrea**, you are the best!! I consider myself very lucky to have had such great technical support during my time in the lab. I will miss you!!

- All former and current members of **AG Wagner** for a great working environment. Thanks for the support. **Iwan**, **Mehari**, **Lea**, **Sussann**, **Julia**, **Silke**, **Sara**, **Hakim** and **Sibel** for all the fun talks, interesting discussions and useful practical tips. **Iwan**, thank you for answering all my queries, computer problems, and your encouragement during my lows. **Sibel**, you were a great support as a friend, colleague, and I will never forget our funny talks and laughs!! Will stay in touch.

- The HiWi students and collaboration partners that I had the privilege and joy to work with. Thanks **Sam**, **Martina**, **Janani, Mirita** and **Thales**.

- Colleagues and group leaders within **SFB766** (Bacterial Cell Envelope) for the great learning opportunities, lively interaction and providing both encouragement as well as criticism.

- **Gisela**, **Inka**, **Dirk**, **Lisa**, **Jan,** and **Stephan** for all the help with official problems, questions, and arrangements during my stay in the institute.

- My dearest **family** – for your unwavering support and faith in me.

- My husband **Neel**, for your unconditional support, love and care. I love you!!

- **Gauri** for being there through highs and lows of my life both professionally as well as personally. I am lucky to have met you and will always be thankful to Tuebingen for giving me a friend for my lifetime.

- **Himanshu**, **Gurleen**, **Shibu**, **Vaidurya**, **Shruti**, **Bogdan**, **Shwetha**, **Nanda**, **Suryesh**, **Iqra**, **Bilal, Krithika, Jialin** and **Sandra** for adding fun to my life. Thanks **Iqra** for proofreading my thesis.